HARD X-RAY IMAGING AND TOMOGRAPHY

P. Cloetens
ESRF,
the European Synchrotron
ID16A

cloetens@esrf.eu

With thanks to:
J. Baruchel, S. Bohic, J.C. da Silva, M. di Michiel, D. Karpov
A. Pacureanu, F. Peyrin, A. Rack, M. Salome, P. Tafforeau, Y. Yang

The European Synchrotron | ESRF

X-ray (absorption) imaging is not a new technique….

History : 1895, G.C. Röntgen

First X ray made in public. Hand of the famed anatomist, Albert von Kölliker, made during Roentgen's initial lecture before the Würzburg Physical Medical Society on January 23, 1896.

CRUMPLING OF SILVER NANOWIRES BY ENDOLYSOSOMES STRONGLY REDUCES TOXICITY

Fibroblast cell

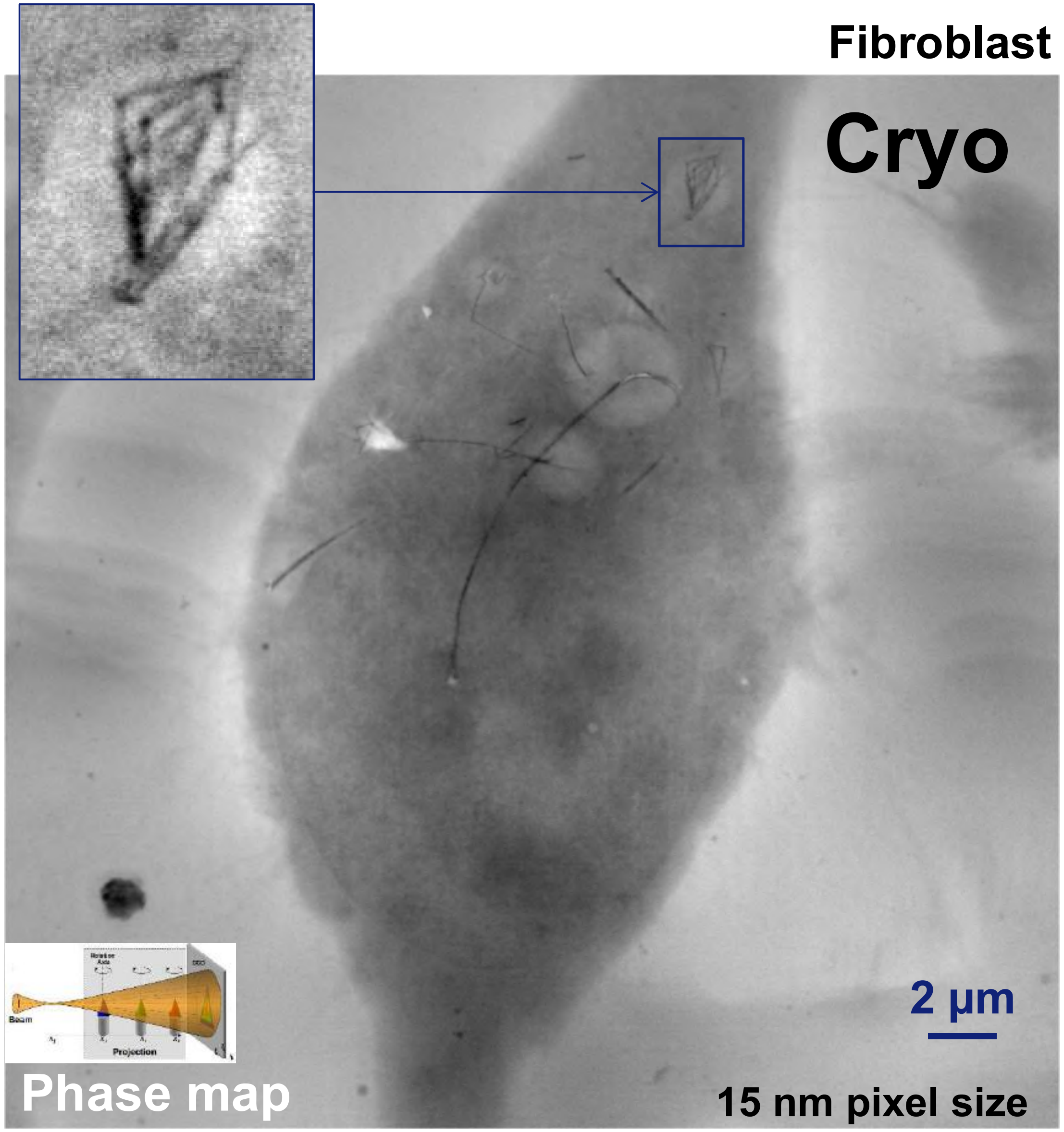

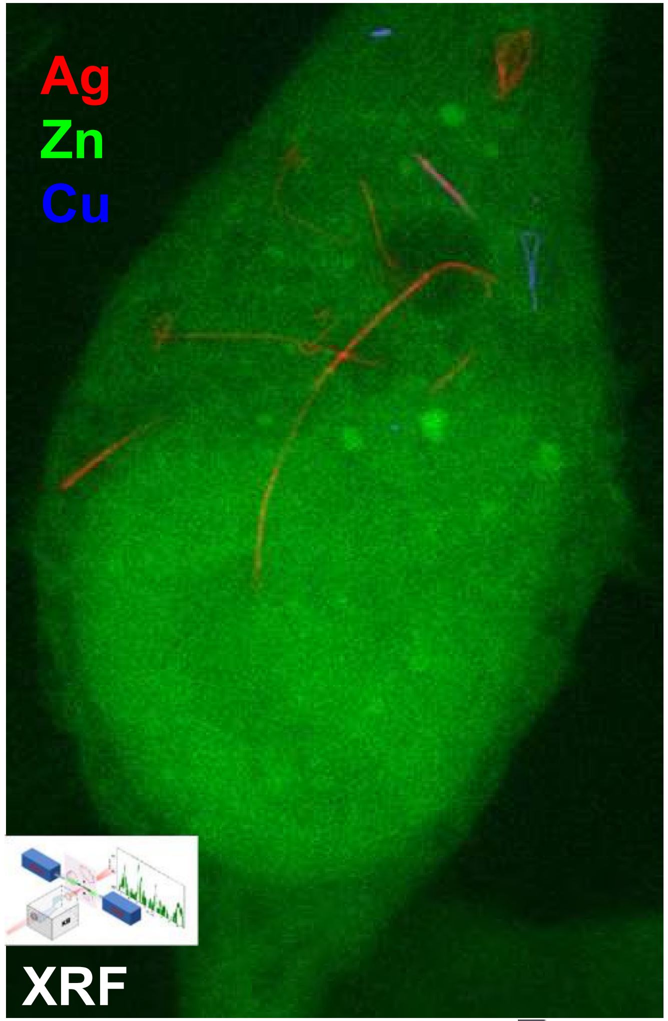

50 nm pixel size

33 nm Ag nanowires

S Lehmann, A E Prada, L Charlet, B Gilbert (LBNL) et al, *PNAS*, 116, 14893 (2019)

CRUMPLING OF SILVER NANOWIRES BY ENDOLYSOSOMES STRONGLY REDUCES TOXICITY

30 nm voxel size

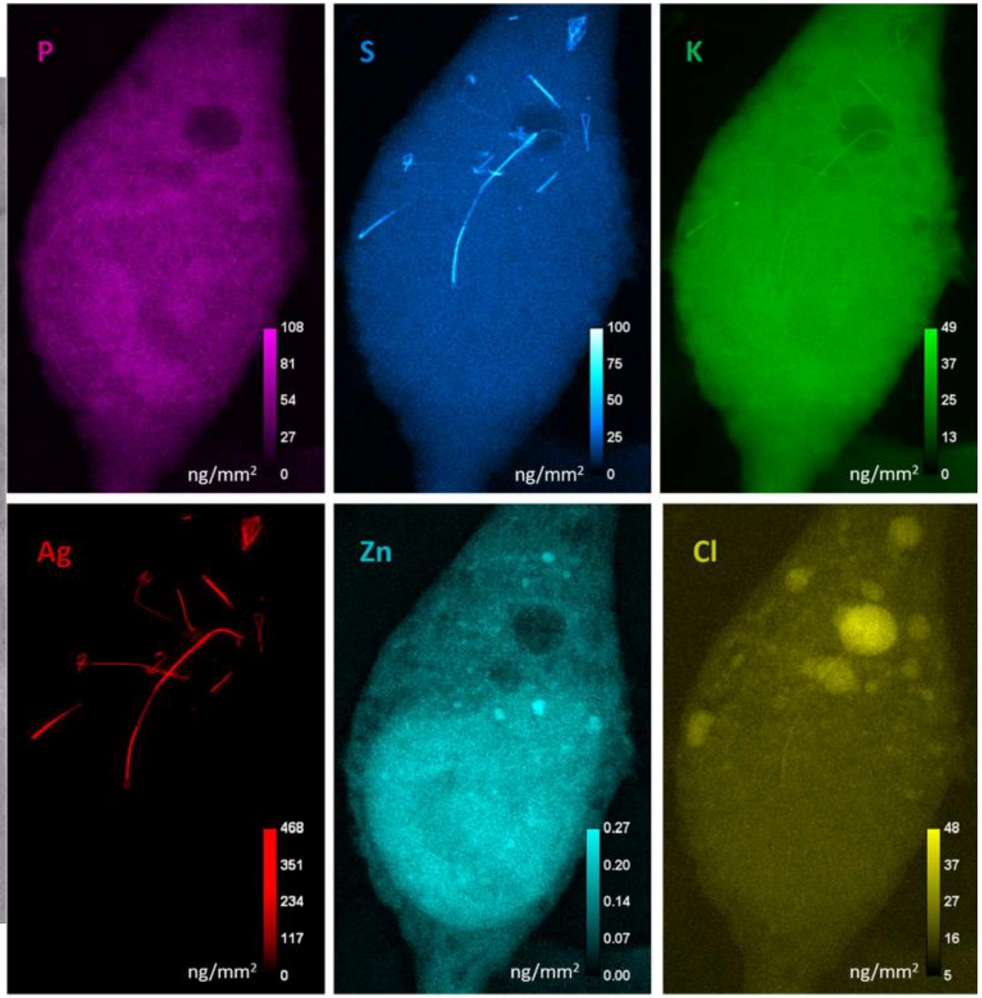

S Lehmann, A E Prada, L Charlet, B Gilbert (LBNL) et al, *PNAS*, 116, 14893 (2019)

X-RAY IMAGING   X-RAY MICROSCOPY

"Micron scale"

- Tomography
- (Spatial) Resolution
- Absorption / Phase Contrast
- Generalized Tomography

  Fluorescence, Diffraction, SAXS

"Nano-scale"

- Techniques
- Full-field & Dark-field Microscopy
- CDI / Far-field Ptychography
- Nano-probe techniques
- In-line Holography

Inhomogeneous sample

(density, composition, domains, phases, defects, …)

→ requires a **"local" investigation**

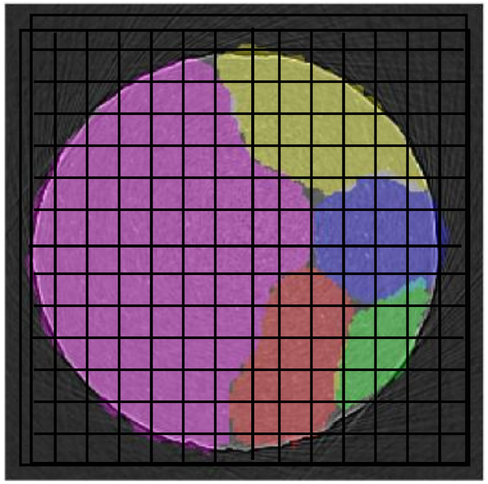

Two main techniques:

Full-field Techniques
with Parallel Beam

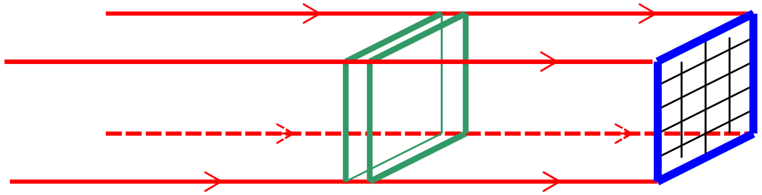

Scanning Techniques
with Focused Beam

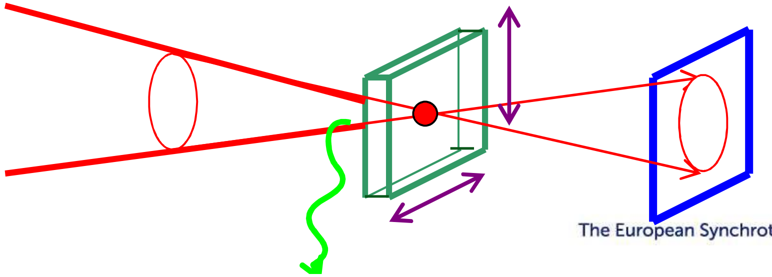

X-RAY MATTER INTERACTIONS USED FOR X-RAY IMAGING

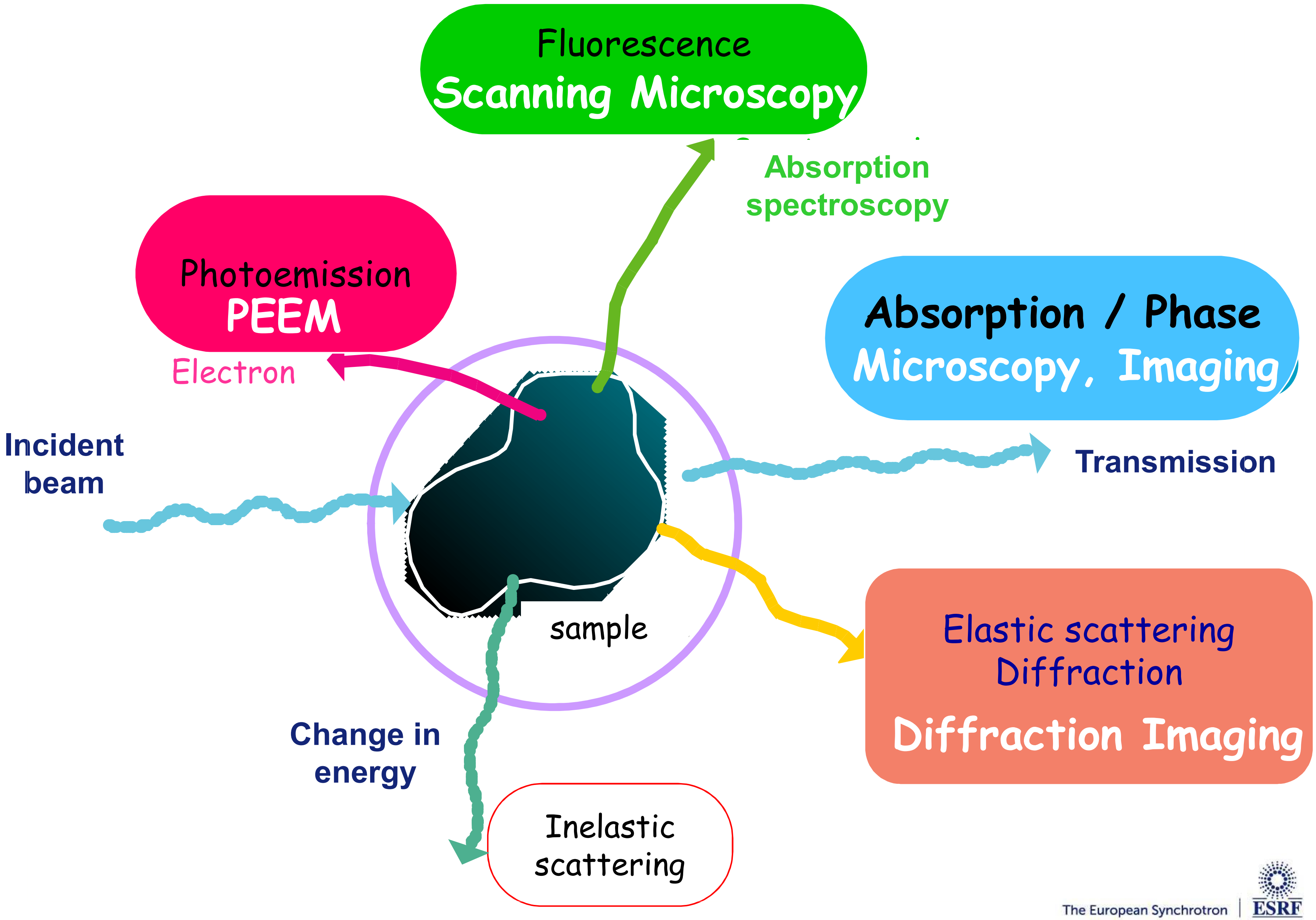

MAIN ASSETS OF HARD X-RAYS IN MICROSCOPY

- Combine **high spatial resolution** on **'thick' samples** in 3D
- **Multi-modal approach**; natural and quantitative contrast from electron density, elements, chemistry and (crystalline) structure
- **Access to large volumes** (representative elementary volume)
- **Dynamics**: follow evolving systems with fast 2D and 3D techniques (mostly non-destructive)

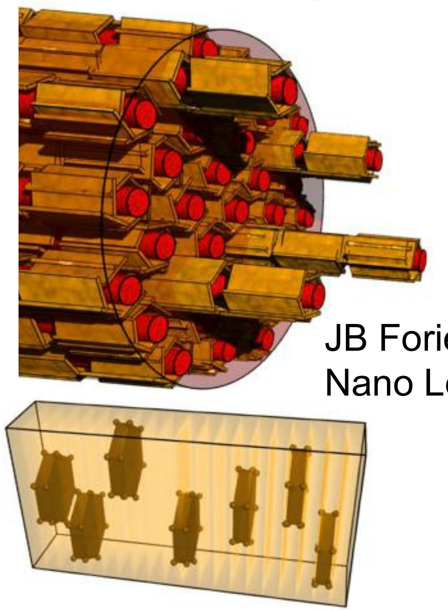

JB Forien, P Zaslansky et al.
Nano Lett. 15 (2015) 3729

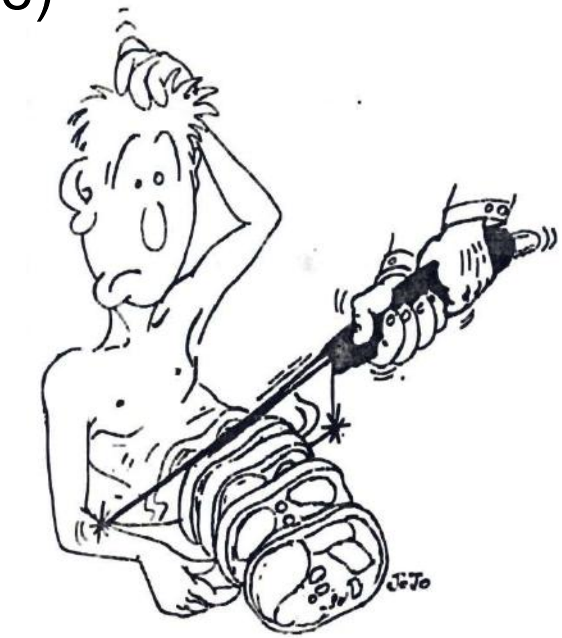

Goal: **quantitative imaging**:
= ***measuring*** a given *object* quantity as a function of *space* and *time*

$\alpha(\boldsymbol{r},t)$

with $\boldsymbol{r} = (x,y,z)$ or (x,y)

and α can be $n = 1 - \delta + i\,\beta$
lattice distortion u
element concentrations
(electron) density …

Always put a **scale bar** and **color bar**!

X-rays well suited:
Weak and linear interaction, but not always (e.g. dynamical diffraction)
But
'Poor' instrumentation compared to light / electron microscopy

COMPUTED TOMOGRAPHY (2D → 3D)

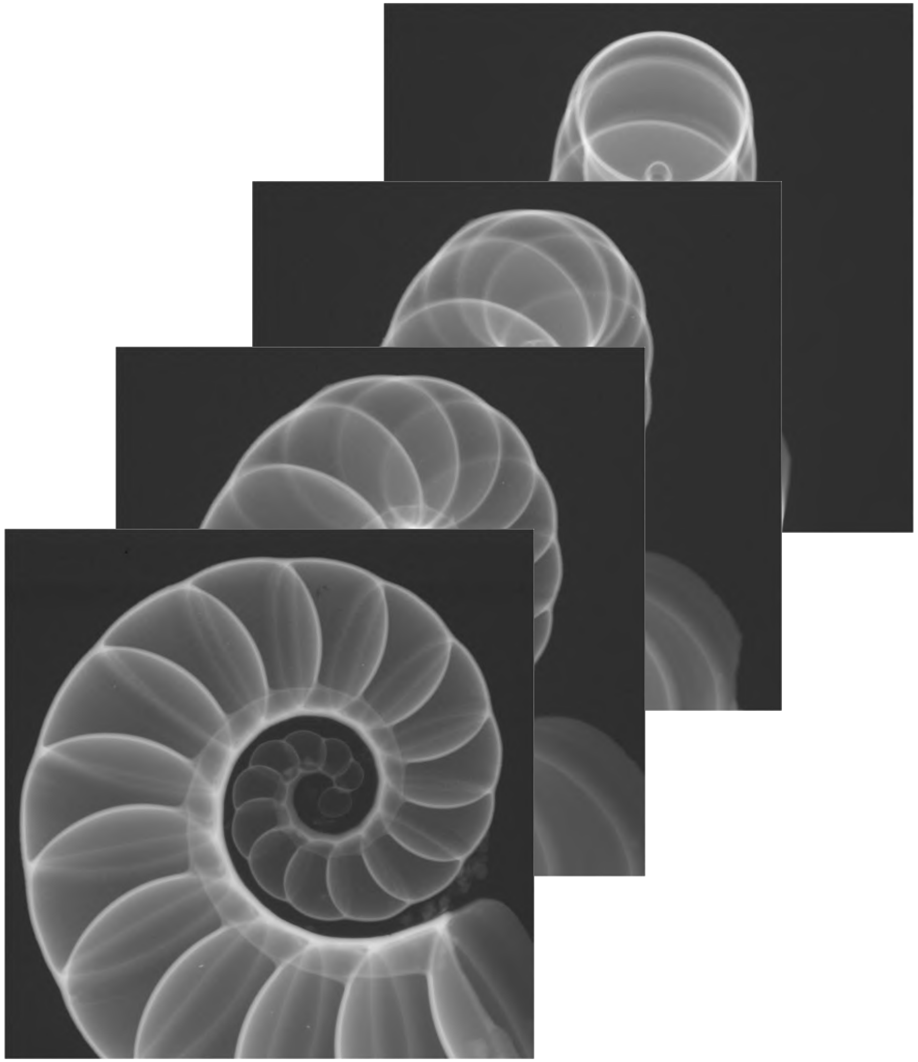

N 2D projections

Volume Rendering

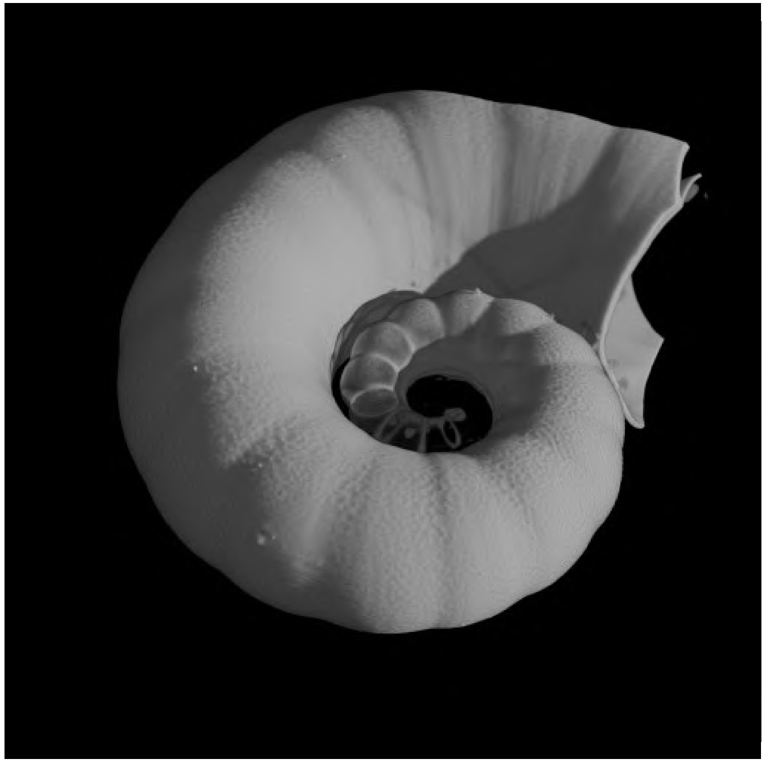

Reconstructed 3D volume

Lambert-Beer law

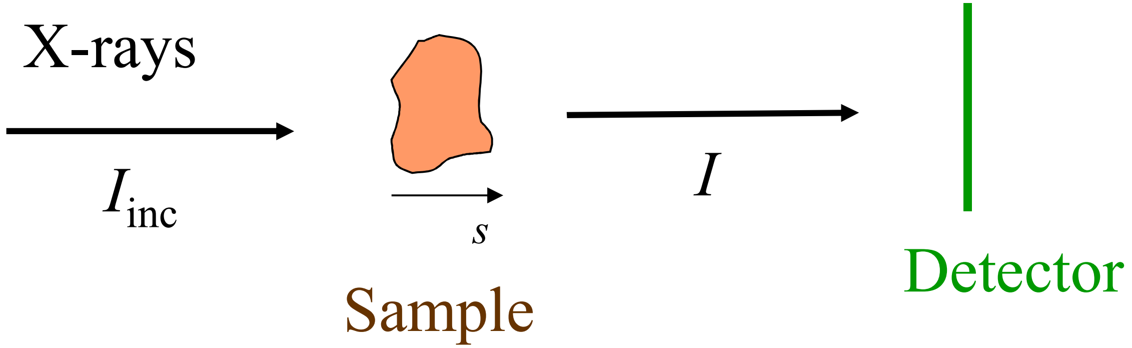

$$\frac{I}{I_{\text{inc}}} = \exp \int -\mu ds \qquad \ln \frac{I_{\text{inc}}(x')}{I(x')} = \int \mu(x,y) ds$$

μ, linear attenuation coefficient

LATERAL AND DEPTH RESOLUTION

Radiography → Sum of the attenuation along a ray

→ Good lateral resolution

→ No depth resolution

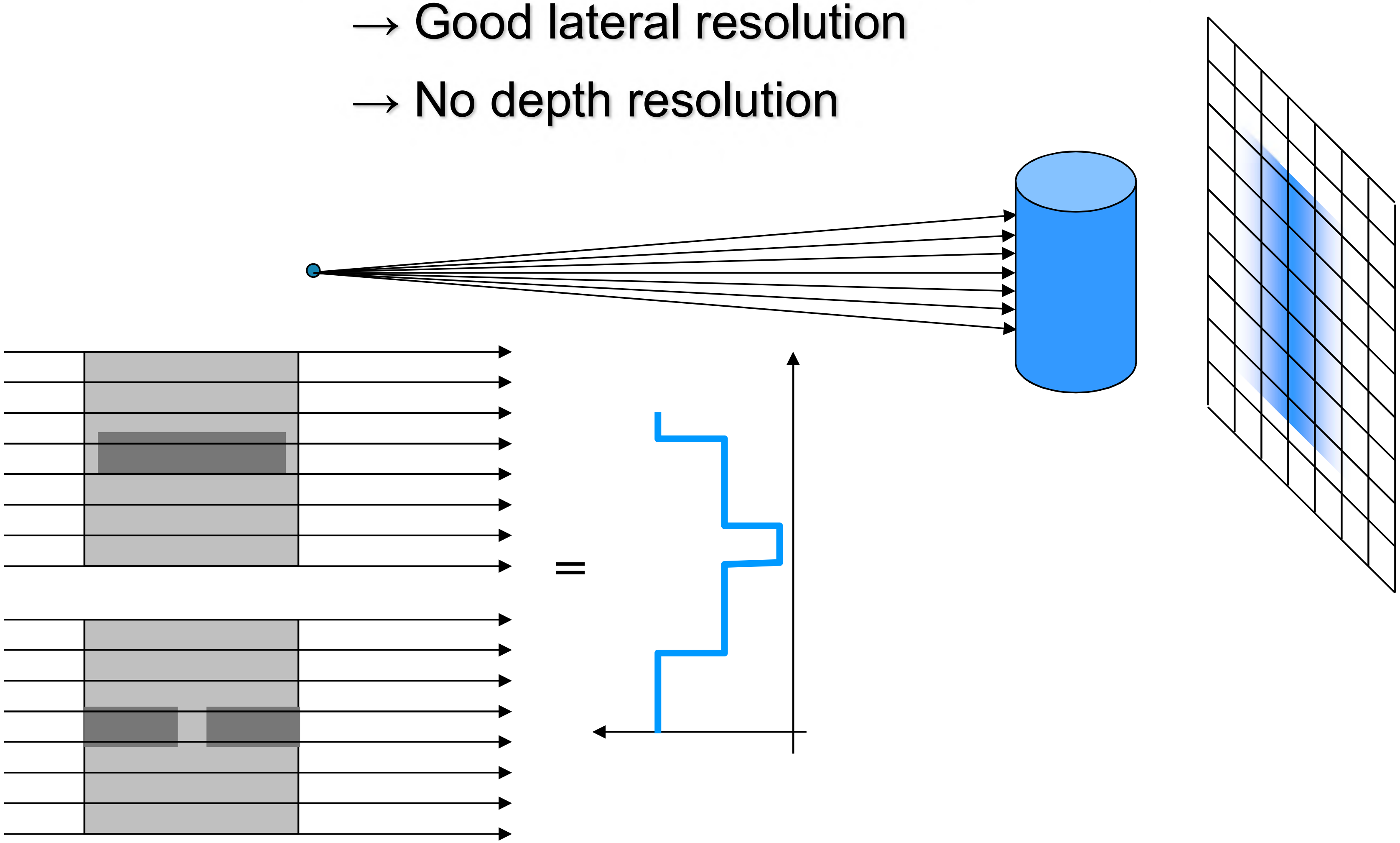

To distinguish the 2 : take 2 projections at 90 degrees

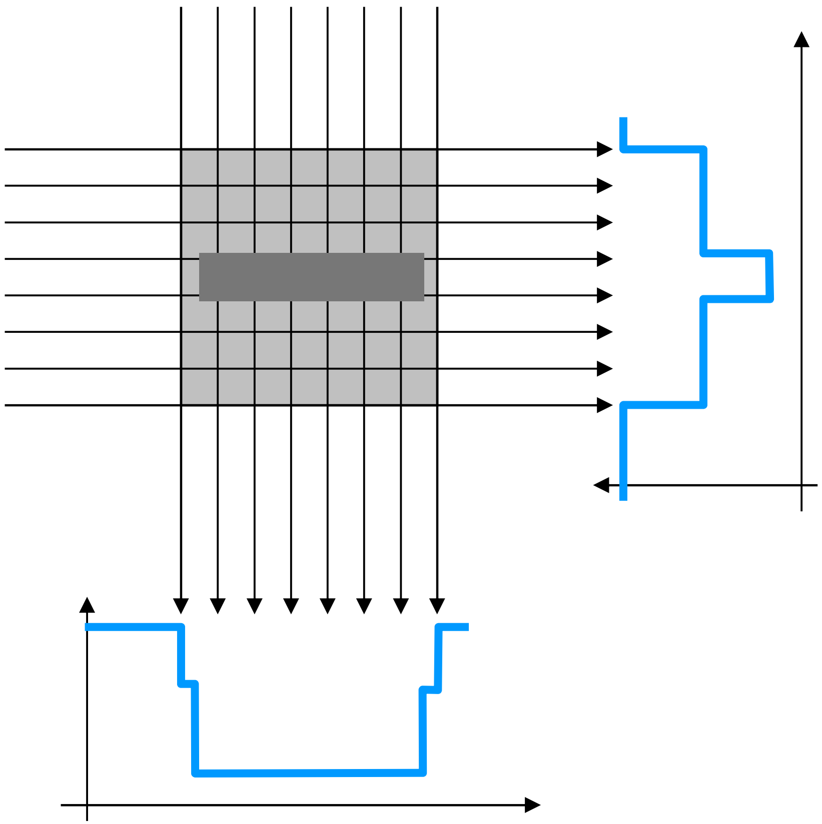

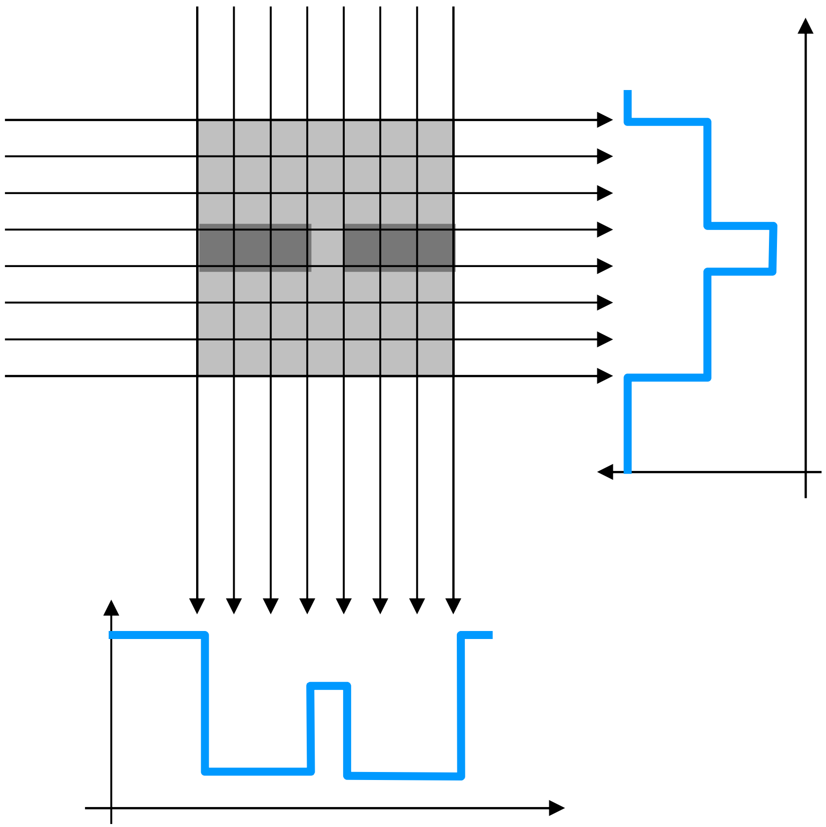

RADON TRANSFORM: EXAMPLES

Image Space

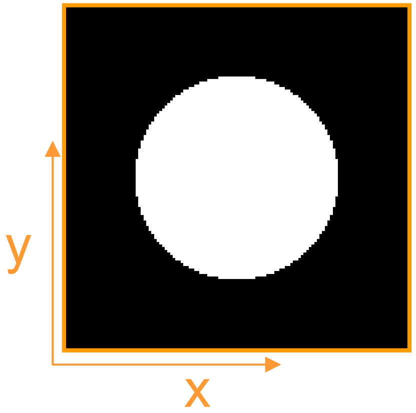

Same projection ∀ θ

amplitude

Gray level

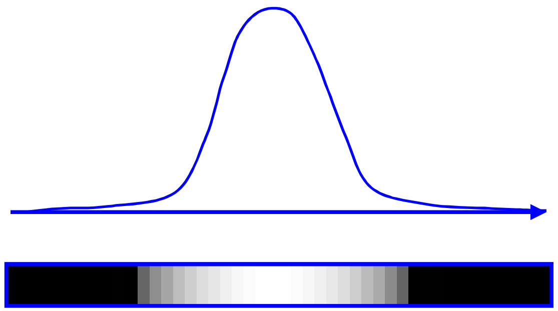

Radon Space
= **sinogram**

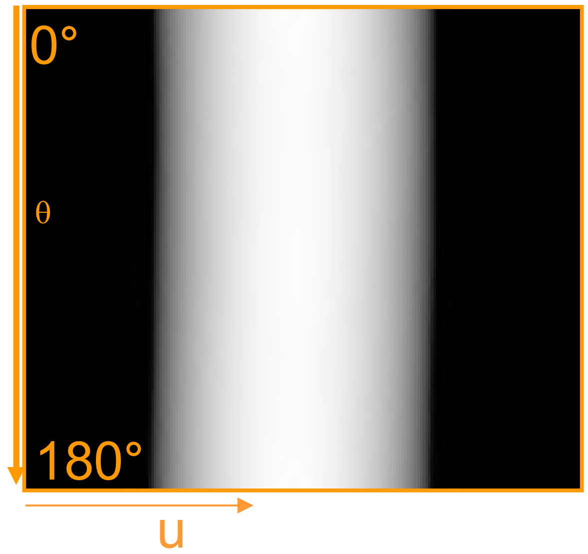

RADON TRANSFORM: EXAMPLES

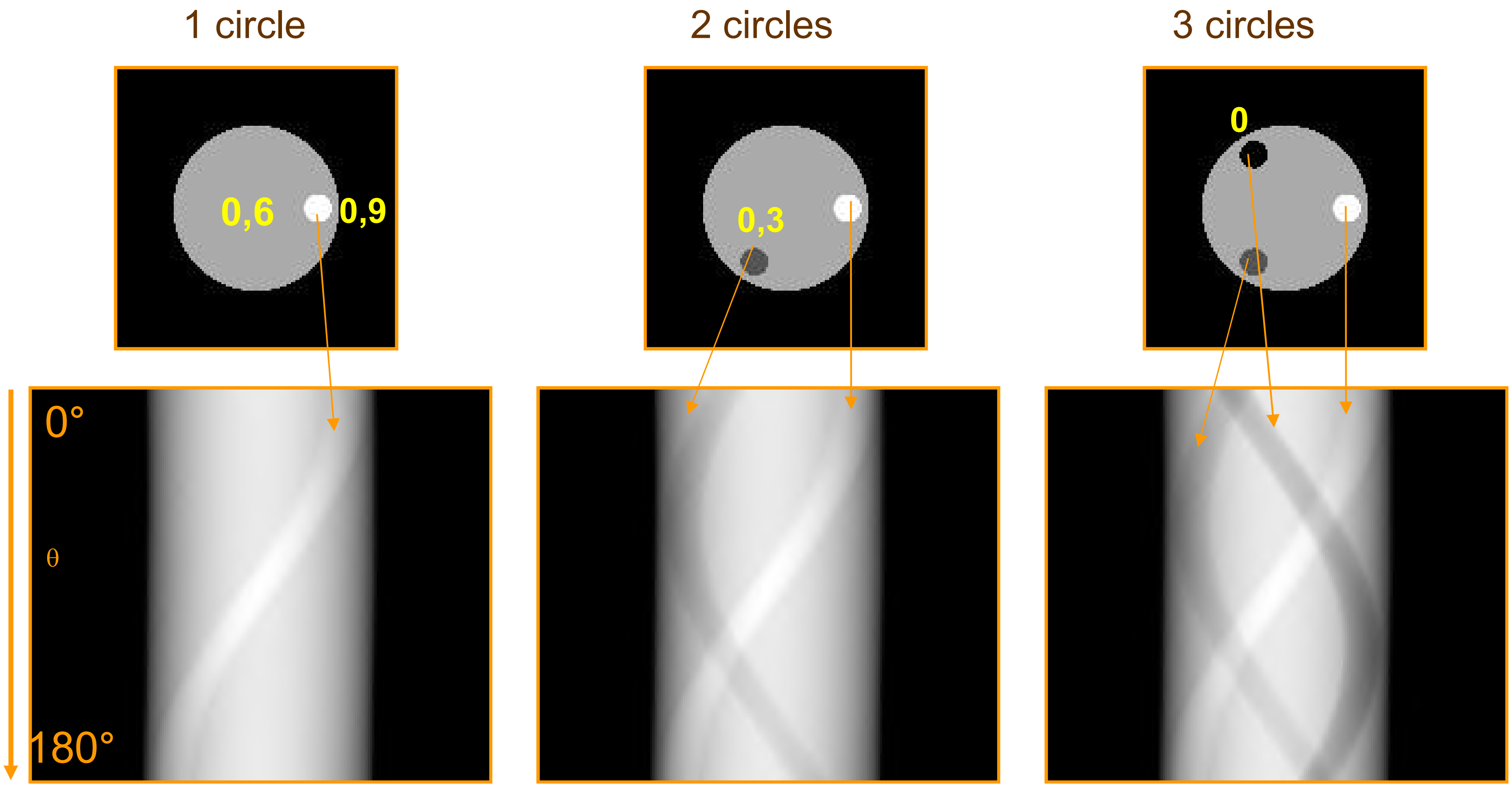

RECONSTRUCTION: (FILTERED) BACK-PROJECTION

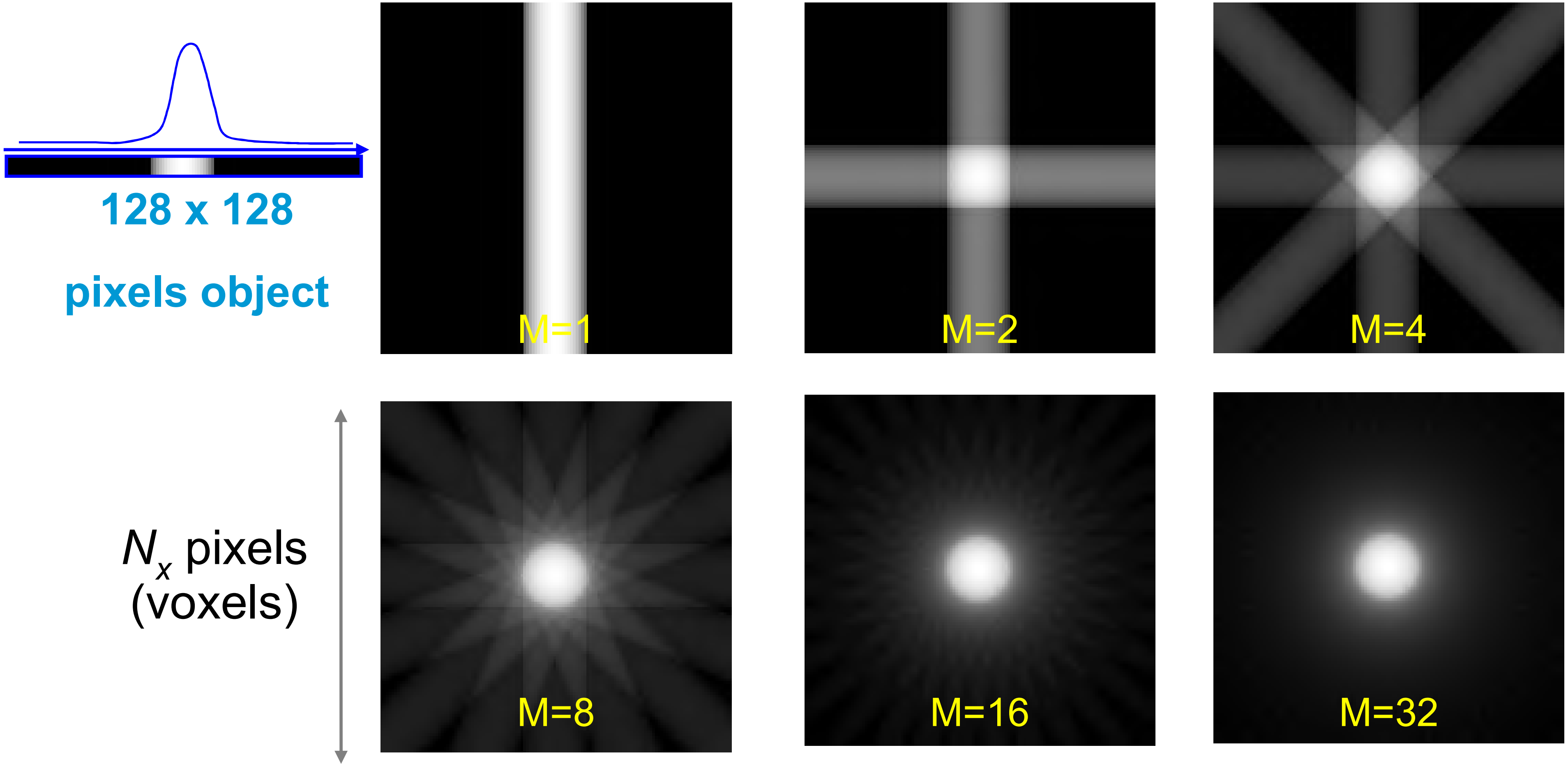

Correct result using: **Filtered Back-projection**

Number of projections: Theory: $M = \frac{\pi}{2} N_x$ Practice: $M \approx N_x$

Absorption/Phase tomography: analytic method, FBP using e.g. Nabu

Diffraction/Fluorescence tomography: algebraic methods, MLEM, TV using e.g. ASTRA

SPATIAL RESOLUTION (1)

Pixel / Voxel size

Often stated as ‘resolution’ in tomography!

Correct sampling requires: $f_{max} < f_{Nyquist} = \frac{1}{2pixelsize}$

Rayleigh Criterion for resolving two adjacent objects

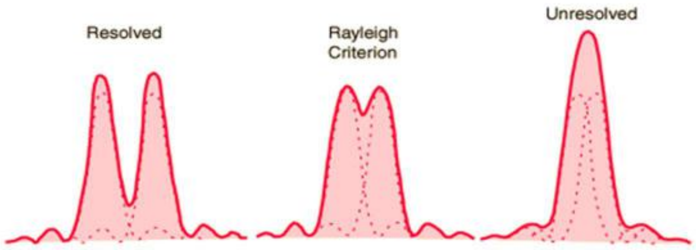

Point spread function - Transfer function

$R_{Rayleigh} = c\ \lambda/NA$

Noise-less world

Abbe criterion:

Resolution depends on **wavelength** and **numerical aperture**. There is an upper limit for a given wavelength.

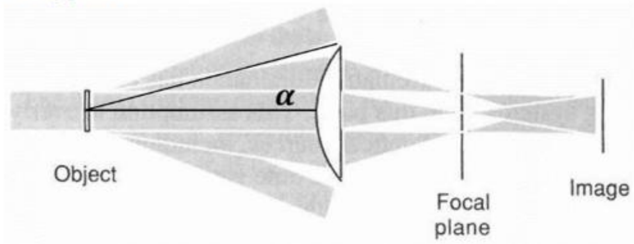

$$\Delta x = \frac{\lambda}{2n \sin \alpha}$$

Rose Criterion: influence of noise on spatial resolution

Photon statistics and/or dose limit the obtainable resolution

SNR > 5 for detection

e.g. tomography (Flannery 87) $N_{phot} \propto \frac{D^4}{R^4} \frac{\exp(\mu D)}{[\mu D(\sigma/\mu)]^2}$

With sample diameter D constant: if R ↓ then N_{Phot} ↑ as $(1/R)^4$

Detection Limit:

Smallest object that can be detected

will depend on contrast and noise

can be << $R_{Rayleigh}$ especially using phase contrast

Precision:

on the position of an object for example

$$Precision \propto \frac{R_{Rayleigh}}{\sqrt{N_{phot}}}$$

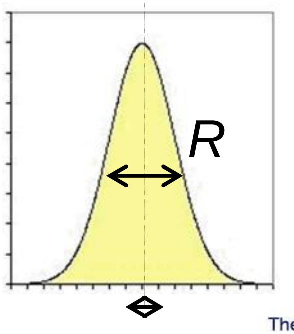

Edge Profile

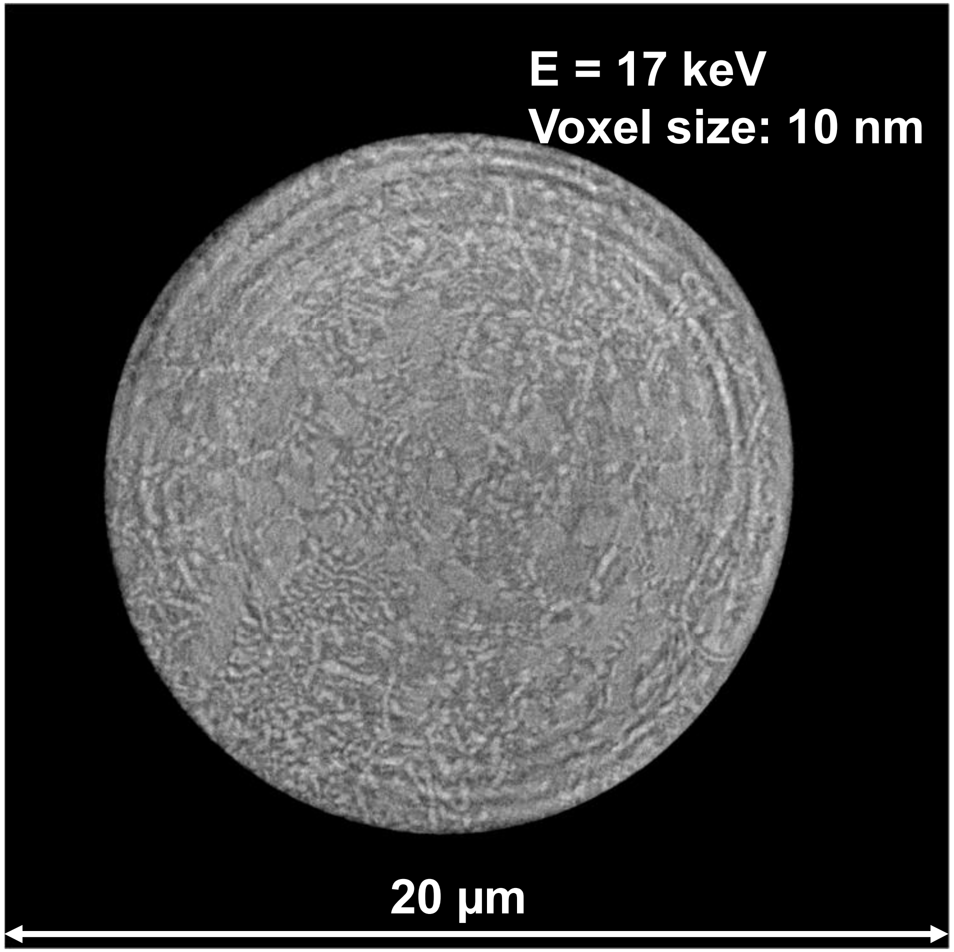

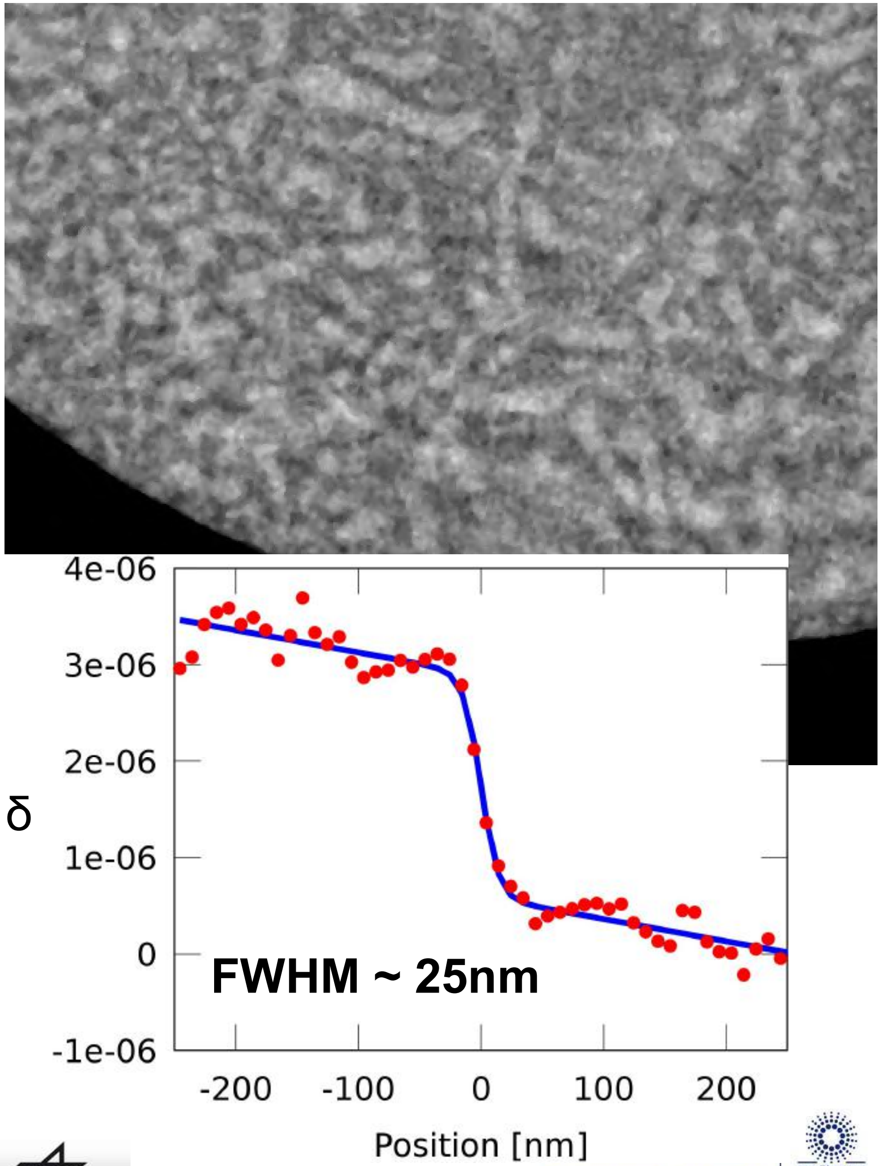

Ultrafine eutectic Ti/Fe alloy by additive manufacturing

Sample: G. Requena, German Aerospace Center (DLR)

ESTIMATION OF THE 3D SPATIAL RESOLUTION

Fourier Shell Correlation

Actually measures the *consistency* of two measurements

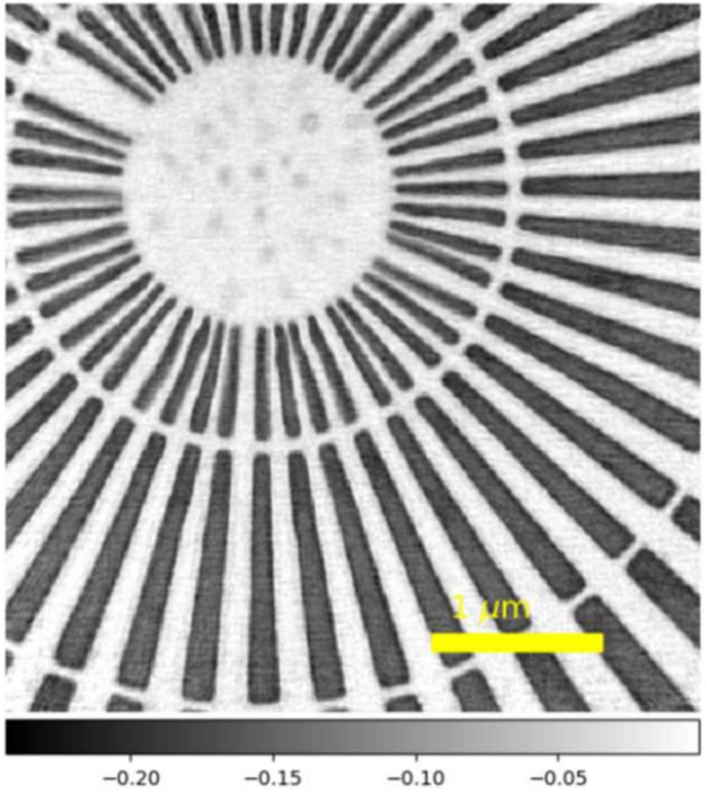

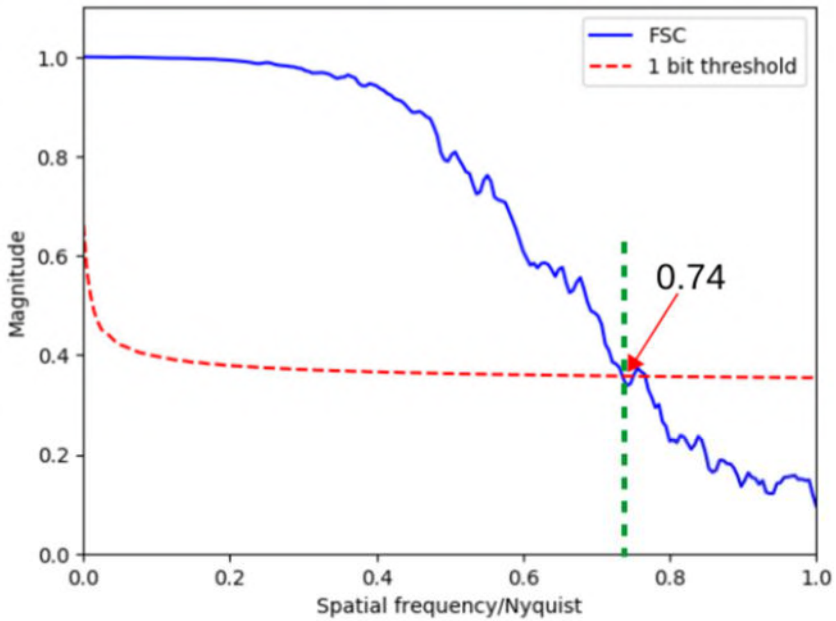

Resolution estimate:

$$\frac{10\ nm}{0.74} = 13.51\ nm$$

$$\mathrm{FSC}_{12}(r_i) = \frac{\sum_{r \in r_i} F_1(r) \cdot F_2(r)^*}{\sqrt{\sum_{r \in r_i} F_1^2(r) \cdot \sum_{r \in r_i} F_2^2(r)}}$$

M. van Heel, M. Schatz,
Fourier Shell Correlation threshold criteria,
J. Struc. Biol. 151 (2005) 250.

ABSORPTION VS. PHASE

Simple transmission

Absorption

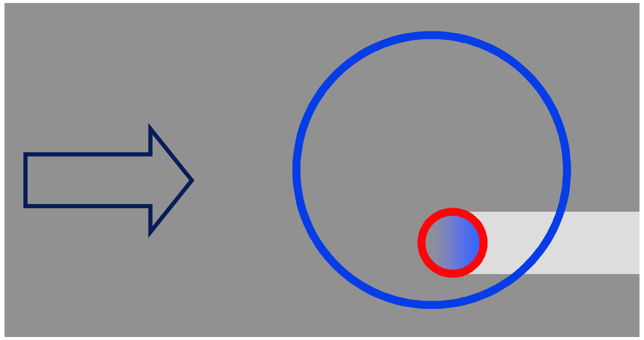

$\beta \propto \mu$

Phase

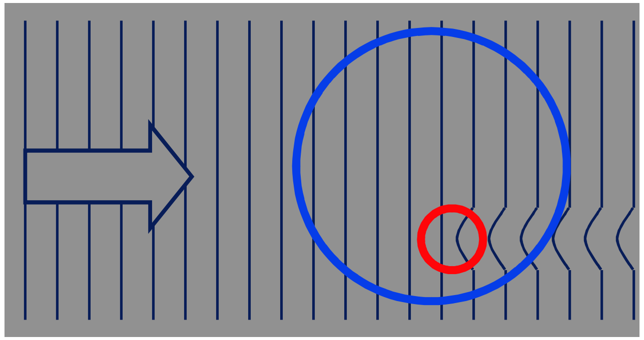

$\delta \propto$ electron density

- Dream 1: **Low Dose**

  Increase the energy

  Absorption contrast ↓ replaced by phase contrast

- Dream 2: Improve the **Sensitivity**

  Absorption contrast too low high spatial resolution

  light materials

  similar attenuation

- Weak interaction with matter
- Refractive index *n* (X-rays):

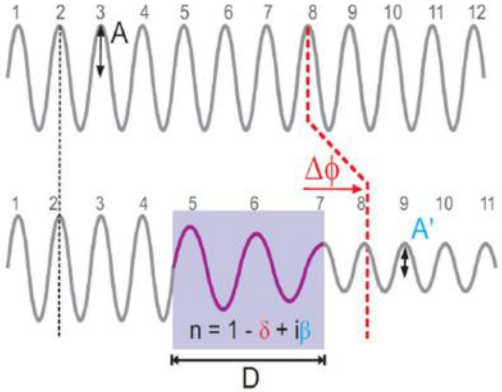

from C. Grünzweig, PhD thesis

$$n = 1 - \delta + i\beta$$

$\delta >> \beta$

10^{-6} 10^{-9}

β – Absorption index

- photo-electric effect
  Compton scattering
- strong energy dependence
- $\beta = (\lambda / 4\pi).\mu$
  linear attenuation coefficient μ

$$\beta = \frac{r_c \lambda^2}{2\pi V} \sum f_p''$$

δ – Refractive index decrement

- proportional to
  electron density
- inversely proportional to
  energy^2
- $$\delta = \frac{r_c \lambda^2}{2\pi V} \sum \left(Z_p + f_p' \right)$$

$\approx 1.3\ 10^{-6}\ \rho\ \lambda^2$

ρ in g/cm^3, λ in Å

PHASE CONTRAST VS ABSORPTION

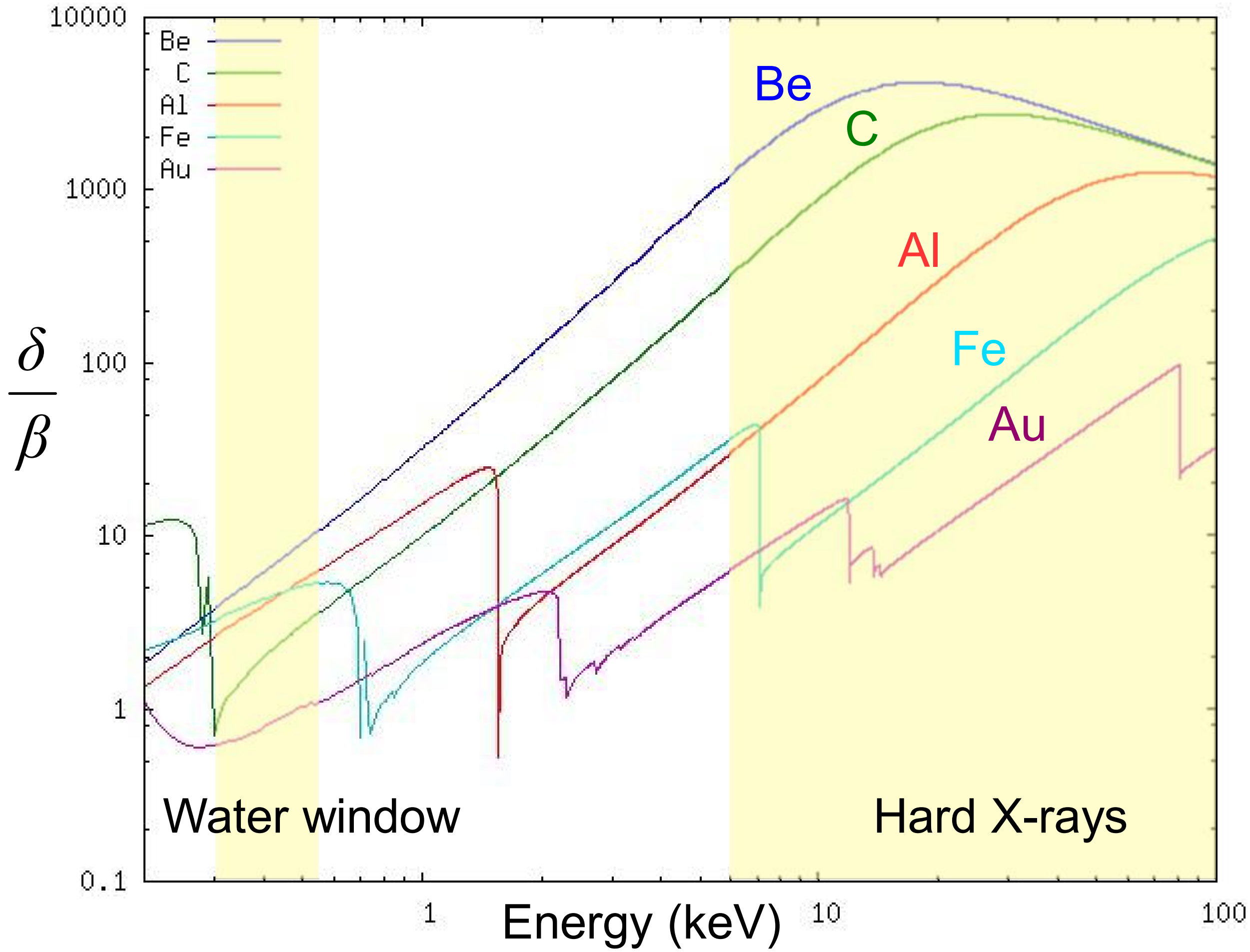

Gain of up to a few 1000 !

'Subtraction' of images around a K-edge:

→ coronary angiography

→ brain permeability

→ lung ventilation, …

→ Concentration maps of I, Gd, …

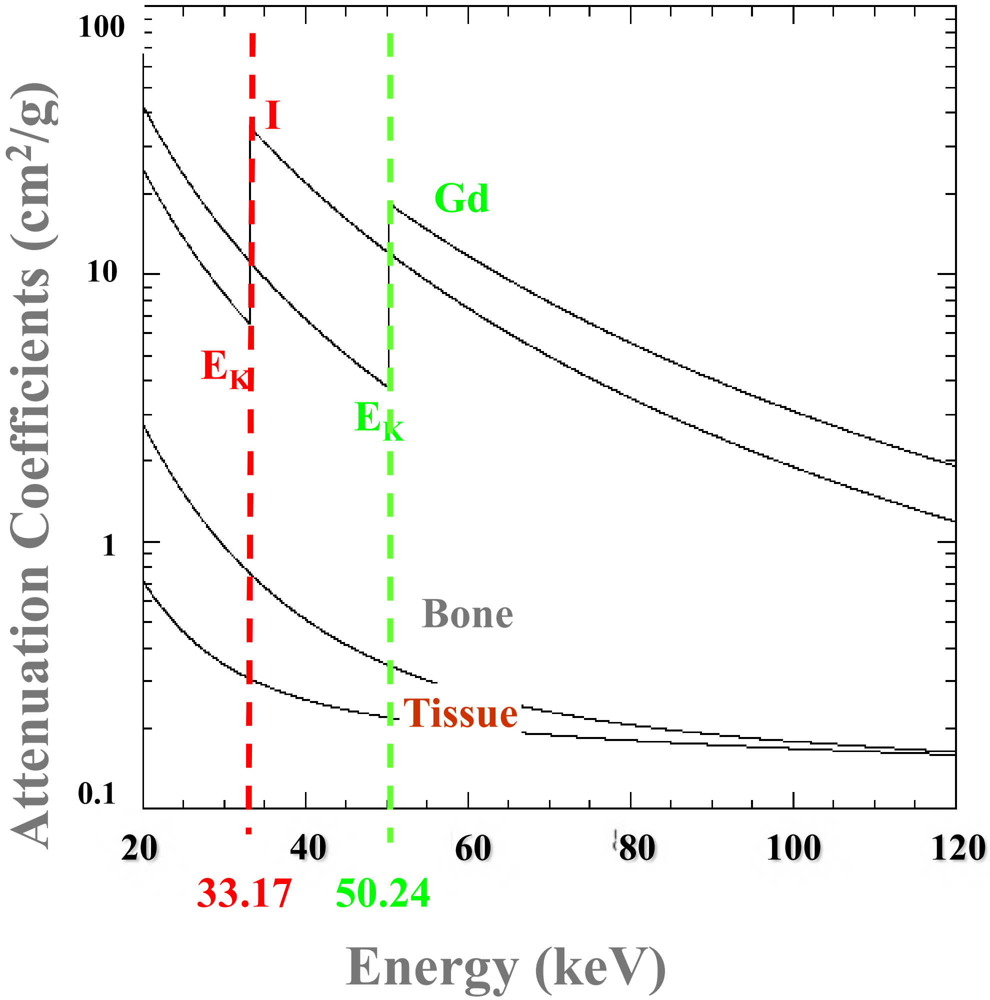

ABSORPTION: K-EDGE SUBTRACTION IMAGING

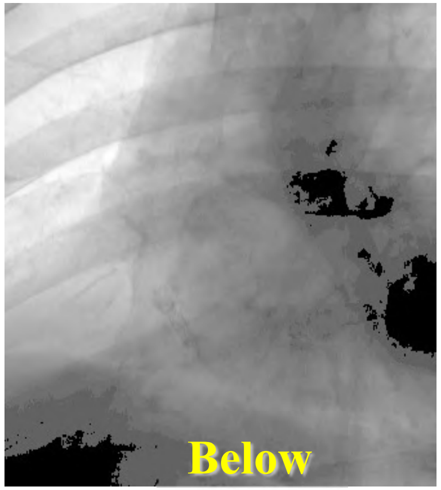

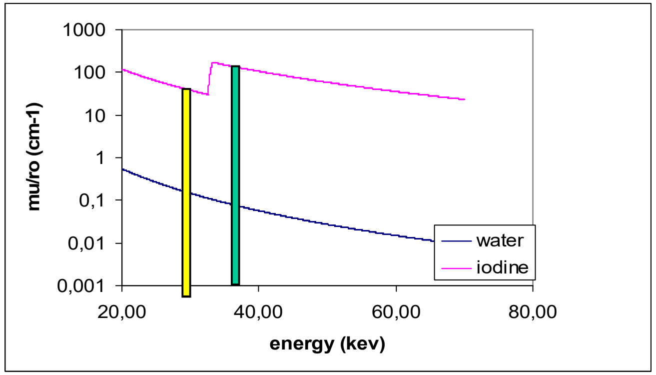

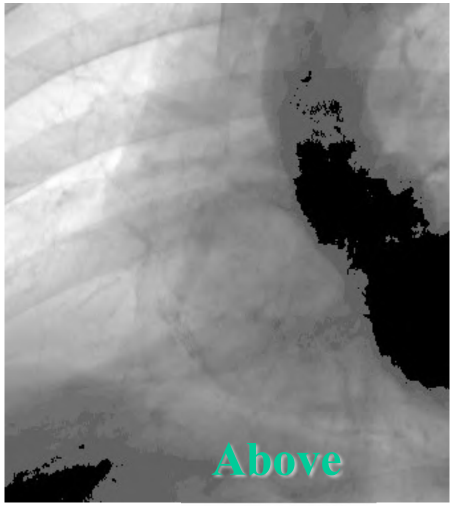

subtraction of images recorded above and below the "absorption edge" of iodine

K-edge subtracted image:

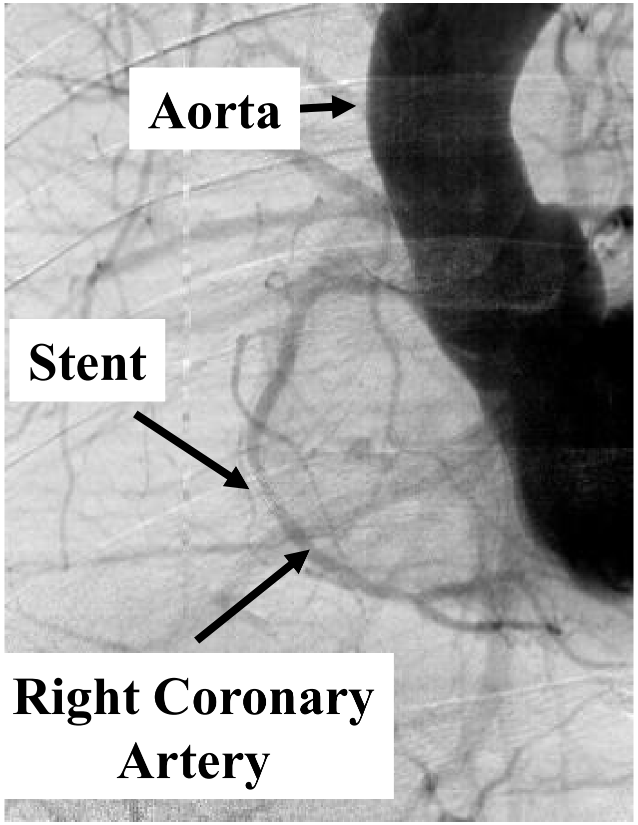

Tissues display nearly the same absorption

→ Iodine is seen

Elleaume, Estève et al.

TRANSMISSION THROUGH A SAMPLE

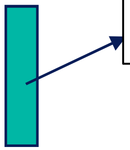

refractive index $n = 1 - \delta + i\beta$

Δz

$$e^{ik_{medium}\Delta z} = e^{i\frac{2\pi}{\lambda} n \Delta z} = e^{i\frac{2\pi}{\lambda}\Delta z} . e^{-i\frac{2\pi}{\lambda}\delta\Delta z} . e^{\frac{-2\pi}{\lambda}\beta\Delta z}$$

Transmission function

projection of the refractive index distribution

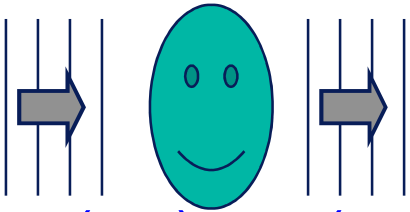

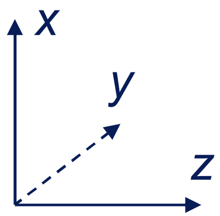

$u_{inc}(x,y)$ $u_0(x,y) = T(x,y).\, u_{inc}(x,y)$

Amplitude $A(x,y) = e^{-B(x,y)} = e^{-\frac{2\pi}{\lambda}\int \beta(x,y,z)dz}$

$T(x,y) = A(x,y).e^{i\varphi(x,y)}$

Phase $\varphi(x,y) = -\frac{2\pi}{\lambda}\int \delta(x,y,z)dz$

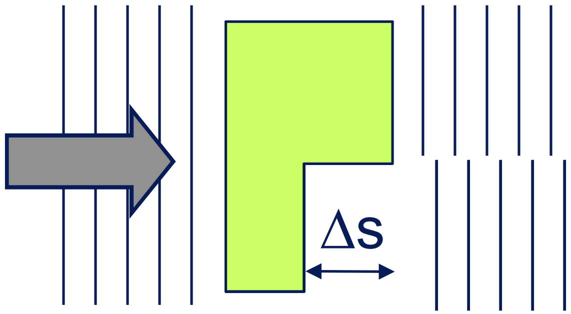

Phase Retardation

$$\Delta\varphi = -\frac{2\pi}{\lambda}\delta.\Delta s$$

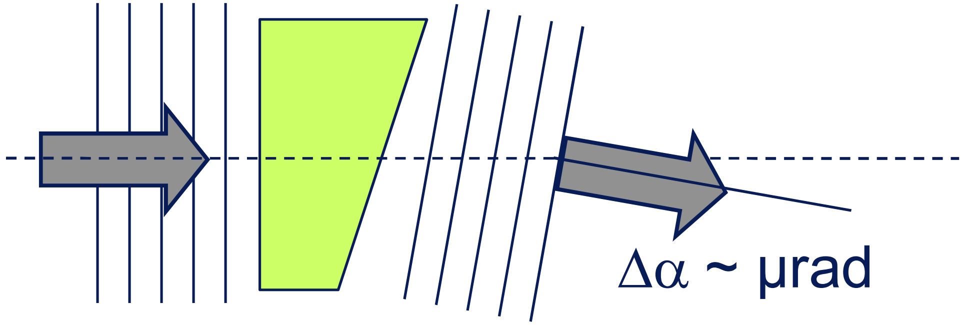

Deflection

⇔

Phase gradients

$$\Delta\alpha = -\frac{\lambda}{2\pi}\frac{\partial\varphi}{\partial x}$$

At zero distance:

Intensity $I_0 = |u_0|^2 = I_{inc}.\exp\left(-\int \mu dz\right)$

⇒ all phase information is lost

SUMMARY PHASE CONTRAST IMAGING METHODS

Interferometry φ

Differential Phase Contrast Imaging

Analyser-based PCI $\frac{\partial \varphi}{\partial x}$ + Dark-field

Grating-based PCI $\frac{\partial \varphi}{\partial x}$ + Dark-field

Speckle-based PCI $\frac{\partial \varphi}{\partial x, y}$ + Dark-field

Edge Illumination PCI $\frac{\partial \varphi}{\partial x}$

Propagation-based $\frac{\partial^2 \varphi}{\partial^2 x} + \frac{\partial^2 \varphi}{\partial^2 y}$

Speckle-based Phase Contrast Imaging

$$\frac{\partial \varphi}{\partial x, y}$$

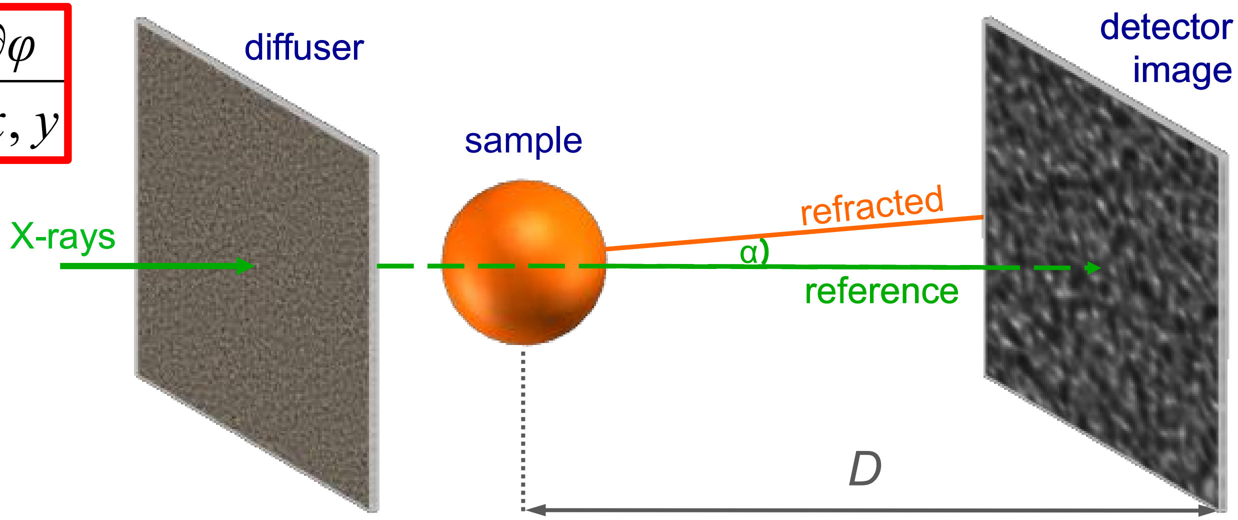

S. Berujon et al., Phys. Rev. A 86, 063813 (2012).

K. Morgan et al., Appl. Phys. Lett. 100, 124102 (2012).

refraction in sample

$$\alpha_{x,y} = \frac{1}{k}\frac{\partial \varphi}{\partial x, y} = \frac{v_{x,y}}{D}$$

displacement of speckle pattern

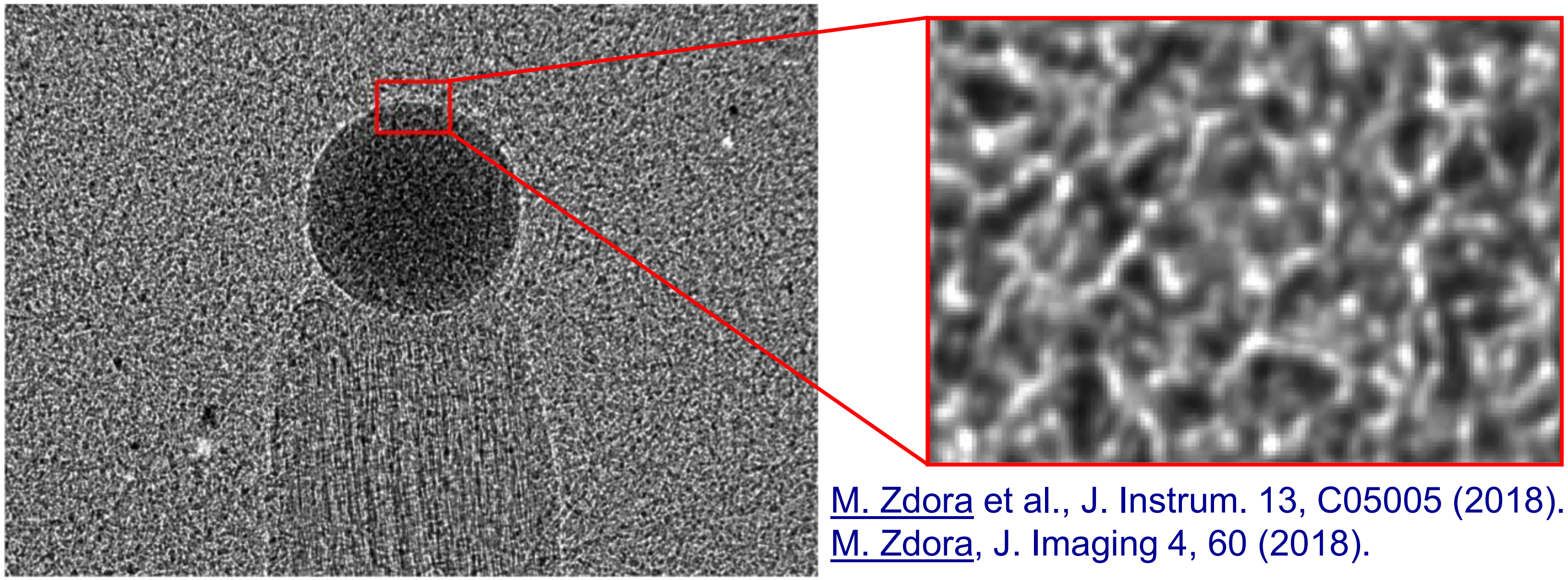

M. Zdora et al., J. Instrum. 13, C05005 (2018).
M. Zdora, J. Imaging 4, 60 (2018).

From M Zdora

Speckle-based Phase Contrast Imaging

$$\frac{\partial \varphi}{\partial x, y}$$

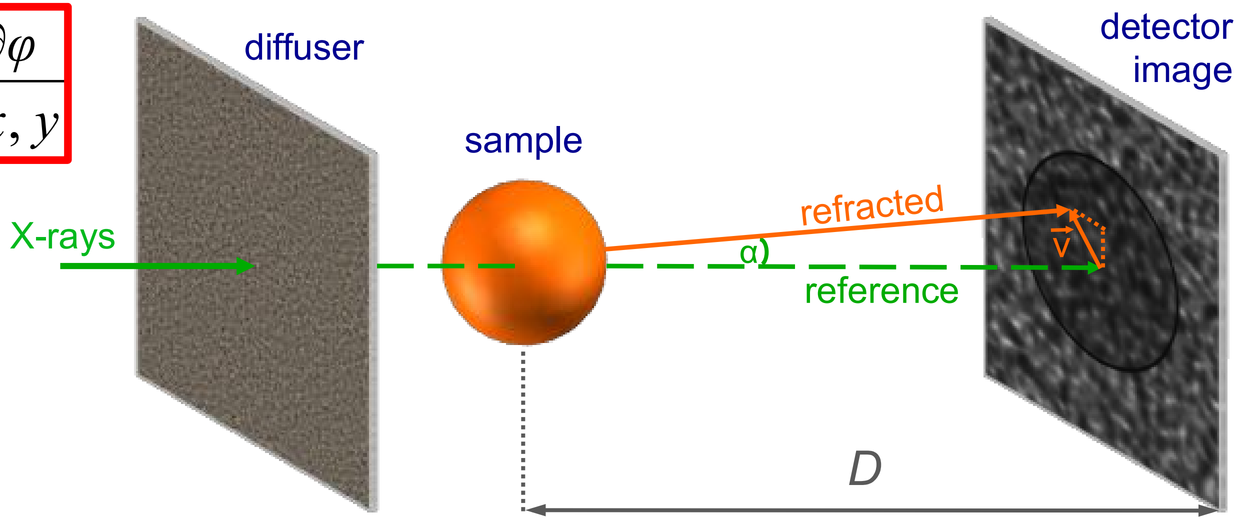

S. Berujon et al., Phys. Rev. A 86, 063813 (2012).

K. Morgan et al., Appl. Phys. Lett. 100, 124102 (2012).

$$\alpha_{x,y} = \frac{1}{k}\frac{\partial \varphi}{\partial x, y} = \frac{v_{x,y}}{D}$$

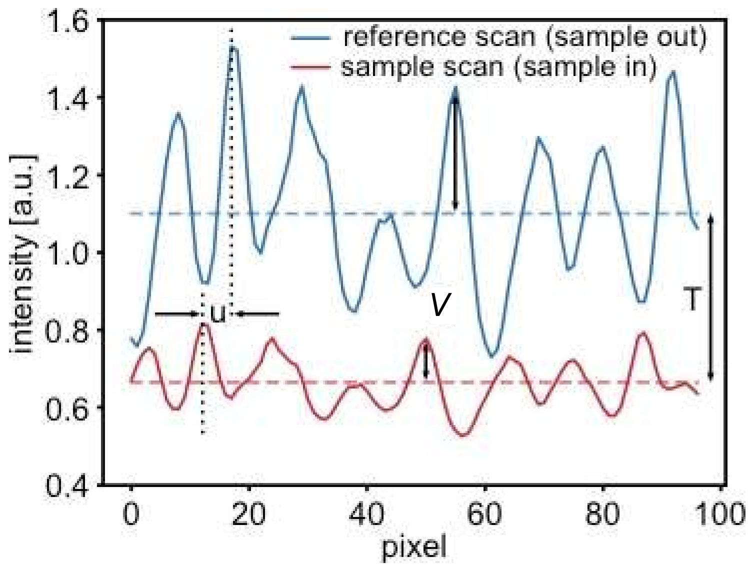

3 complementary image signals:
- Differential phase in horizontal ***and*** vertical direction
- Transmission
- Dark-field (scattering)

M. Zdora et al., J. Instrum. 13, C05005 (2018).

From M Zdora

Speckle-based Phase Contrast Imaging

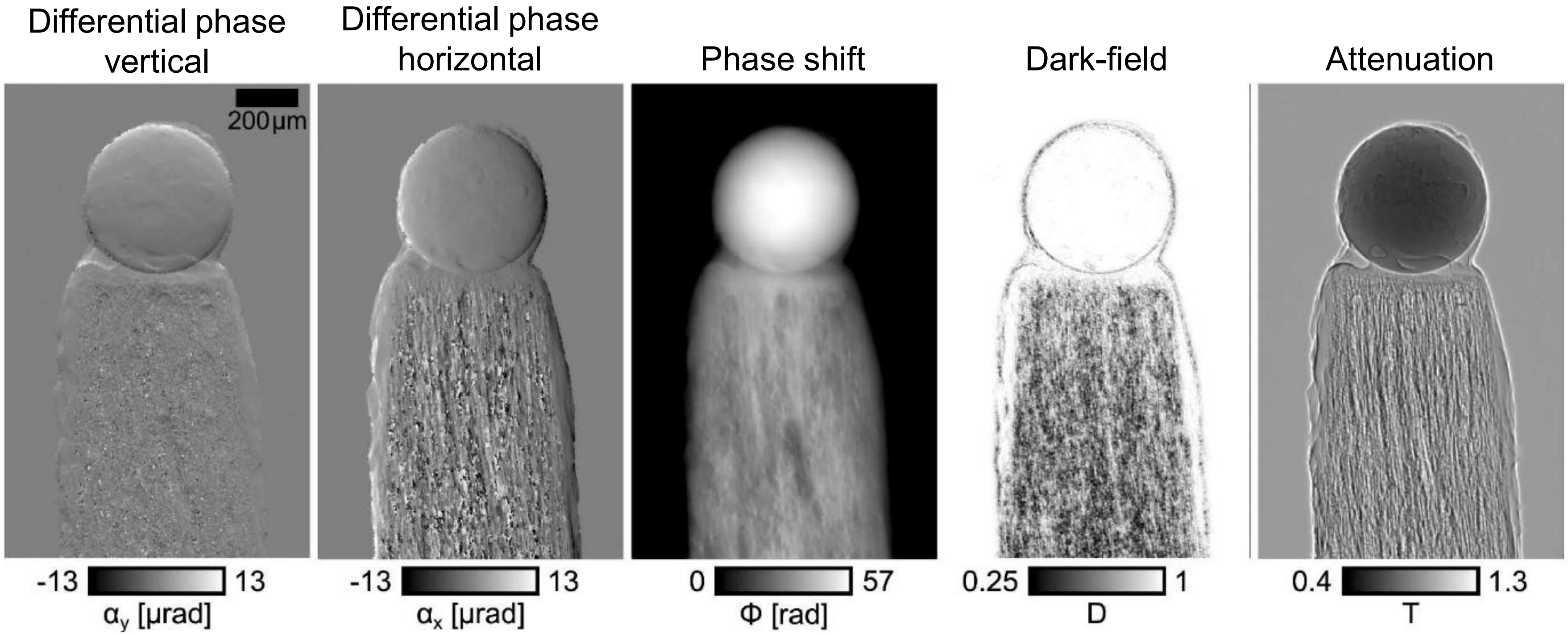

M. Zdora et al., J. Instrum. 13, C05005 (2018).
M. Zdora, J. Imaging 4, 60 (2018).

3 complementary image signals:

- Differential phase in horizontal ***and*** vertical direction
- Dark-field (scattering)
- ‘Attenuation’

From M Zdora

In-line Holography
Fresnel diffraction

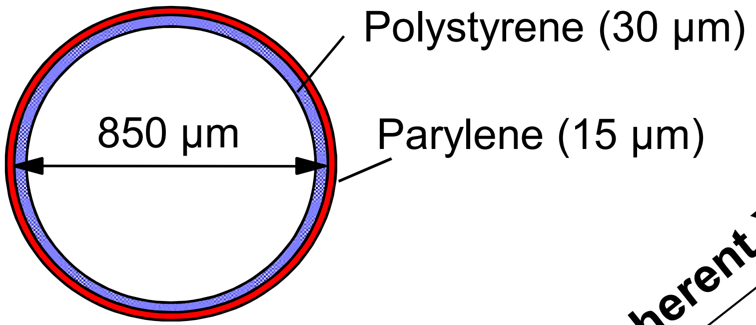

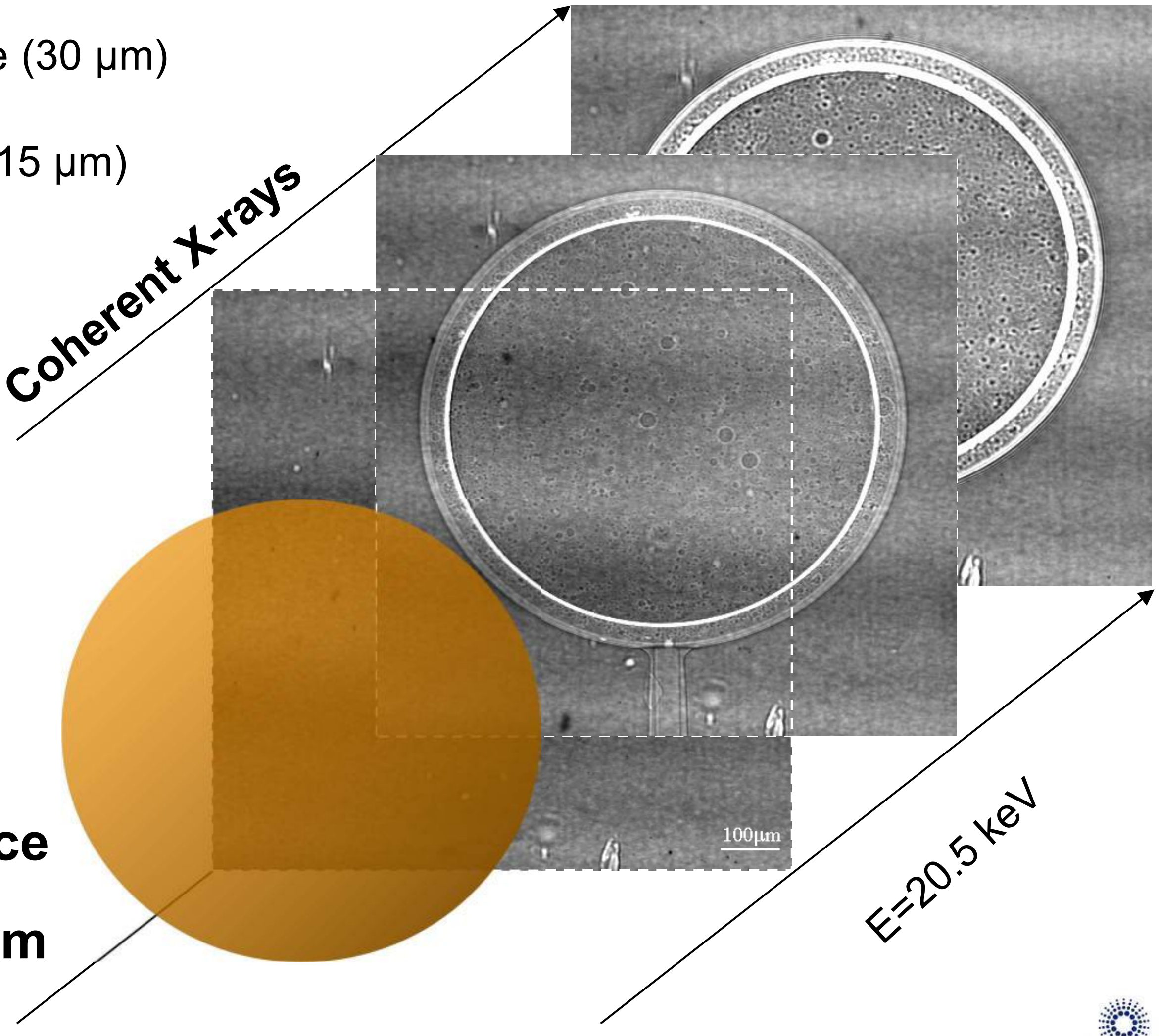

Attenuation at zero distance

Phase contrast downstream

FRESNEL DIFFRACTION IN REAL SPACE

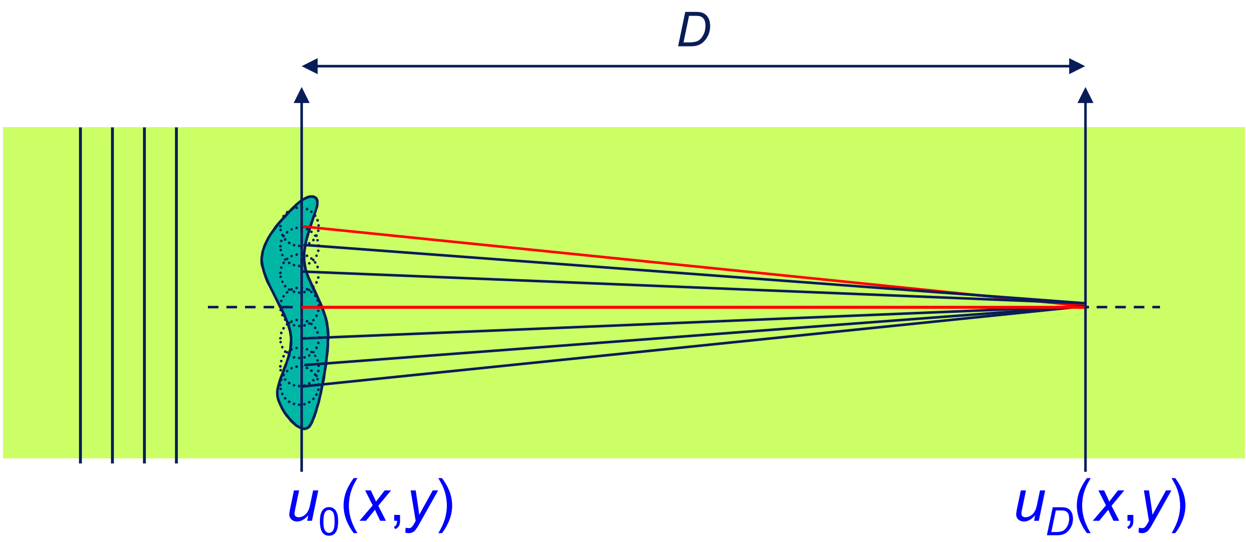

- Fresnel Integral (1D)

$$u_D(x) = \frac{1}{\sqrt{i\lambda D}} \int_{-\infty}^{+\infty} u_0(x_0) \exp\left[-i\frac{\pi}{\lambda D}(x-x_0)^2\right] dx_0$$

  - Convolution in real space
    Multiplication in reciprocal space
  - Small angles paraxial approximation

FRESNEL DIFFRACTION IN REAL SPACE

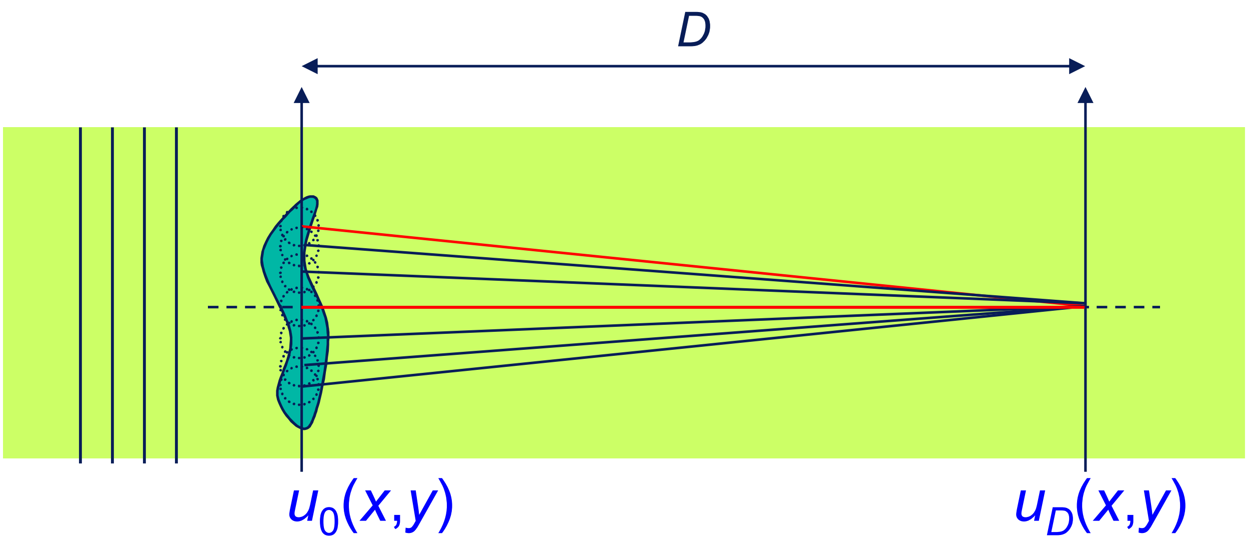

- *In principle*: complete object contributes to a point of the image
  In practice: only finite region: first Fresnel zone

radius $r_F = \sqrt{\lambda D}$

- First Fresnel zone determines the sensed lengthscale
  Distance to be most sensitive to object with size a $D_{opt} = \dfrac{a^2}{2\lambda}$

For example at λ = 0.5Å (25 keV)

a = 1 μm ⇒ D = 10 mm

a = 40 μm ⇒ D = 16 m

- Fresnel Integral becomes Fourier Transform if $\sqrt{\lambda D} \gg \text{object size}$

IMAGING REGIMES WITH COHERENT X-RAYS

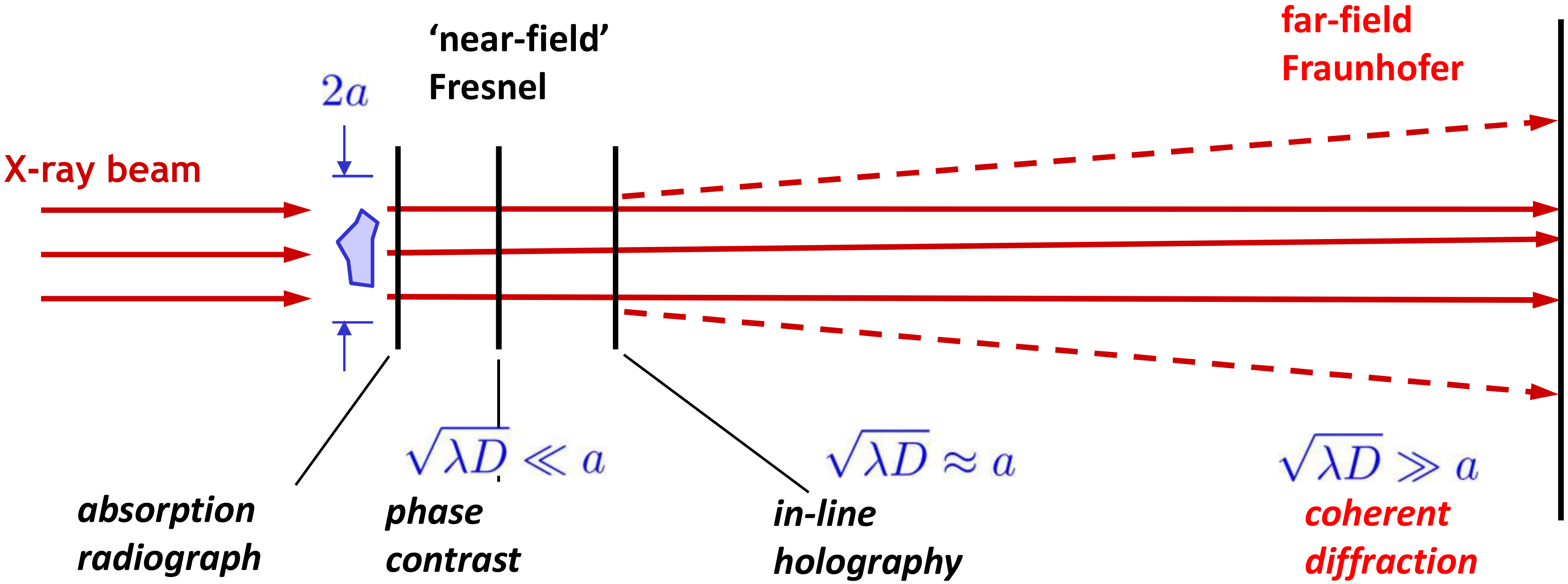

Kagoshima (1999)

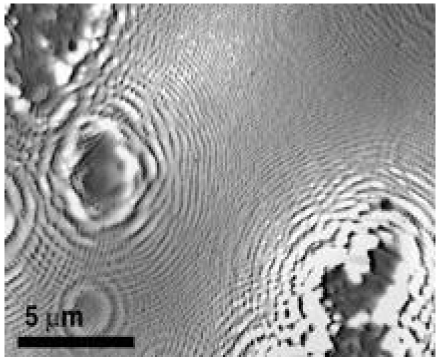

Jacobsen (1990)

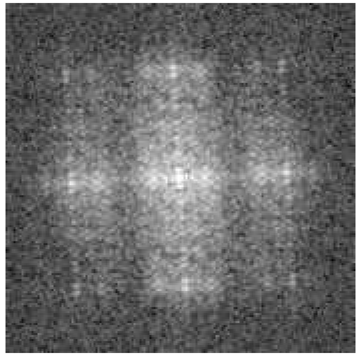

Miao (1999)

Courtesy Prof. Oleg Shpyrko (UCSD)

Fresnel number $F = \frac{a^2}{\lambda D}$

SINGLE-BUNCH PHASE CONTRAST IMAGING

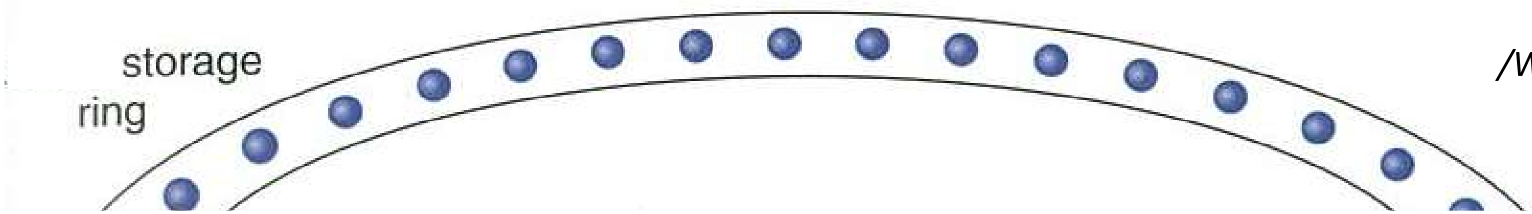

/Willmott, 2011/

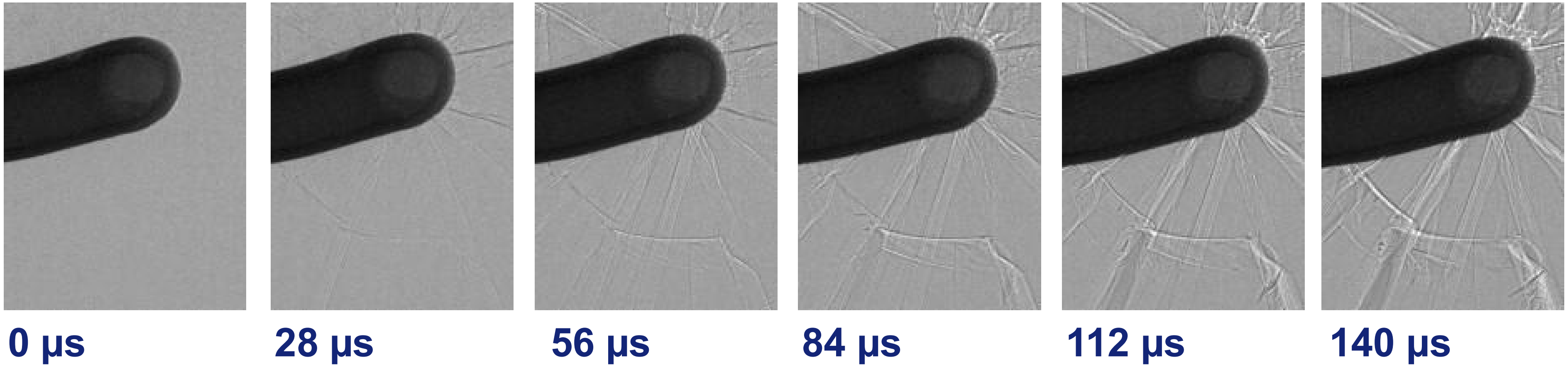

single bunch:

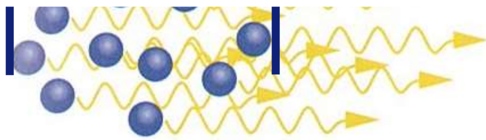

- revolution 2.8 µs
- 4 bunches = 1.4 MHz frame rate
- Approx. 160 ps flash exposure

Rack, Scheel, Reichert et al., J Synch Rad 21, no. 4 (2014)

GAS-GUN FACILITY AT ID19

**in collaboration with D. Eakins, D.Chapman (University of Oxford, UK)*

- **Aims at visualizing microscopic processes**
  - internal damage
  - cracking and spall,
  - twinning and evolving microstructures
  - shocked induced phase transitions
  - growth instabilities
  - void collapse and densification of porous system
- **Example**
  - ❖**cavity collapse dynamics**

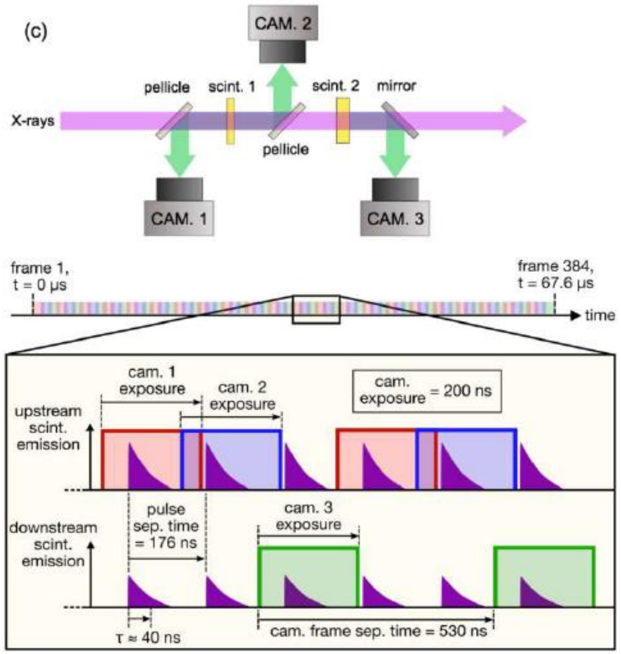

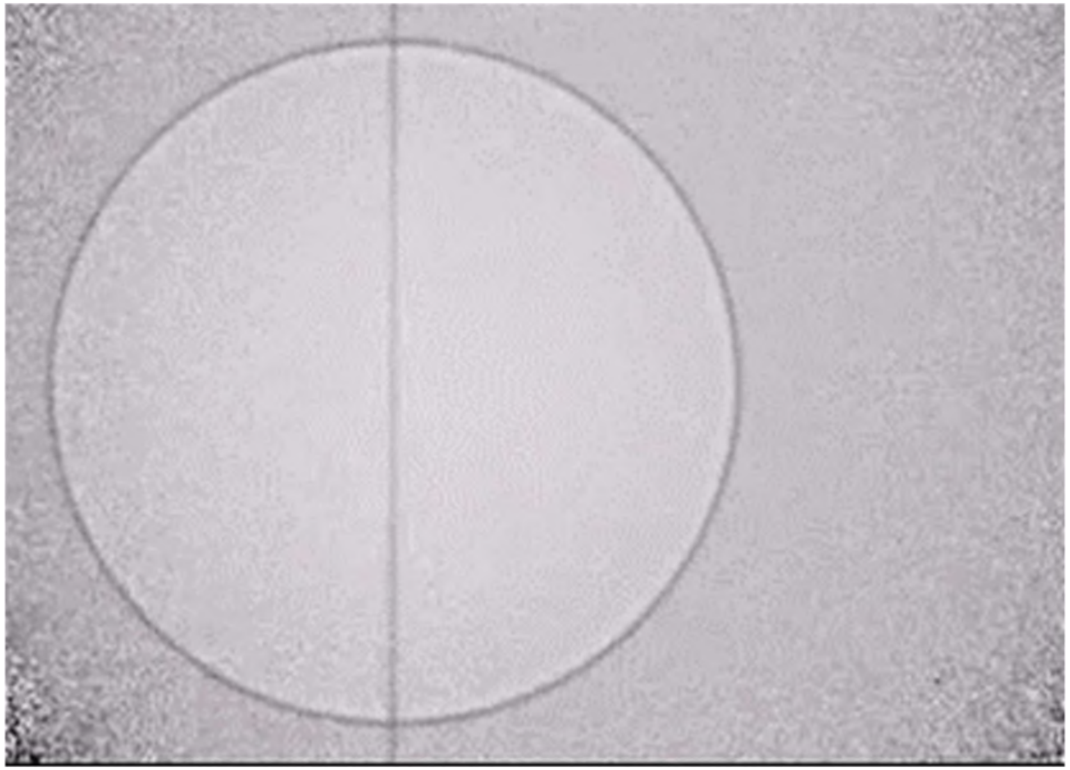

• (2) 3 inter-laced HPV-X2 for (pseudo) 5.6 MFPS

M Olbinado, A Rack

Image(s) $\Rightarrow$ Object ???
Inverse Problem

Linearization with respect to defocus D

Australian School: K. Nugent, T. Gureyev, D. Paganin

TIE (transport of intensity)

$$\frac{\partial I}{\partial z} = -\frac{\lambda}{2\pi}\nabla\left(I\nabla\varphi\right)$$

CTF

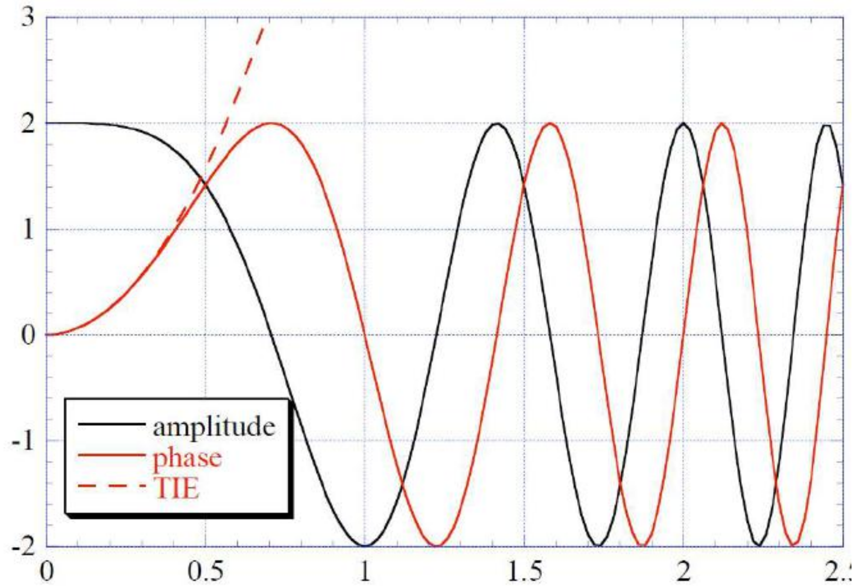

Linearization with respect to object

Flemish School: D. Van Dyck, P. Cloetens, JP Guigay

Transfer Function Approach / Focus variation

Schiske, P. (1968). Zur Frage der Bildrekonstruktion durch Fokusreihen.

Combined in 'Mixed Approach'

JP Guigay, M Langer, R Boistel, P Cloetens, Opt. Lett., 32, 1617 (2007)

PAGANIN APPROACH (TIE VARIANT)

- Single distance reconstruction for **homogeneous objects**
  Valid for **short distance**, **arbitrary absorption (!)** and **constant** δ/β
  Paganin, D. et al, J. Microsc., 206, 33-40 (2002).
- Pro's:
  - Single distance
  - Most correct of simple approaches (arbitrary absorption)
  - Robust: homogeneity assumption has regularizing effect
- Contra's:
  - Weak distance, weak contrast → contrast is not optimized
  - Not adapted to very inhomogeneous objects
  - Low-pass filter → resolution is deteriorated

$$resolution \approx \sqrt{\lambda D}$$

$$\int \mu dz = -\ln\left(FT^{-1}\left\{ \frac{FT(I_D)}{\pi\lambda D f^2 \frac{\delta}{\beta} + 1} \right\} \right)$$

BM18: HIERARCHICAL PHASE-CONTRAST TOMOGRAPHY

Main techniques:
- Hierarchical tomography
- Propagation phase-contrast imaging

Main beamline specifications:
- *Energy range:**80-240** keV (**25-280** in the future)*
- *220m long beamline, up to 36m for propagation phase-contrast*
- *Current sample size **0.5m and 30 kg***
- *Future sample size up to **2.5m and 300** kg*
- *High automation level for high throughput **(regular improvements)***

EBS and refurbishment improvements:
- *Smallest possible X-ray source of the EBS*
- *Beam of 35cm with highest coherence worldwide for high-energy X-ray imaging*
- *Large pixel range (0.85 - 120 um)*

45m long experimental hutch with large polychromatic beam at high energy

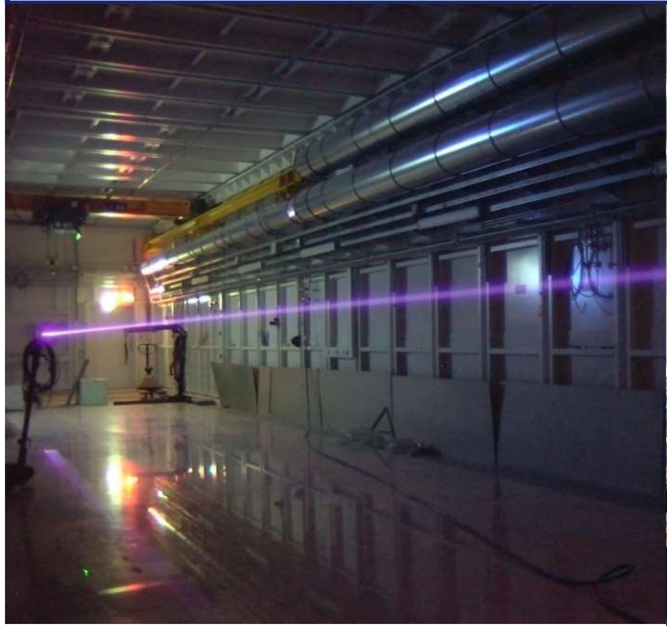

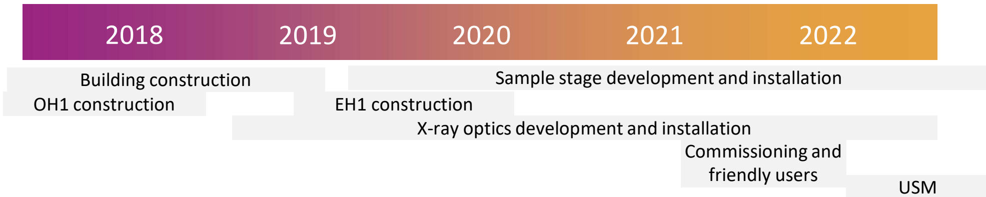

STREAMLINE

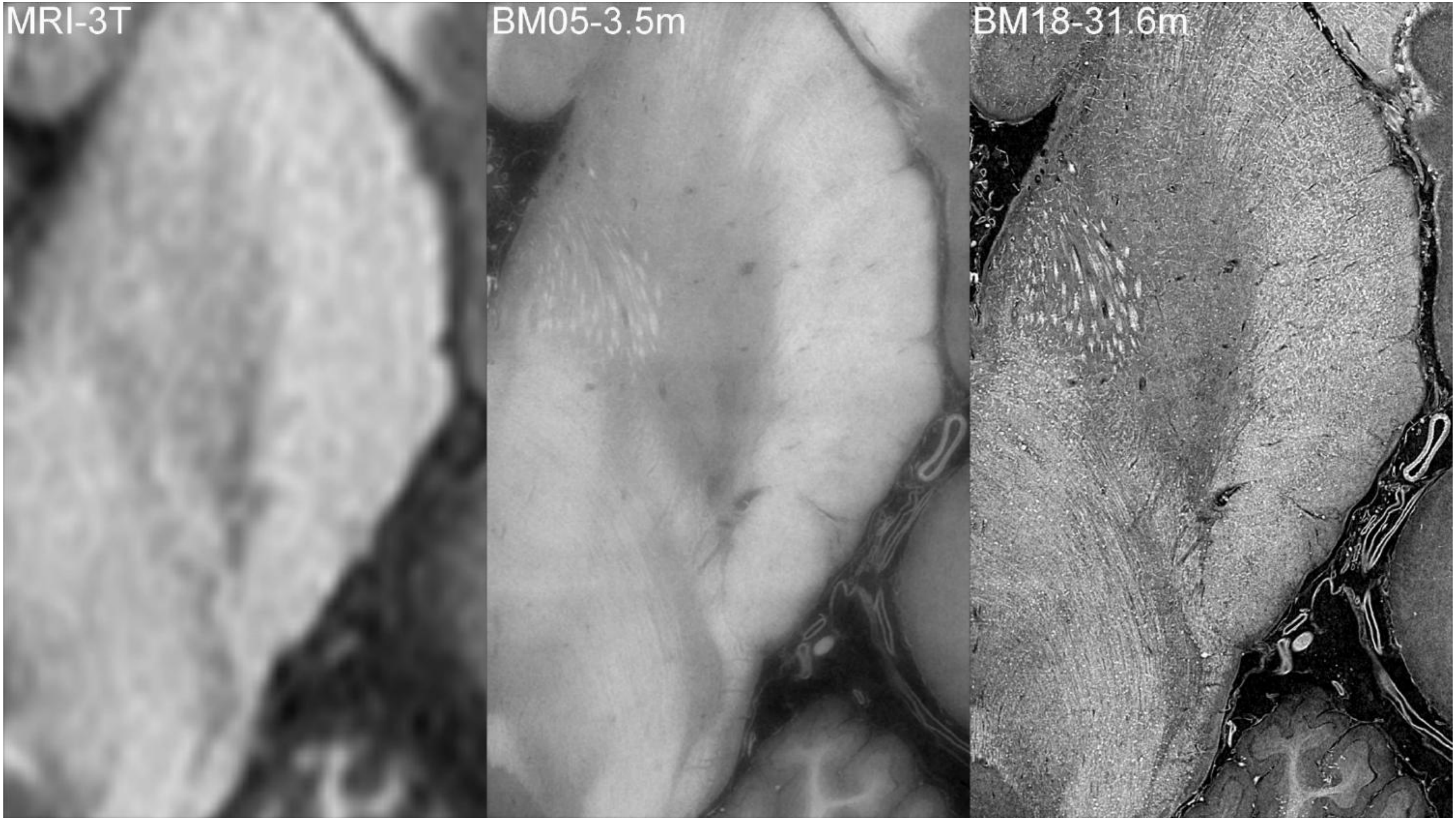
MRI-3T
BM05-3.5m
BM18-31.6m

- **Fourier Transforms of the intensity and phase are linearly related**

$$I_D(\boldsymbol{f}) = \delta_{Dirac}(\boldsymbol{f}) - 2\underbrace{\cos(\pi\lambda D\boldsymbol{f}^2)}_{\text{amplitude contrast factor}} \cdot B(\boldsymbol{f}) + 2\underbrace{\sin(\pi\lambda D\boldsymbol{f}^2)}_{\text{phase contrast factor}} \cdot \varphi(\boldsymbol{f})$$

valid in case of a slowly varying phase, weak absorption

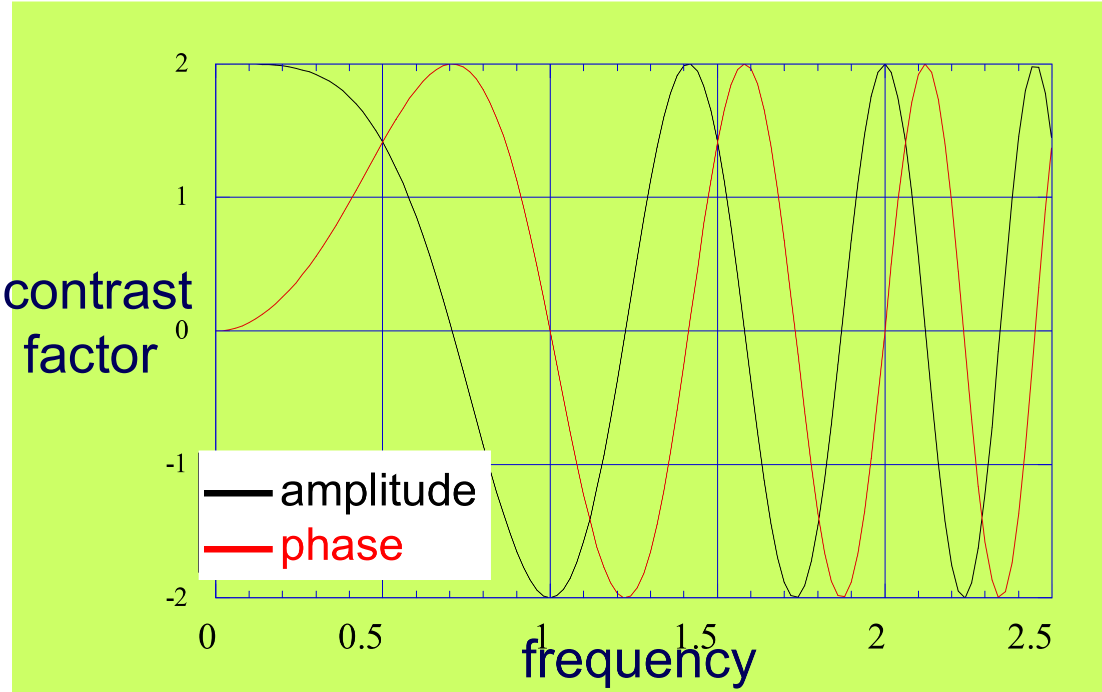

CONTRAST TRANSFER FUNCTIONS

Decreasing linewidth
Increasing spatial frequency

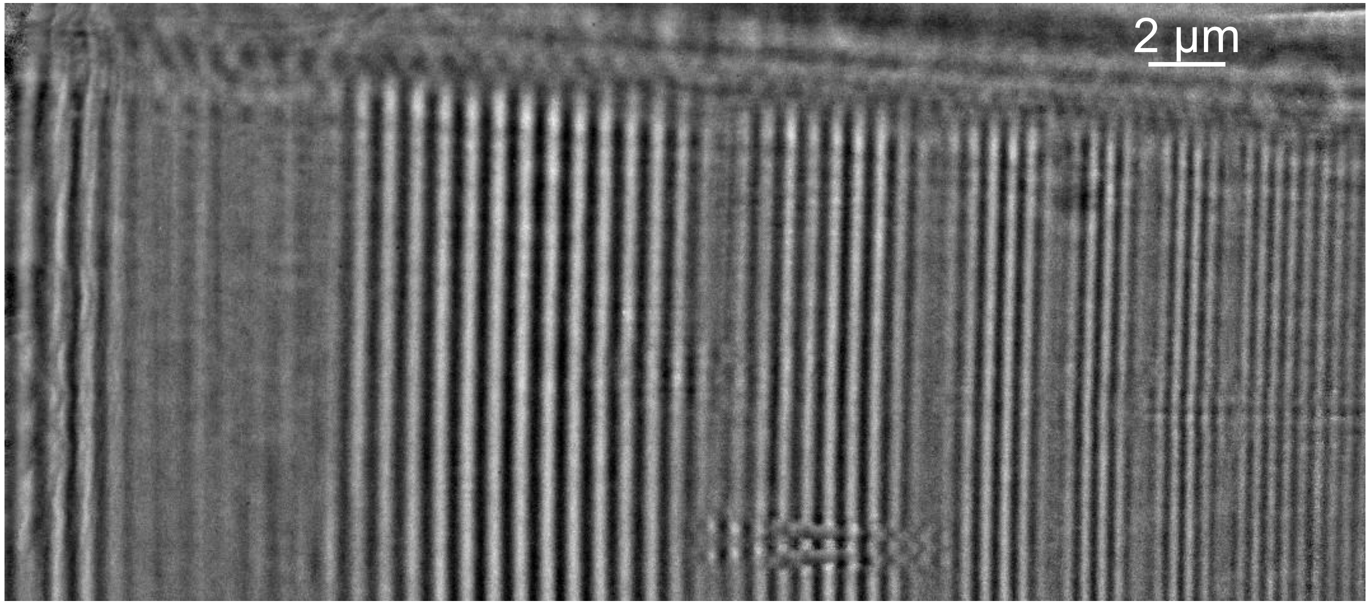

period ≈ 720 nm

period ≈ 530 nm

period ≈ 610 nm

Object invisible !

Contrast depends strongly on period or spatial frequency

HOLO-TOMOGRAPHY

1) phase retrieval with images at different distances

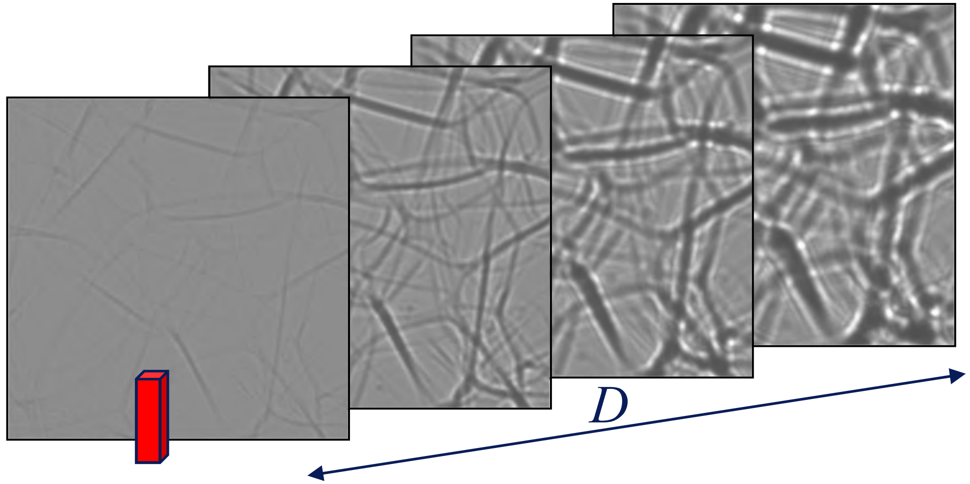

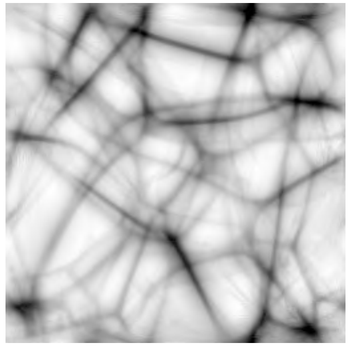

Phase map

2) tomography: repeated for ~ 1000 angular positions

3D distribution of δ or the electron-density
improved resolution
straightforward interpretation
processing

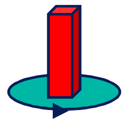

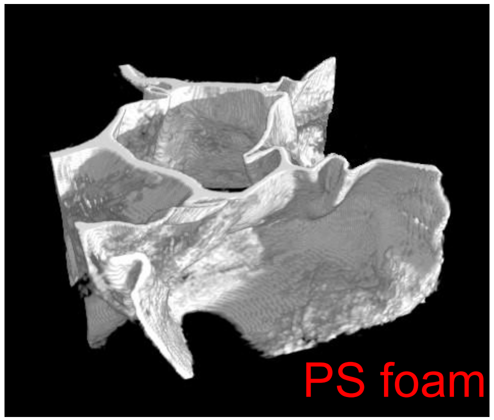

P.Cloetens et al., Appl. Phys. Lett. 75, 2912 (1999)
JP Guigay, M Langer, R Boistel, P Cloetens, Opt. Lett., 32, 1617 (2007)
M. Langer, P Cloetens, A Pacureanu, F Peyrin, Opt. Lett., 37, 2151 (2012)

ABSORPTION VS. PHASE: AL/SI SEMI-SOLID ALLOY

Absorption

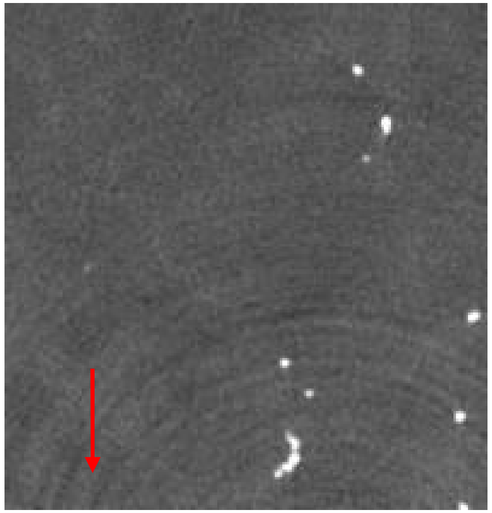

β-map

Phase contrast

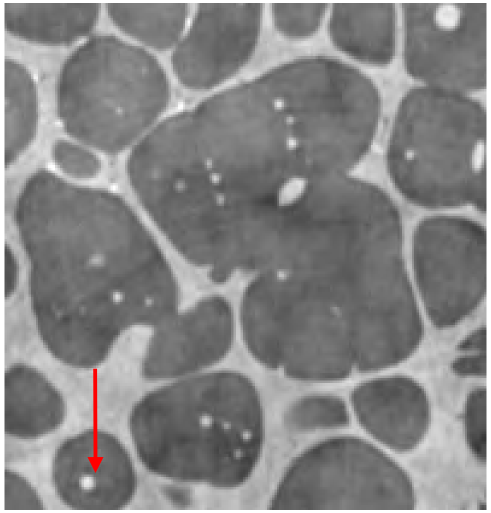

δ-map

E = 18 keV

50 µm

ρ_{Al}~2.7g/cm³

$$\frac{\Delta\rho}{\rho} \approx 2\%$$

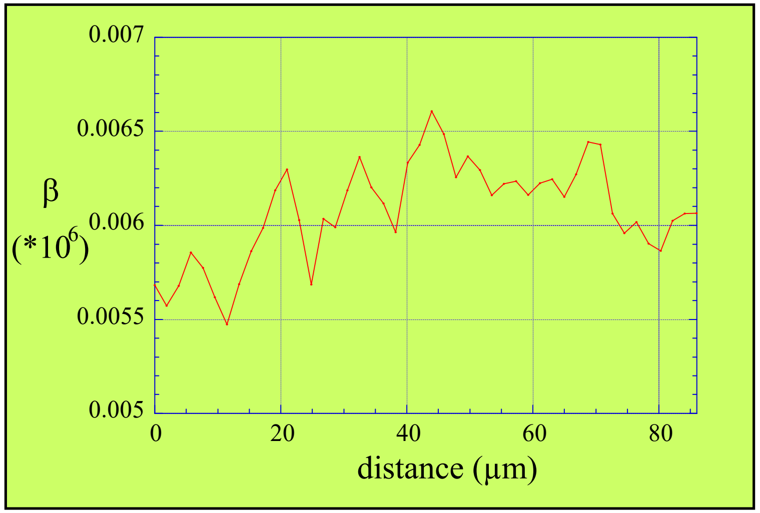

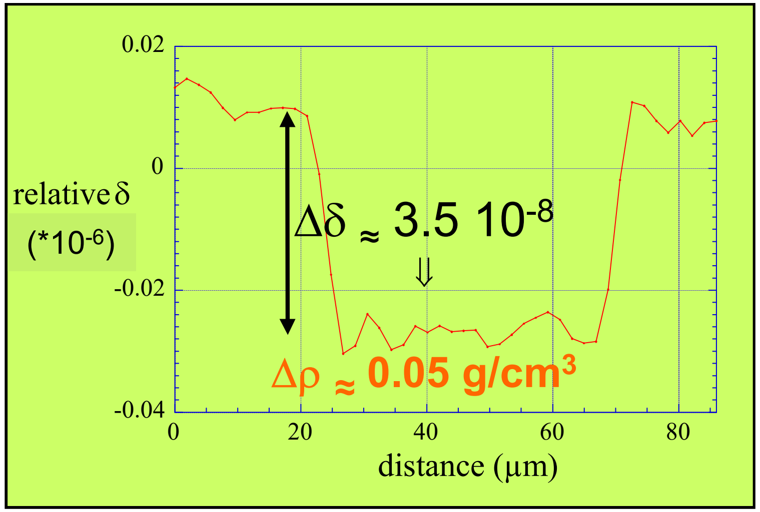

L Salvo, P Cloetens, et al., NIM B, 200 (2003) 273

GENERALIZED TOMOGRAPHY

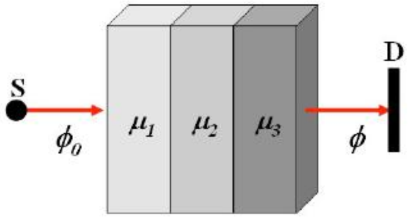

X-ray Absorption & Phase Contrast

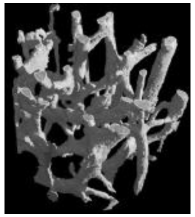

3D morphology

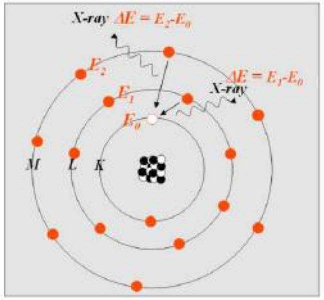

Golosio et al, APL

X-ray Fluorescence

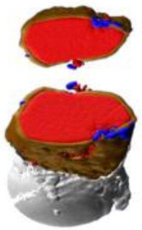

3D element distribution

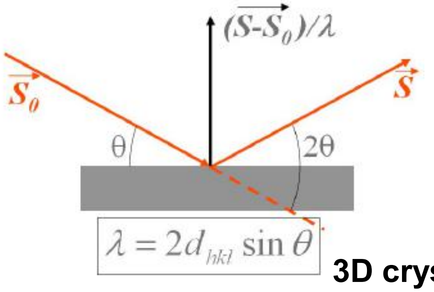

X-ray Diffraction

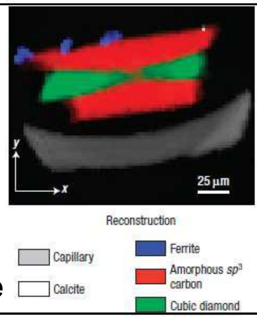

3D crystal phases and much more

Courtesy of P. Bleuet

Back to 1st generation scanner!

Pixel- by-pixel acquisition

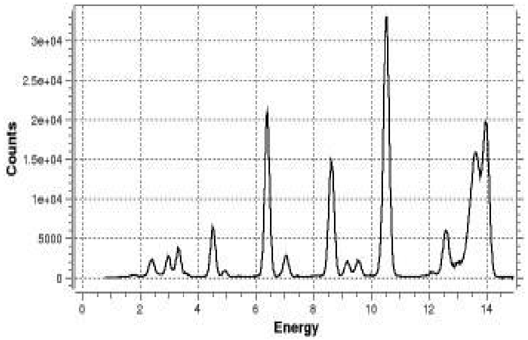

2D-Slice or 3D-Volume

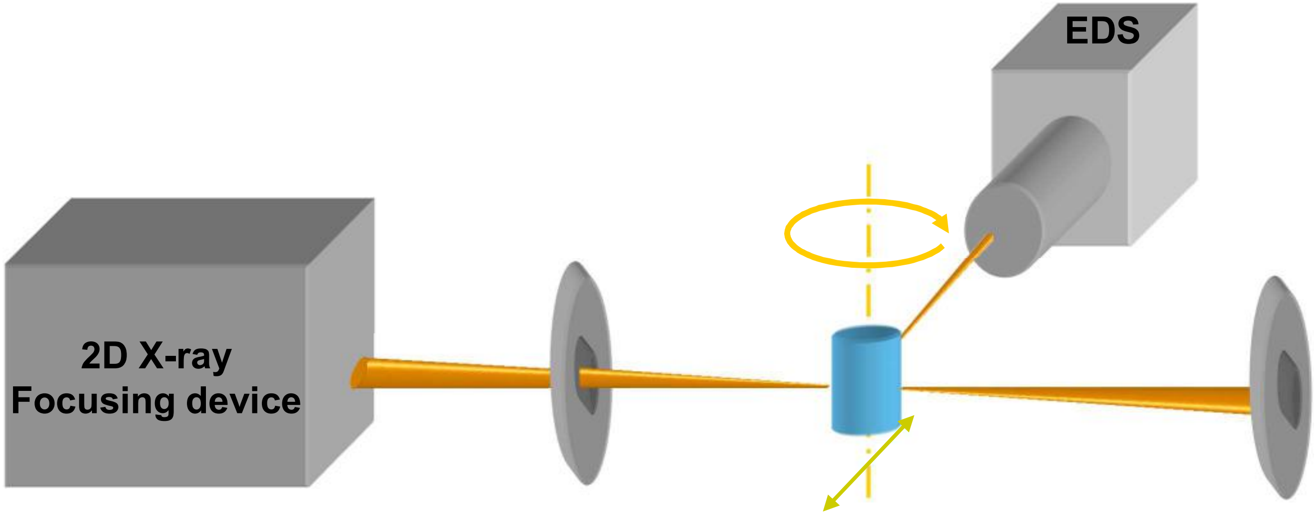

Self-absorption of fluorescence is major problem

3D rendering of a fly ash

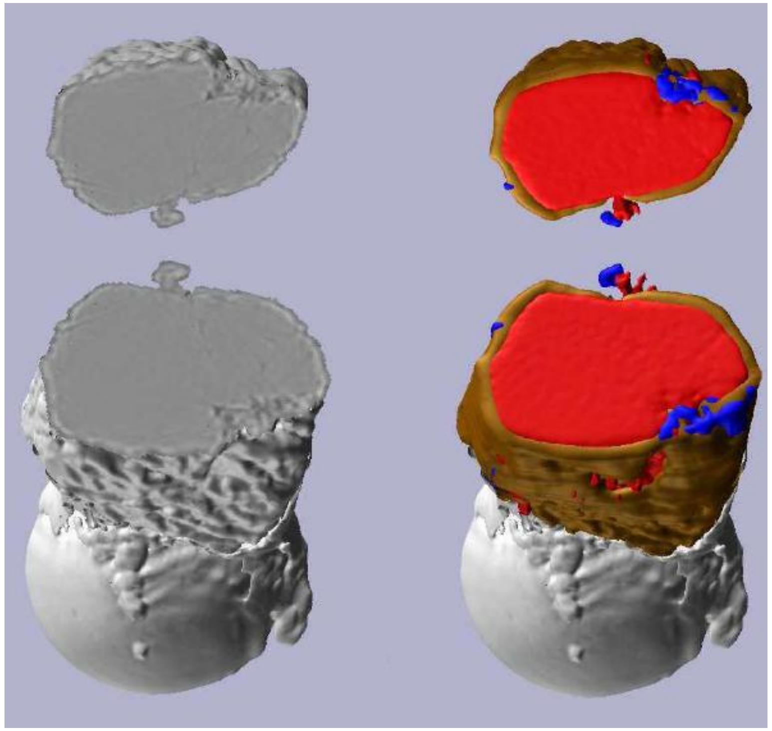

3D rendering, fly ash particle

Left :
Transmission tomography

Right :
Distributions of
Rubidium
Manganese
Iron

.

Voxel size 3×3×3 μm^3.

B. Golosio, et al., *J. Appl. Phys.* **94**, 145-156 (2003) and *Appl. Physics Letters*, (2004)

X-RAY (POWDER) DIFFRACTION TOMOGRAPHY

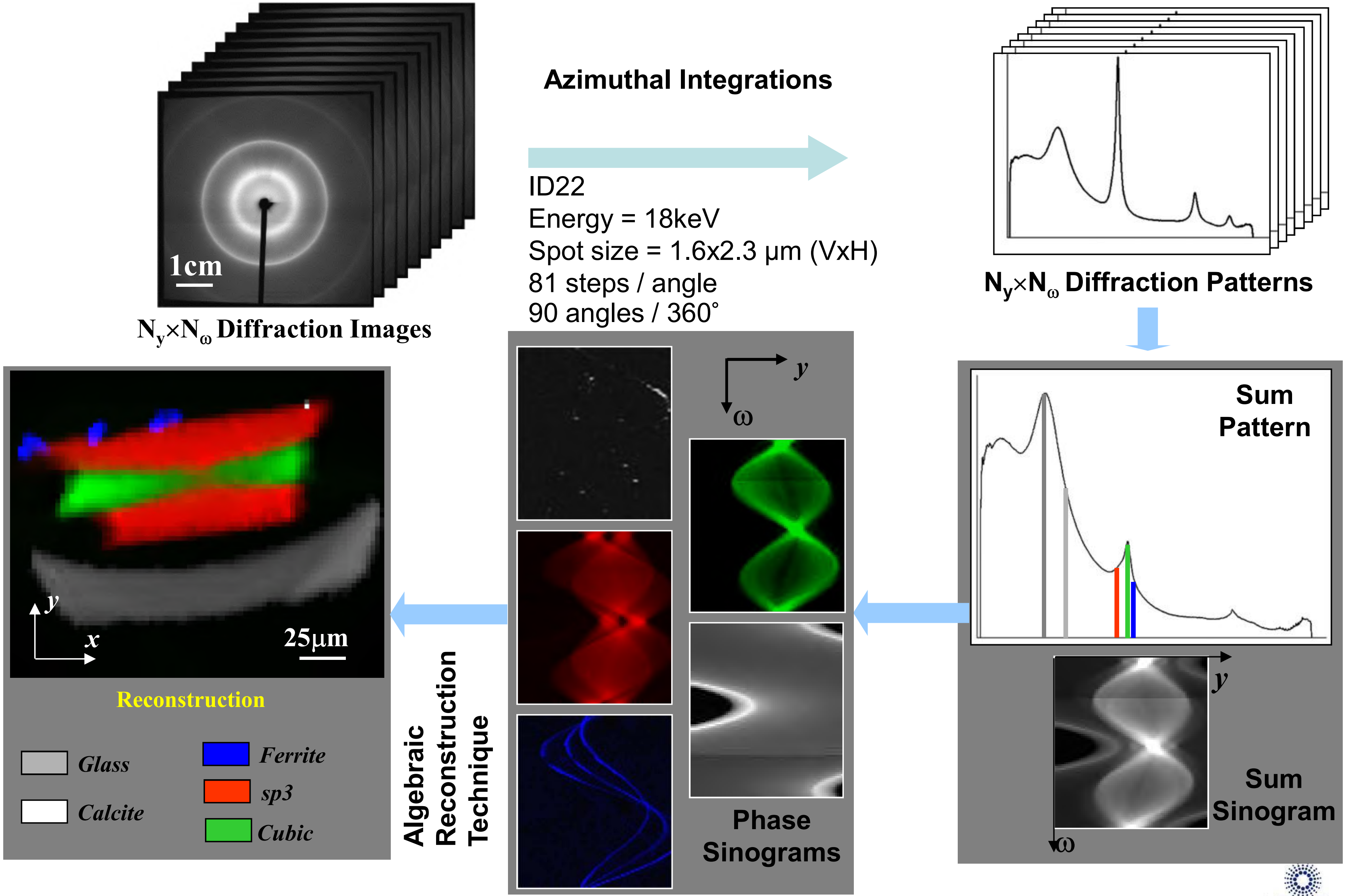

P. Bleuet, et al. *Nature Mater* **7,** 468–472 (2008).

OPERANDO CATALYSIS ON ID15A

Chemical evolution of a catalyst under working conditions

Phases distribution maps in a catalyst

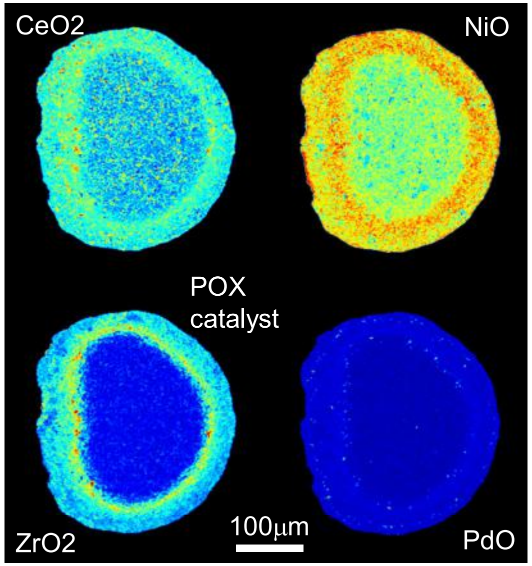

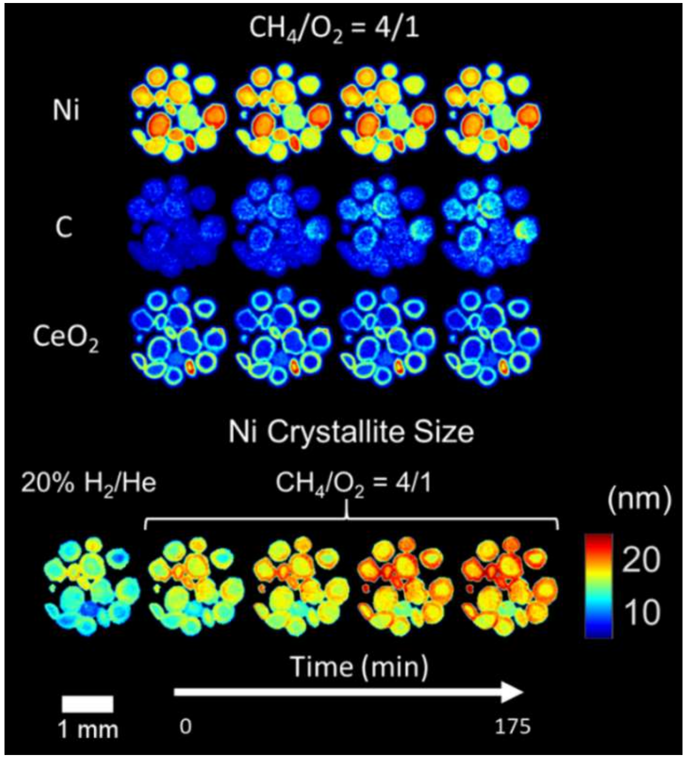

5D operando tomographic diffraction imaging of a catalyst bed
A. Vamvakeros, M. Di Michiel, et al. Nature Communications **9**, 4751 (2018)

PAUL SCHERRER INSTITUT PSI

Scanning SAXS in 3D: A 6D reconstruction

SAXS tensor tomography

Reconstructing 3D real space and 3D reciprocal space

measurements around two axis needed

Marianne Liebi
Now at MAX IV

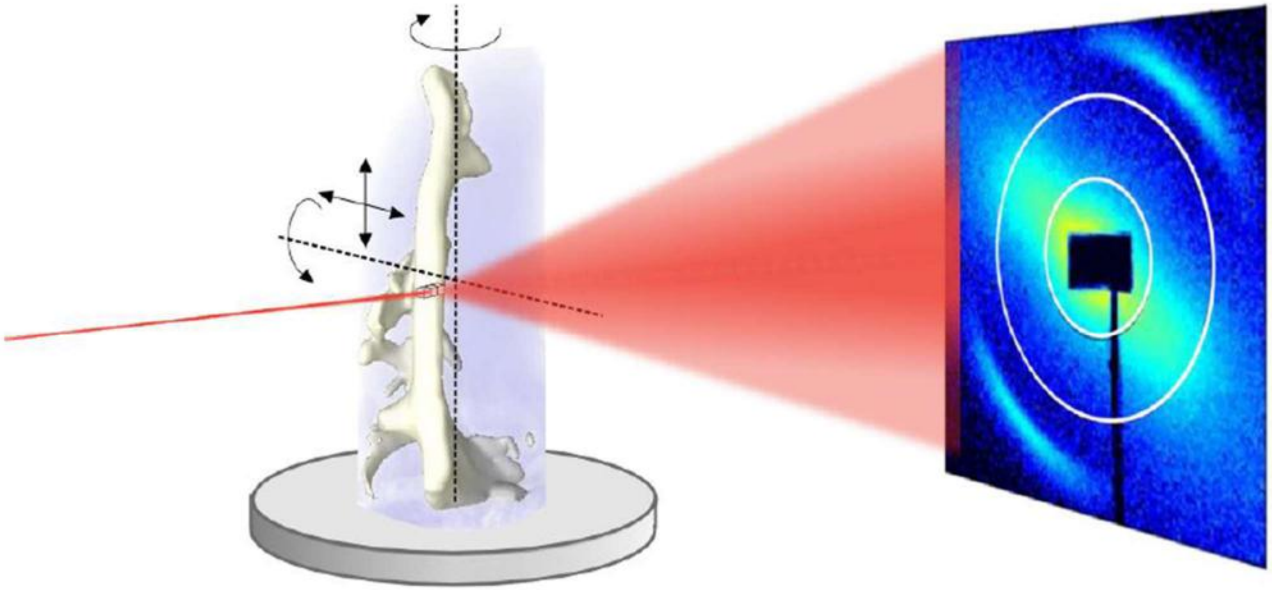

Liebi, M. *et al.* “Nanostructure surveys on macroscopic specimens by small-angle scattering tensor tomography,” Nature **527**, 349 (2015)

PAUL SCHERRER INSTITUT PSI

Scanning SAXS in 3D: A 6D reconstruction

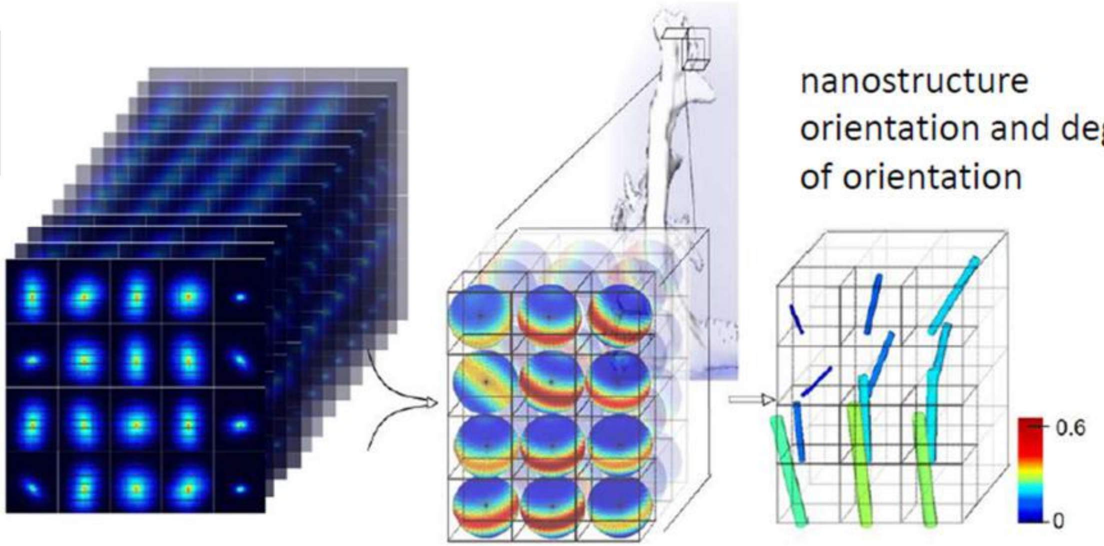

nanostructure orientation and degree of orientation

3D reciprocal space map in each voxel modeled with spherical harmonics

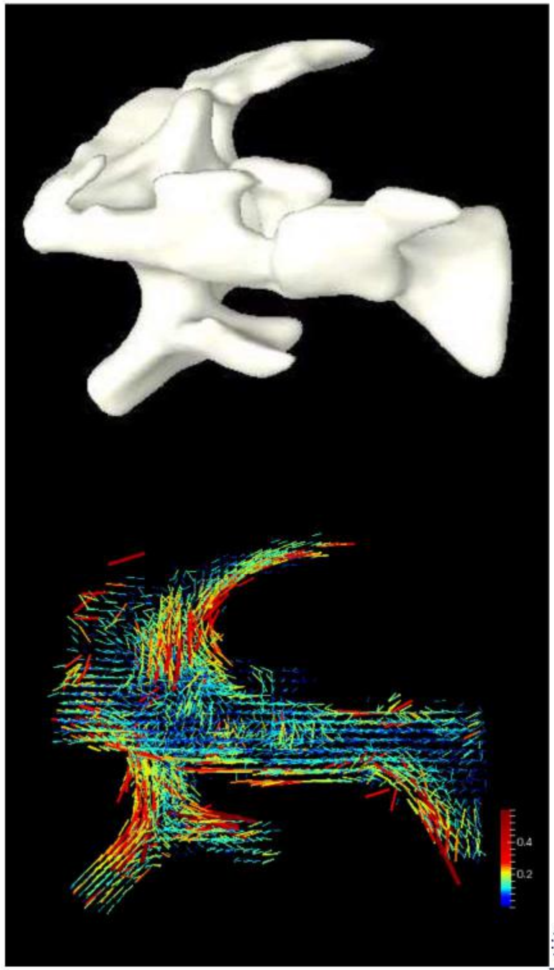

Liebi, M. *et al.* "Nanostructure surveys on macroscopic specimens by small-angle scattering tensor tomography," Nature **527**, 349 (2015)

ESRF

Parallel beam imaging:
Absorption + Phase + Bragg
Dose (in)efficient, ultra fast
Resolution limited by *detector*

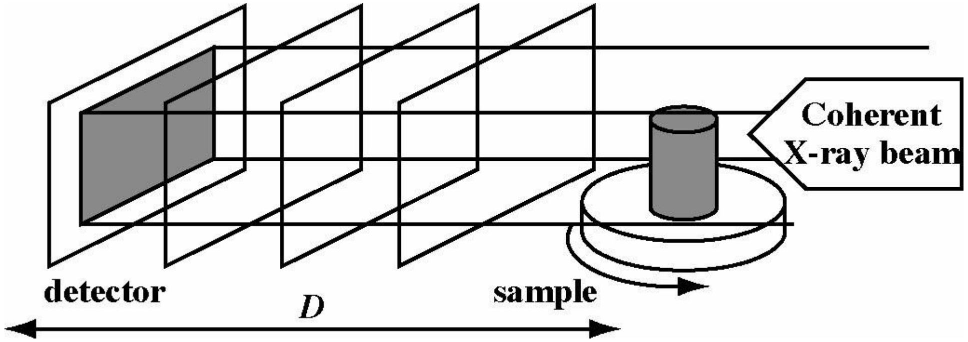

Full-field microscopy:
Absorption + Phase (+ Bragg)
Dose inefficient, fast
Resolution limited by *optics*

TXM (Transmission X-ray Microscopy)

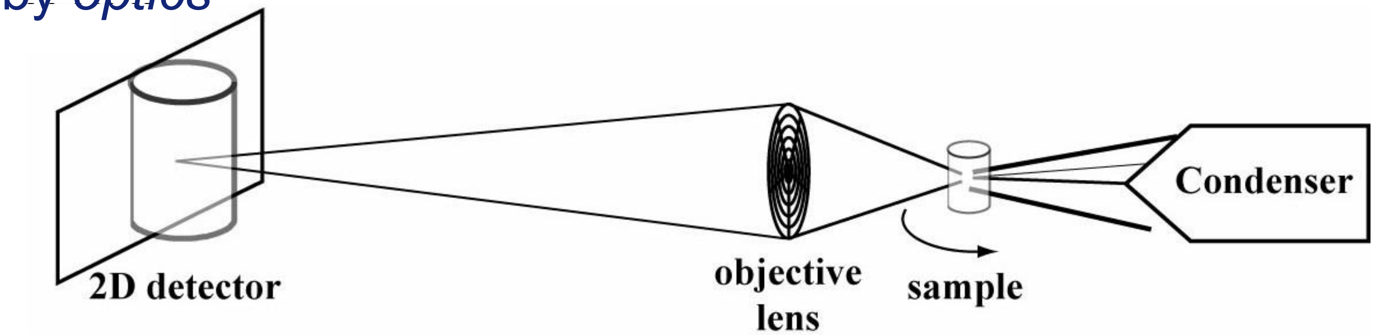

X-RAY MICROSCOPY: COHERENT DIFFRACTION IMAGING SETUPS

CDI:
Phase contrast + Bragg
Dose efficient, ~fast, less robust
Small, isolated object
Resolution limited by *coherent flux*

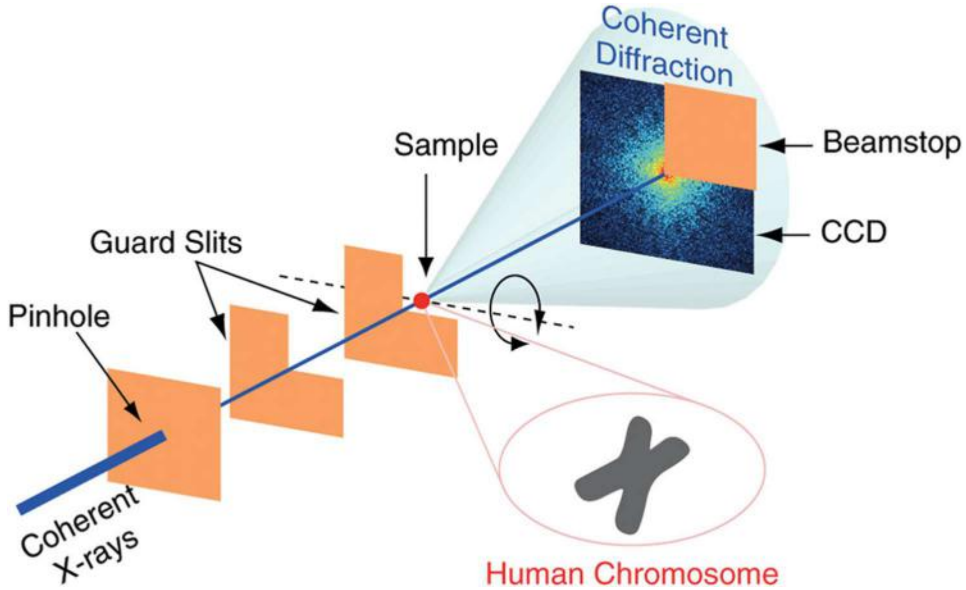

Nishino et al, PRL 102, 018101 (2009)

Ptychography:
Phase contrast (+ Bragg)
Dose efficient, slow, more robust
'Extended' object
Resolution limited by *coherent flux*

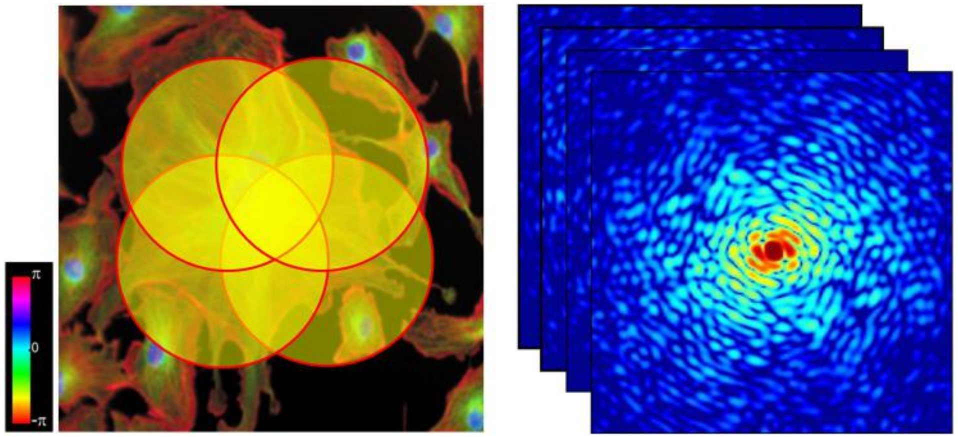

M. Dierolf et al, Europhysics New 39, 22 (2008)

FAR-FIELD X-RAY PTYCHOGRAPHY

Incident X-ray wavefront

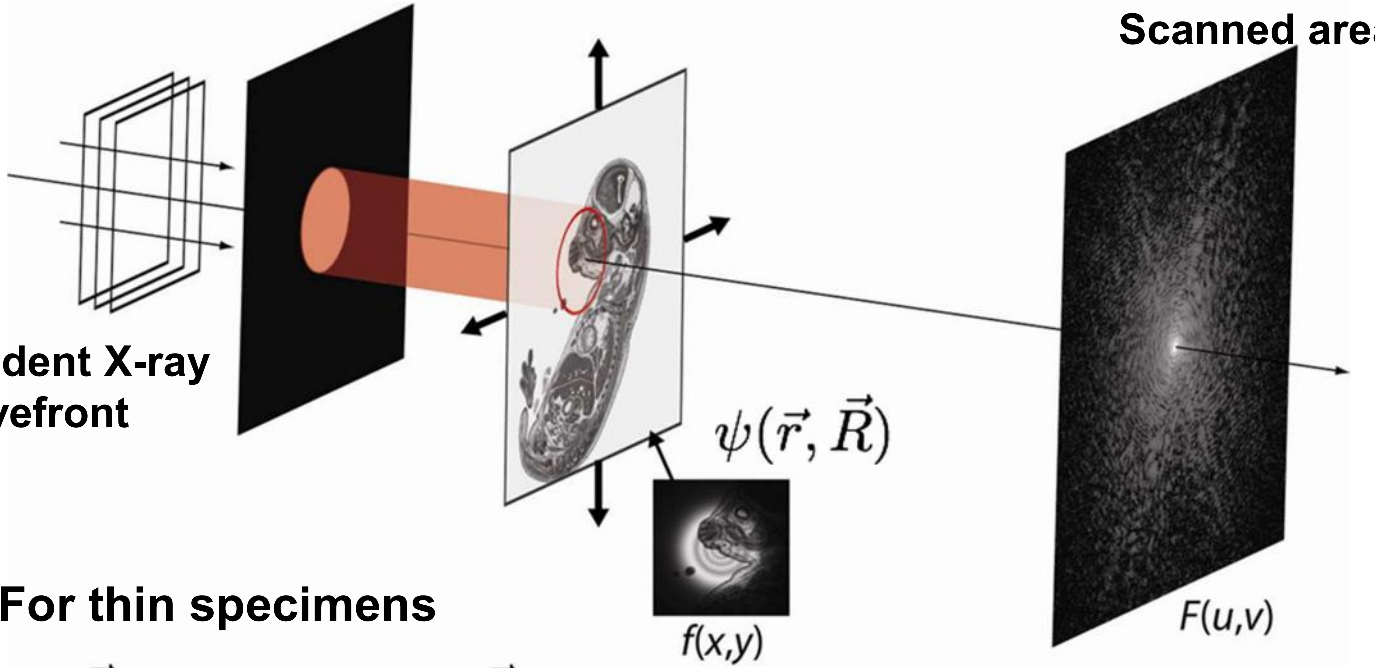

Scanned area Field-of-view

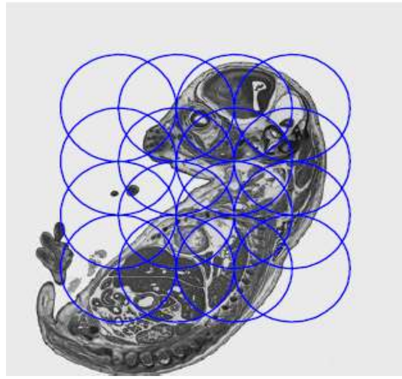

For thin specimens

$$\psi(\vec{r}, \vec{R}) = O(\vec{r})P(\vec{r} - \vec{R})$$

Complex-valued reconstruction

$$I(\vec{q}, \vec{R}) = \left| \mathcal{F}\left\{ \psi(\vec{r}, \vec{R}) \right\} \right|^2$$

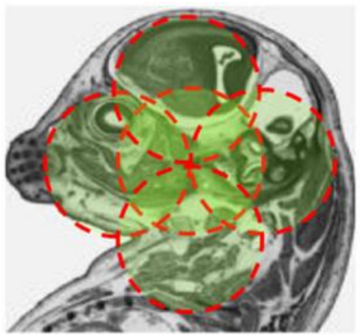

...

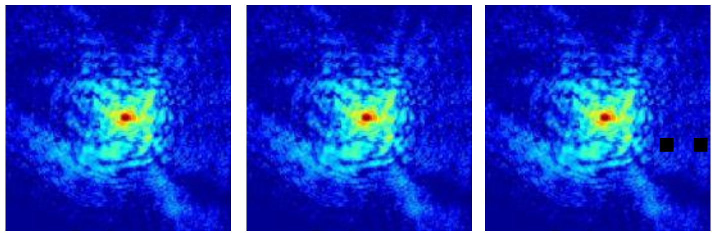

...

R. Hegerl and W. Hoppe, **Ber. Bunsenges. Phys. Chem.** 74, 1148-1154 (1970).
P. Thibault, M. Dierolf et al. **Science** 321, 379-382 (2008).
J. C. da Silva and A. Menzel, **Optics Express** 23, 33812-33821 (2015).

Find the object O(r) and the complex-valued incident illumination P(r) (the probe) consistent with the measured intensities

$$I(\vec{q},\vec{R}) = \left| \int_{-\infty}^{\infty} O(\vec{r})P(\vec{r}-\vec{R})e^{-i\vec{q}\cdot\vec{r}}d\vec{r} \right|^2$$

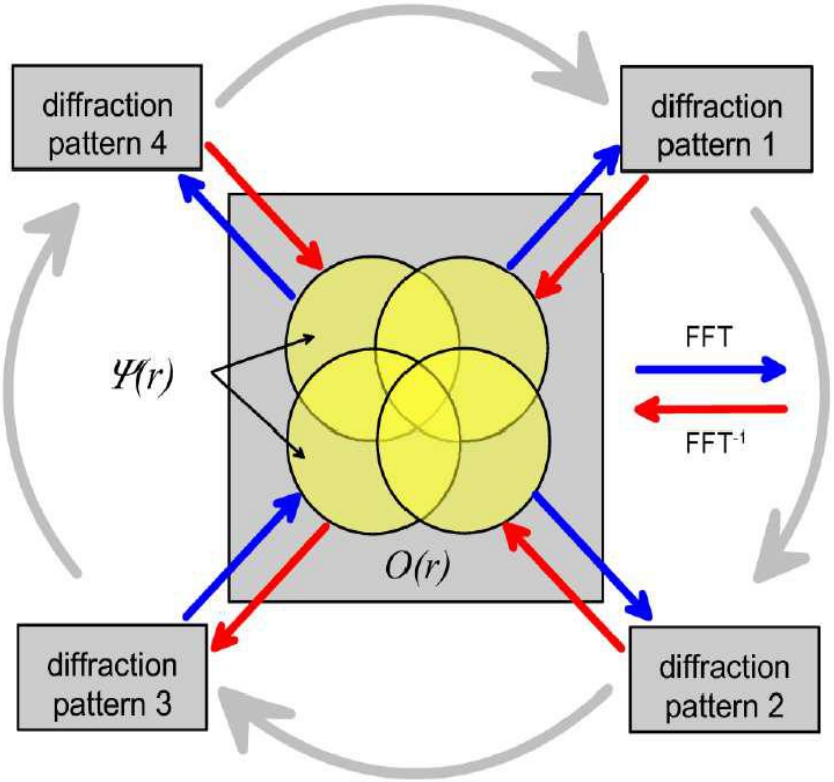

Ptychography Iterative Engine

Figure from M. Dierolf *et al.*, Europhysics New 39 (2008) 22.

Fourier Constraints

Each "view" satisfies each own Fourier Constraint.

Overlap Constraints

Overlapping regions agree and the incident wave field is unique

Redundancy

Redundancy in the data allows to simultaneously reconstruct the probe and the object

THE PTYCHOGRAPHIC PHASE RETRIEVAL IN ACTION

Using Python package Ptypy
(collaborative development B. Enders, P. Thibault)
https://github.com/ptycho/ptypy (private repository)

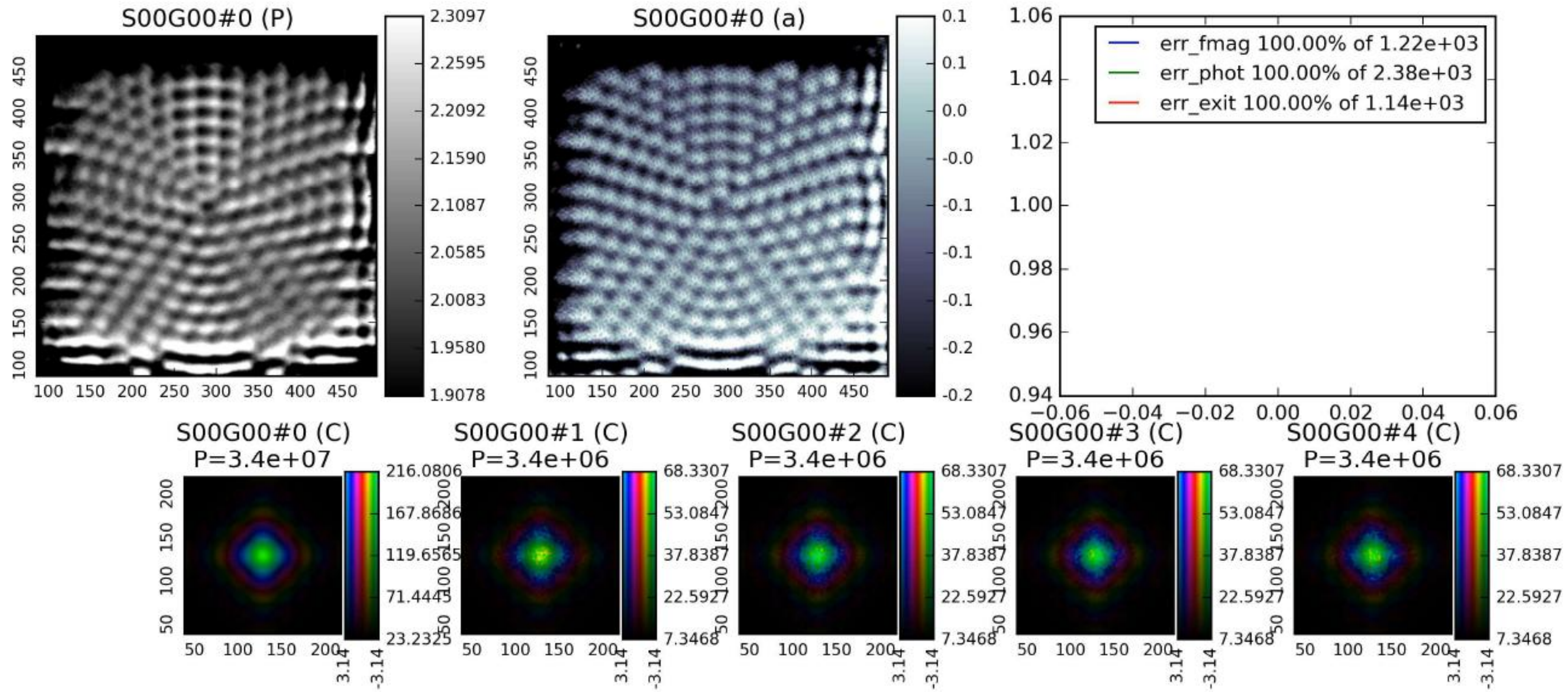

THE PTYCHOGRAPHIC PHASE RETRIEVAL IN ACTION

Using Python package Ptypy
(collaborative development B. Enders, P. Thibault)
https://github.com/ptycho/ptypy (private repository)

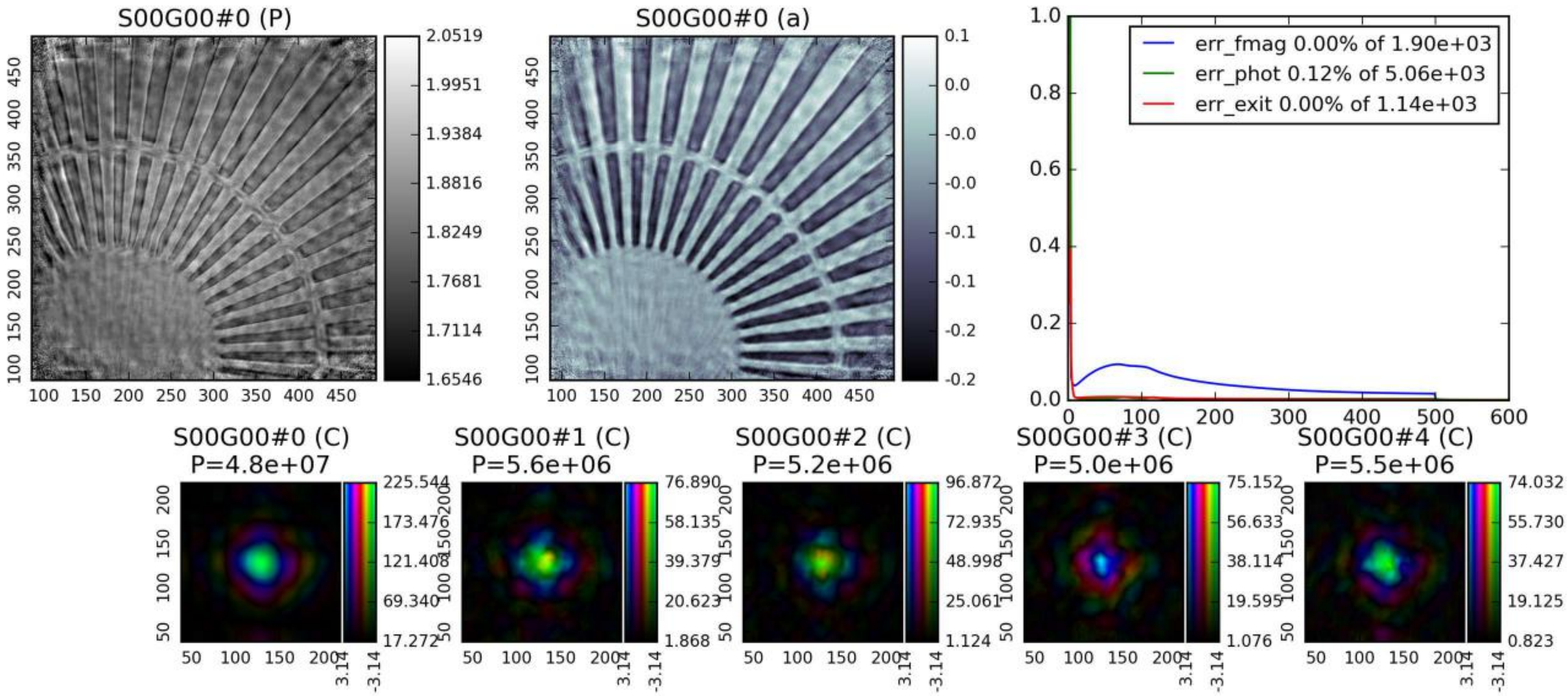

“Partial Coherence effects”: instabilities of optics and positioning motors, detector PSF > 1 pixel, moderate monochromaticity, vibrations of the sample...

P. Thibault and A. Menzel, **Nature** 494, 68-71 (2013)

HIGH SPATIAL RESOLUTION NANOTOMOGRAPHY BY PTYCHOGRAPHY

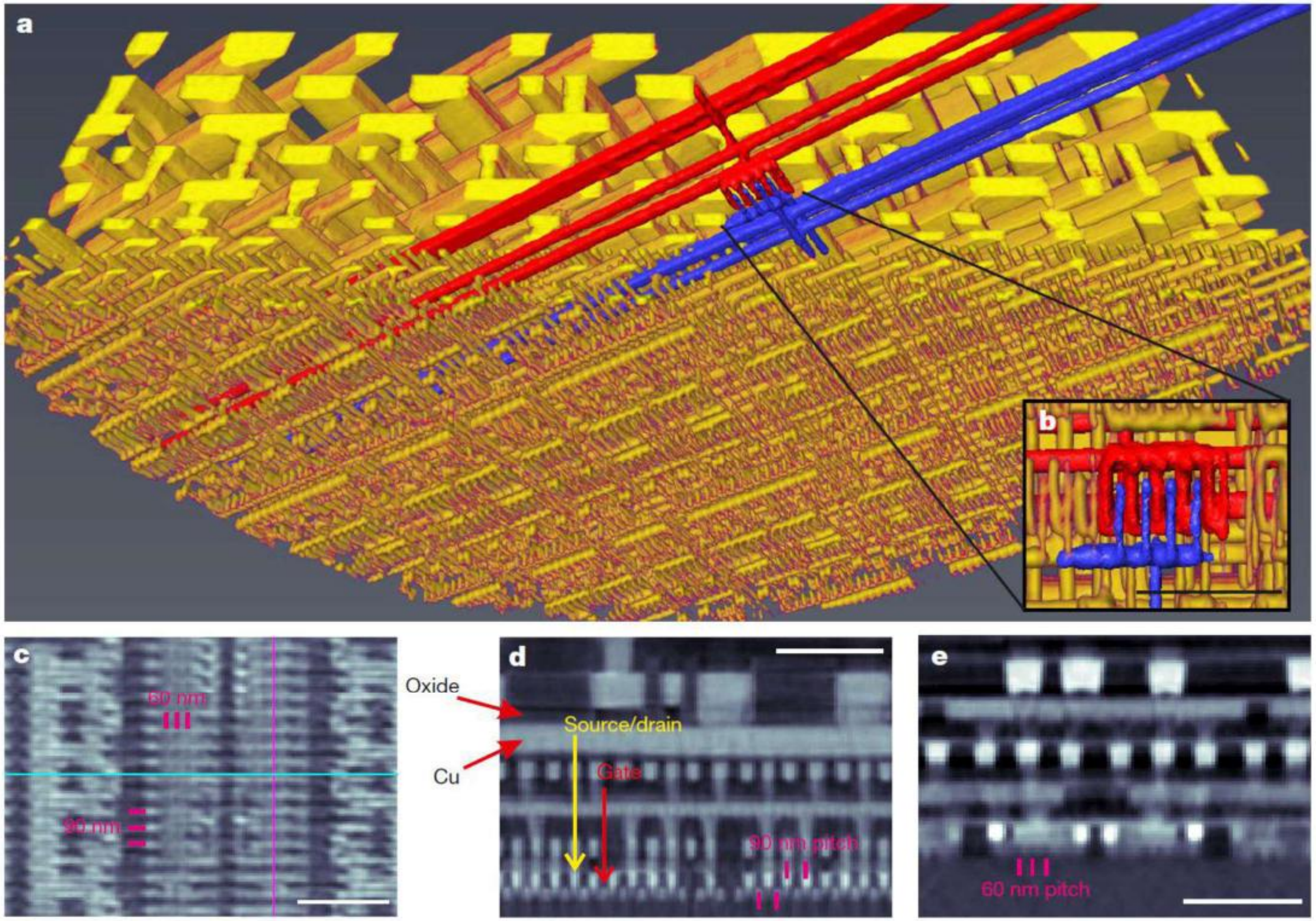

Intel chip,
22 nm technology
Resolution: “14.6 nm”
Scale bars: 500 nm

M. Holler et al., Nature 543, 402 (2017) @ CSAXS/SLS
See also: Burst ptychography, Aidukas et al, Nature (2024)

S(T)XM Scanning (Transmission) X-ray Microscopy:

Micro-analysis
Slow
Rich, trace elements
Phase contrast
Micro-fluorescence
Micro-diffraction
Micro-spectroscopy
Resolution limited by *focus*

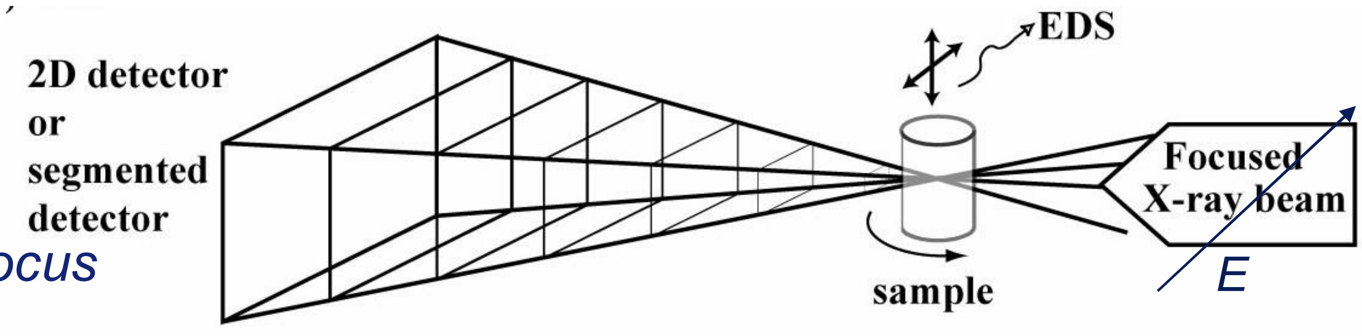

Projection X-ray Microscopy or Holography:

Phase contrast
Dose efficient, fast
Resolution limited by *incoherent focus*

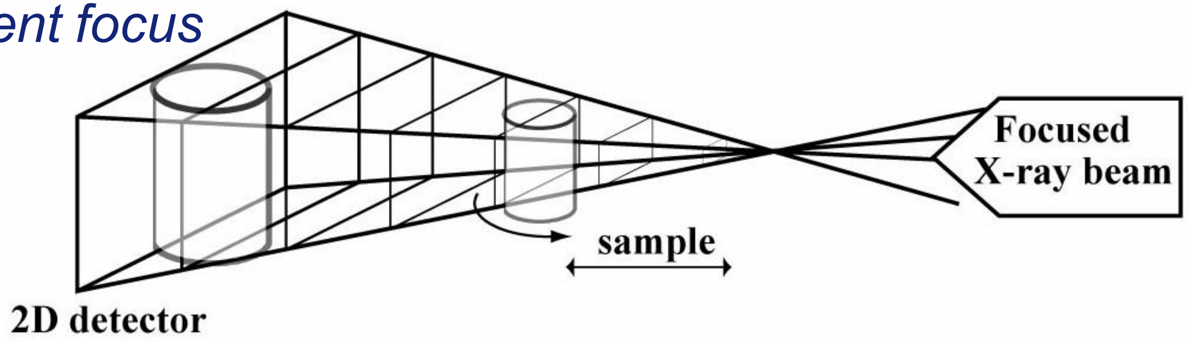

COMBINED X-RAY FLUORESCENCE AND PTYCHOGRAPHY

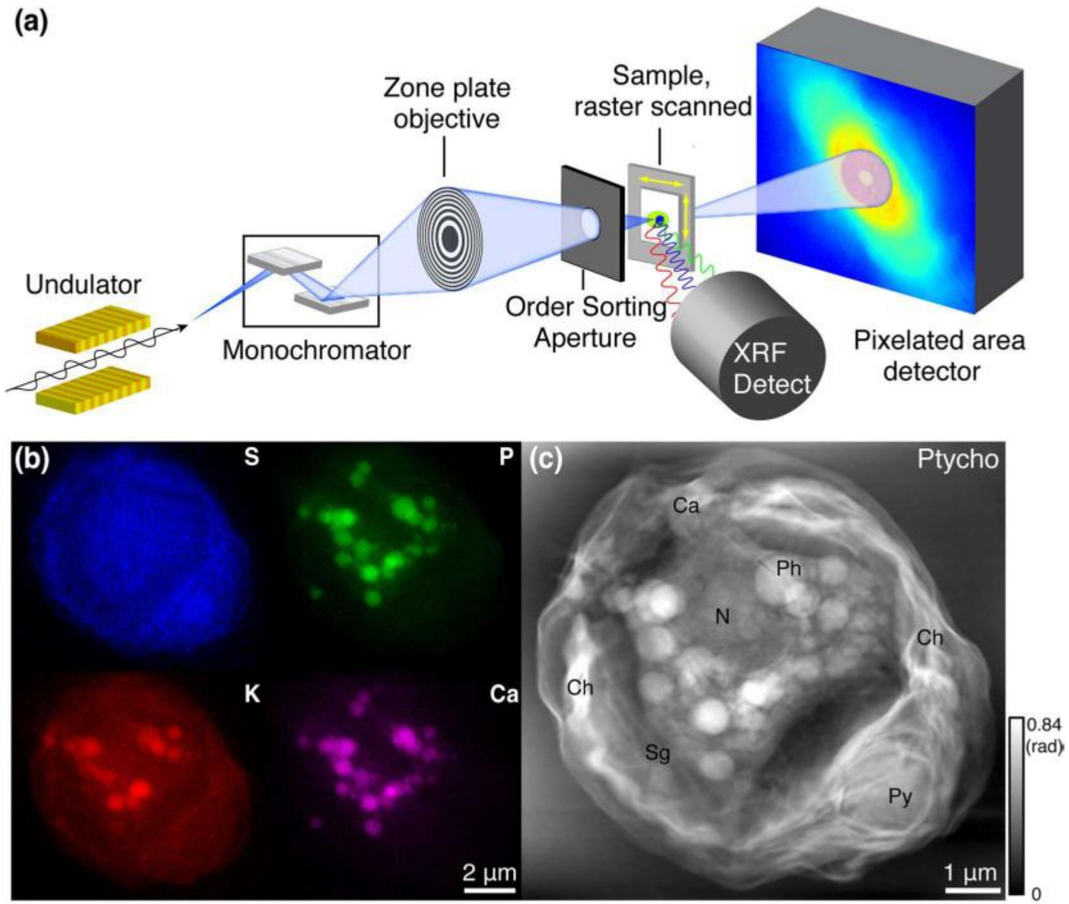

J Deng, D Vine,… Ch Jacobsen
Scientific **Reports** | 7: *445* | 2017

Simultaneous,
using Continuous scanning
Energy: 5.2keV

Required coherence properties rather different (today)
Often preferred to do two successive experiments

ID16B

Multi-technique approach

Tomography | XRF | XAS | XRD | XEOL

Beamline Characteristics:

- Beam modes:
  Pink (10^{-2} bw): 17 to 34 keV
  Monochromatic (10^{-4} bw): 4-30 keV
- Beam size:
  50 x 50 nm^2 (pink); 50 to 100 nm (mono)
- Flux : 10^9 (mono) – 10^{11} (Pink) ph/s
  EBS gain: (x30)
- Operation: in-air, high (900°C) and low (6K) temperature, *in-situ, in-operando*

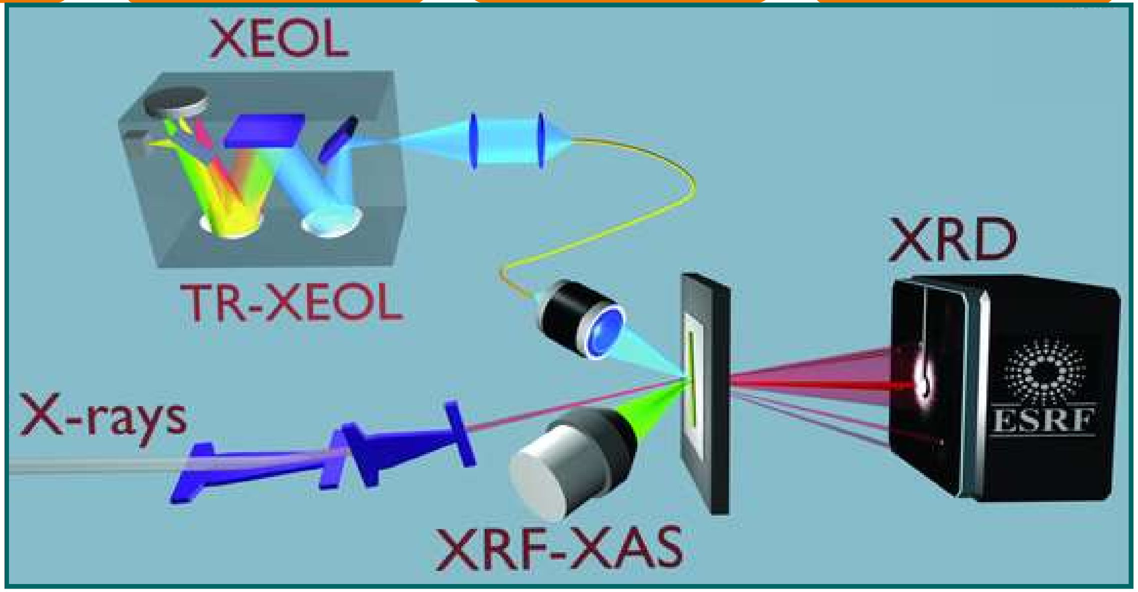

GeSn MICRO-DISKS FOR PHOTONIC APPLICATIONS

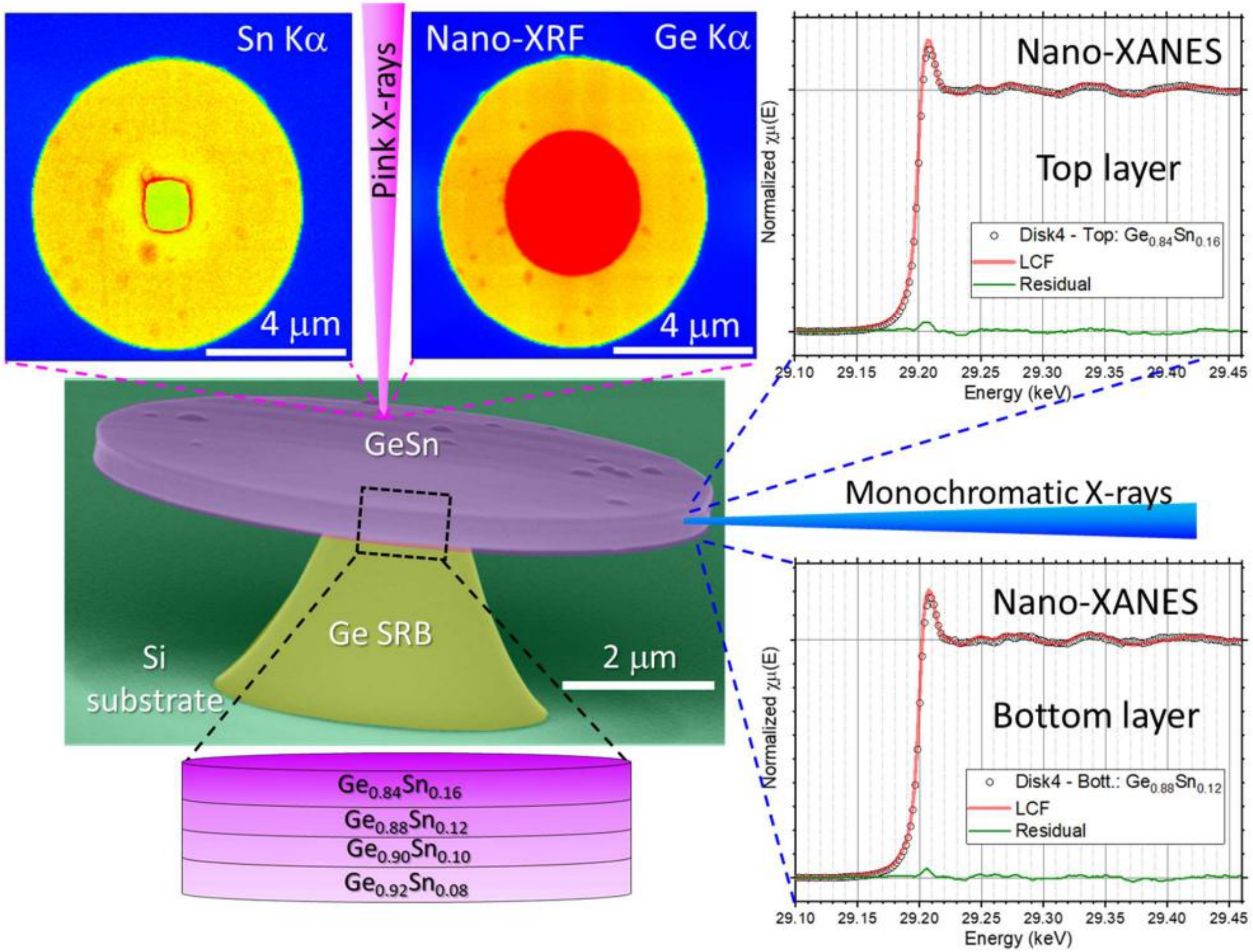

Homogeneity & order in GeSn μ-disks

XRF mapping

- Sn incorporates homogeneously
- Etching to fabricate micro-disk remove GeSn with low SN-concentration.

Nano XANES

- Sn is substitutional to Ge
- Linear combination fitting: No signatures of metallic precipitates in the SGB. Minor fraction of metallic Sn in the SRB disks

J. Segura-Ruiz et al., submitted

ID16A-NI: NANO-IMAGING BEAMLINE

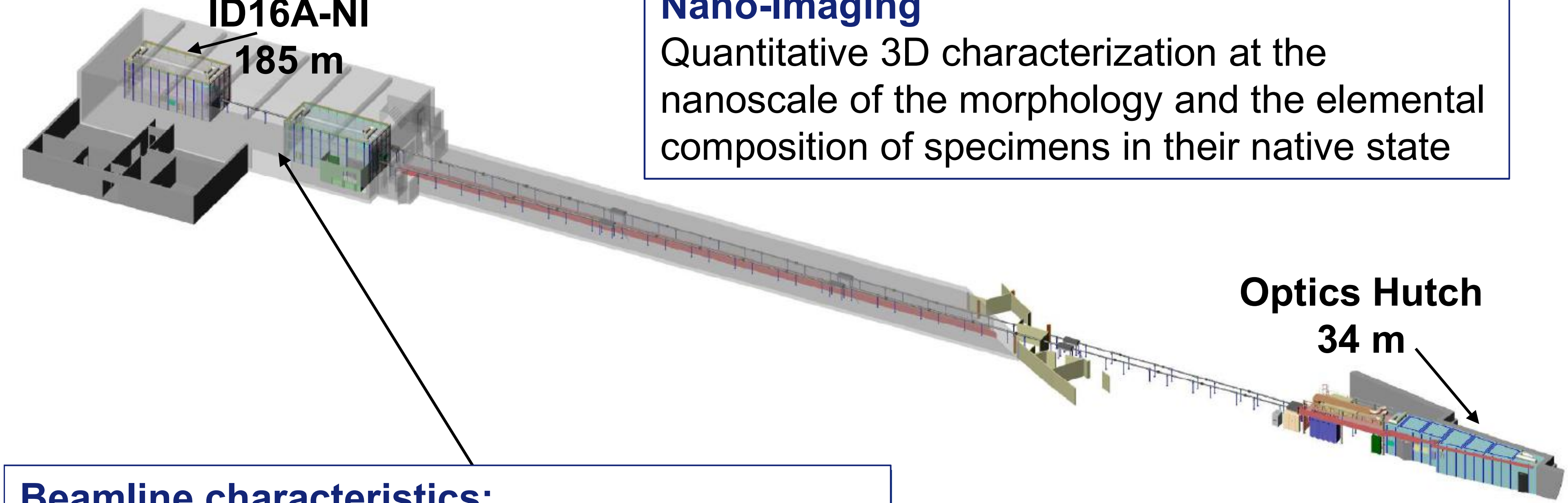

Nano-Imaging
Quantitative 3D characterization at the nanoscale of the morphology and the elemental composition of specimens in their native state

Beamline characteristics:

- Techniques: fluorescence analysis, in-line phase contrast, near-field ptychography
- **Nano-Focus**: (12) 25-35 nm
- Energy: **17 keV** & **33.6 keV**
- Flux: 1.2 10^{13} ph/s & 2.7 10^{12} ph/s @ 0.7%
  in principle…
- Operation: under vacuum, room temperature or **cryo** workflow

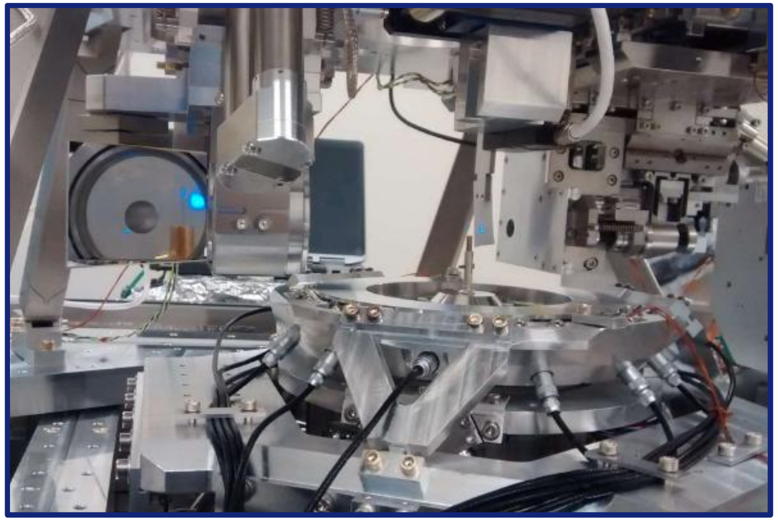

ID16A End-station

X-RAY PHASE CONTRAST

X-RAY FLUORESCENCE

Holography

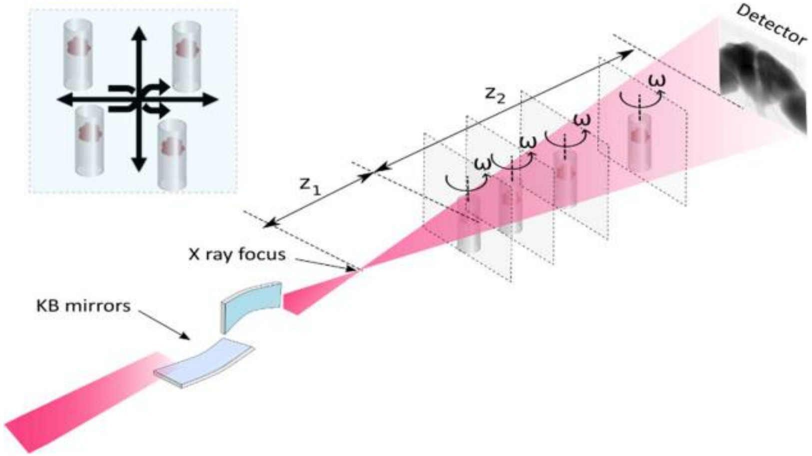

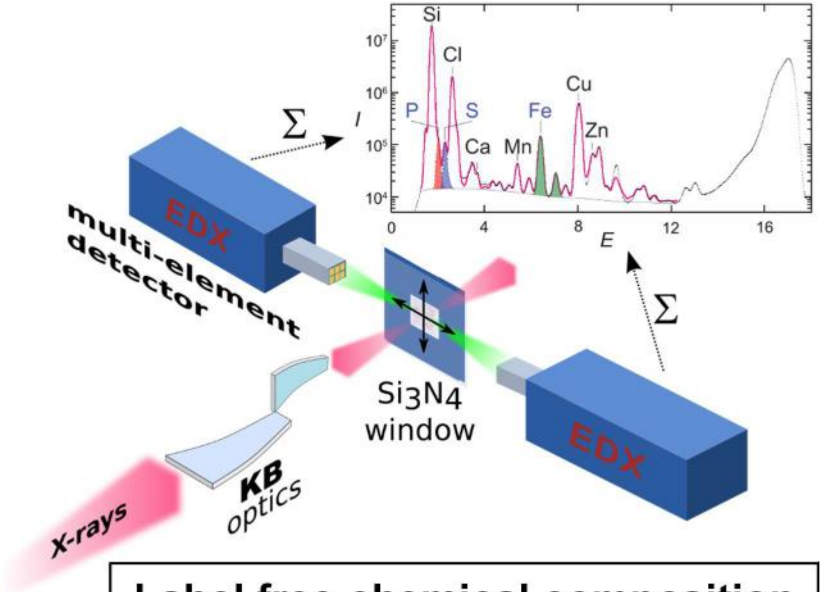

Morphology
Electron Density distribution

Nano
Cryo

Label free chemical composition
(Trace) Element distributions

Near-field Ptychography

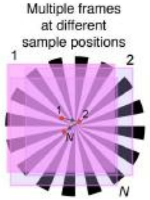

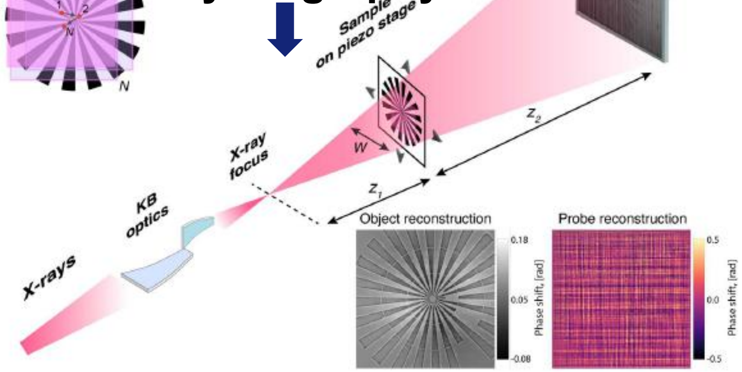

- **Quantitative** 3D reconstructions of $\rho(x,y,z)$, $c_{el}(x,y,z)$
- **Correlative** approaches (Soft X-rays, EM, STED)

50ms dwell-time	Phosphorus	Sulfur	Potassium	Zinc
Limit of detection	$1.2\ 10^{-18}$ g (22,500 atoms)	$3.9\ 10^{-19}$ g (7,300 atoms)	$3.3\ 10^{-19}$ g (5,100 atoms)	$1.9\ 10^{-20}$ g (180 atoms)
Limit of quantification	$2.4\ 10^{-18}$ g (47,700 atoms)	$8.7\ 10^{-19}$ g (16,300 atoms)	$7.7\ 10^{-19}$ g (11,400 atoms)	$3.6\ 10^{-20}$ g (330 atoms)

HOLOGRAPHY: PHASE RETRIEVAL

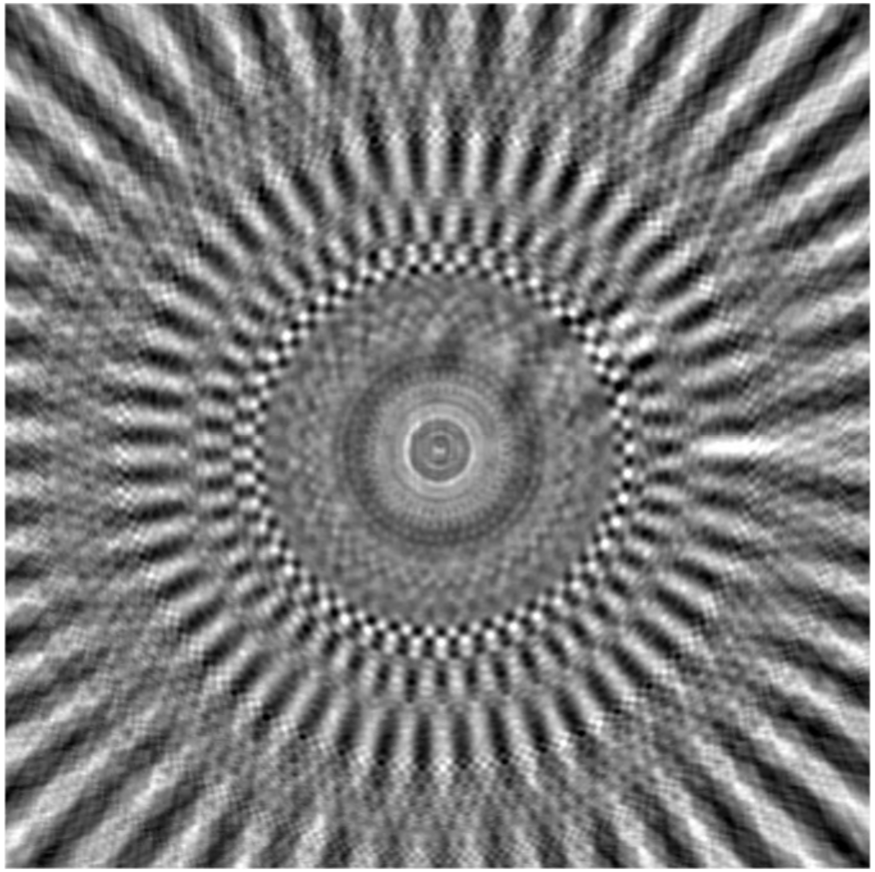

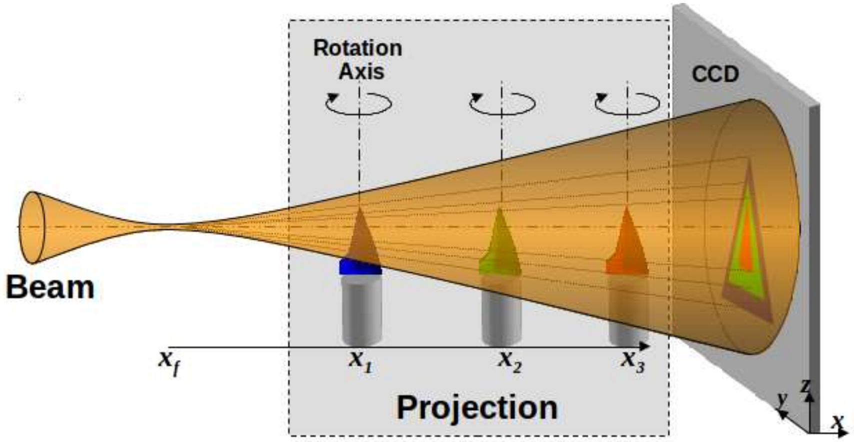

Least squares minimization of cost functional

$$K = \sum_m |I_m^{\exp}(f) - I_m^{calc}[\phi(f)]|^2$$

P.Cloetens et al., Appl. Phys. Lett. 75, 2912 (1999)
P.Schiske, (1968). Zur Frage der Bildrekonstruktion durch Fokusreihen

Single Distance Paganin

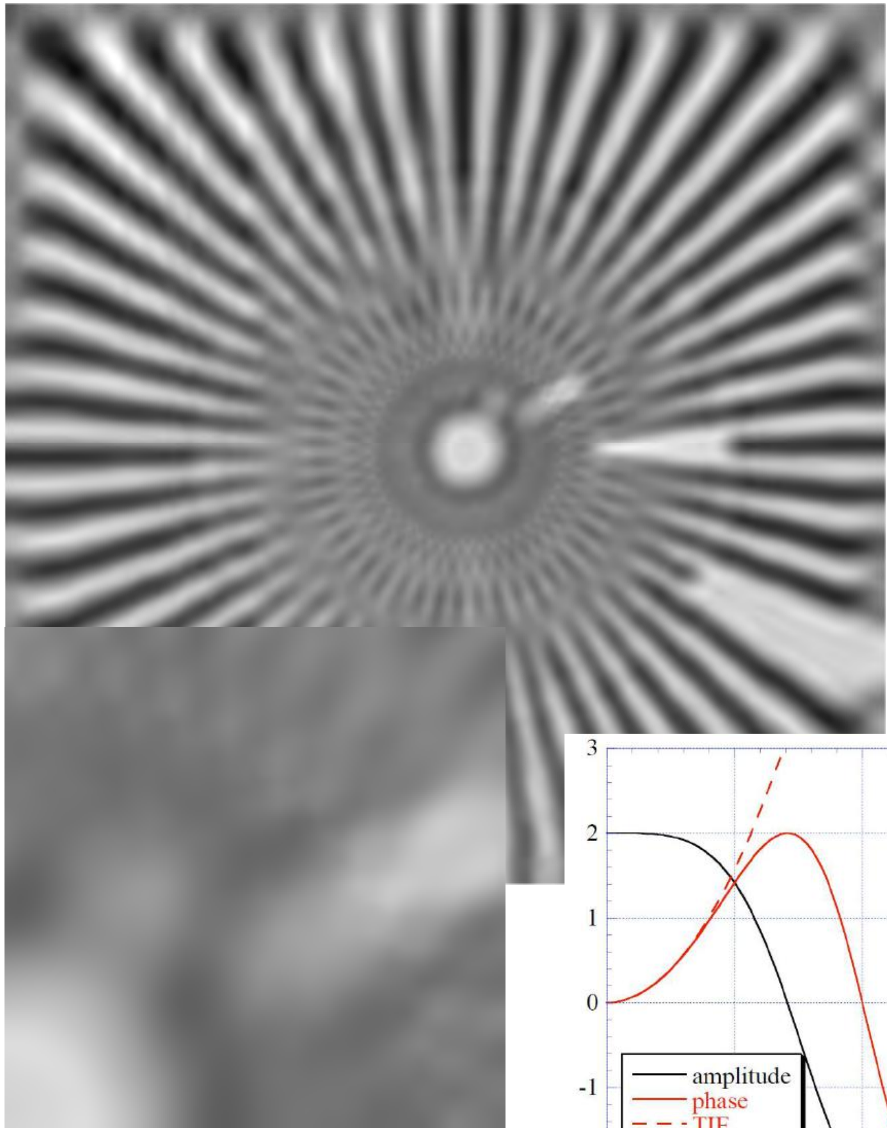

2.5 µm

Multiple Distance Transfer Function

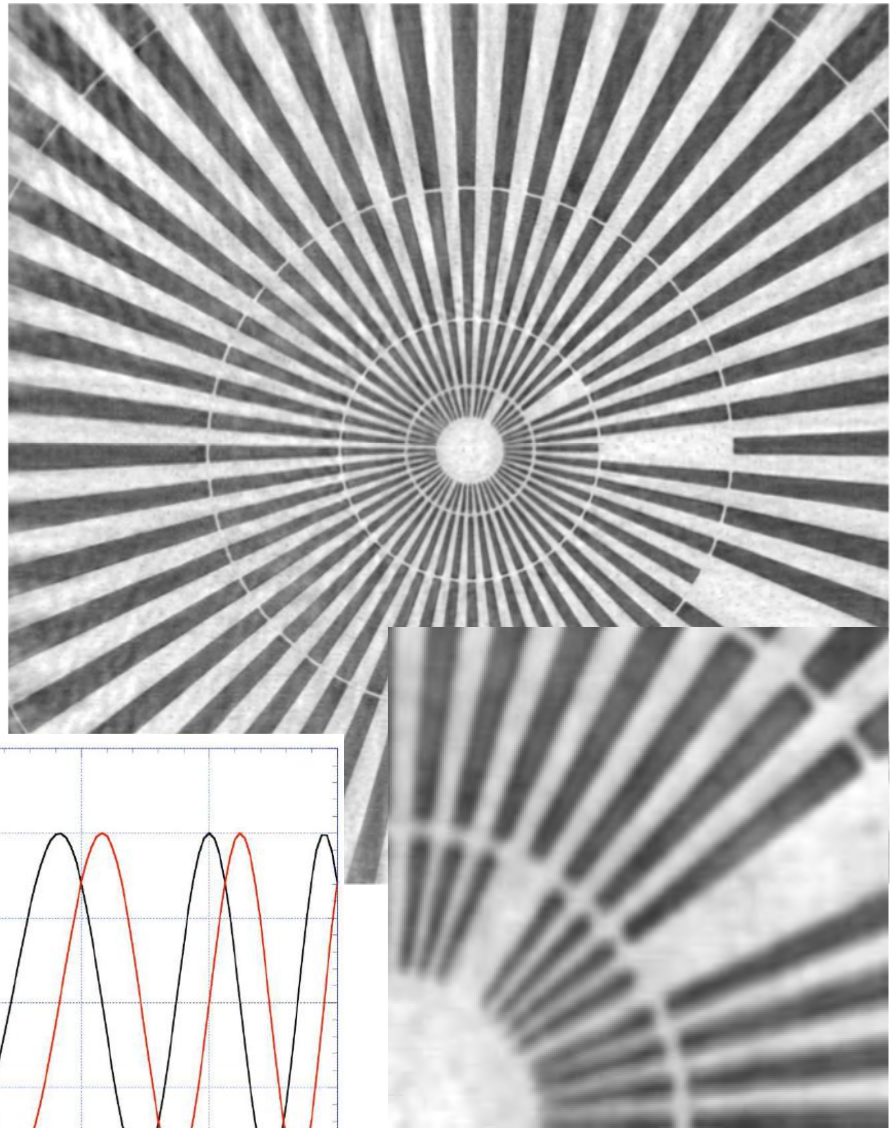

2.5 µm

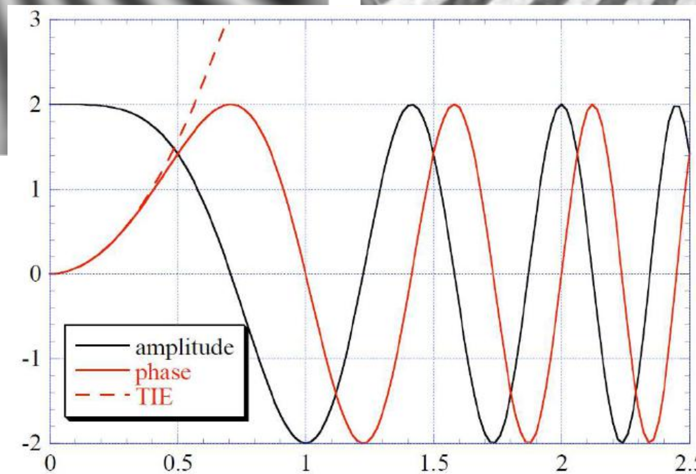

DISCOVER MECHANISMS OF THERAPIES
MESENCHYMAL STEM CELLS AS TREATMENT FOR MULTIPLE SCLEROSIS

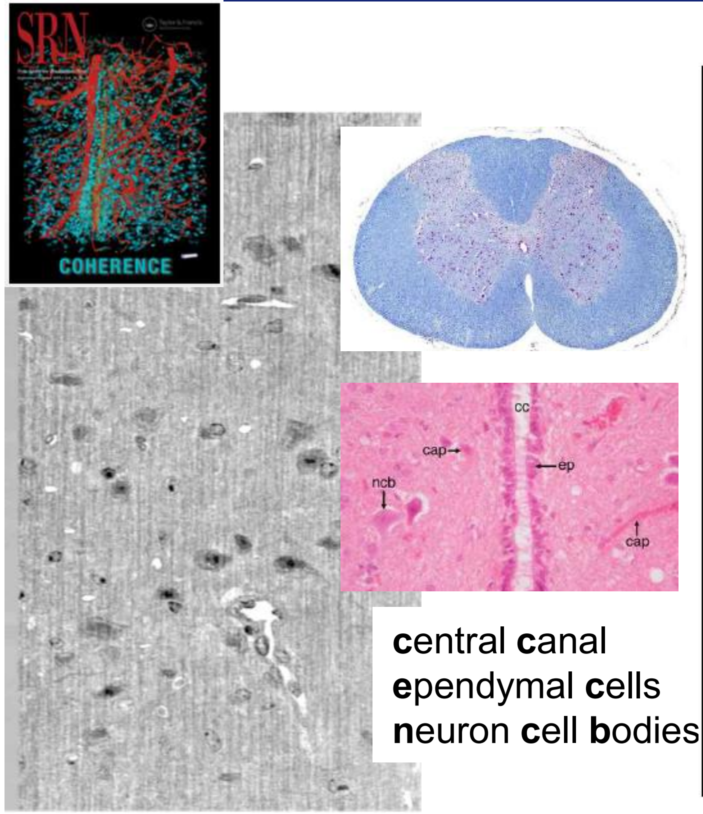

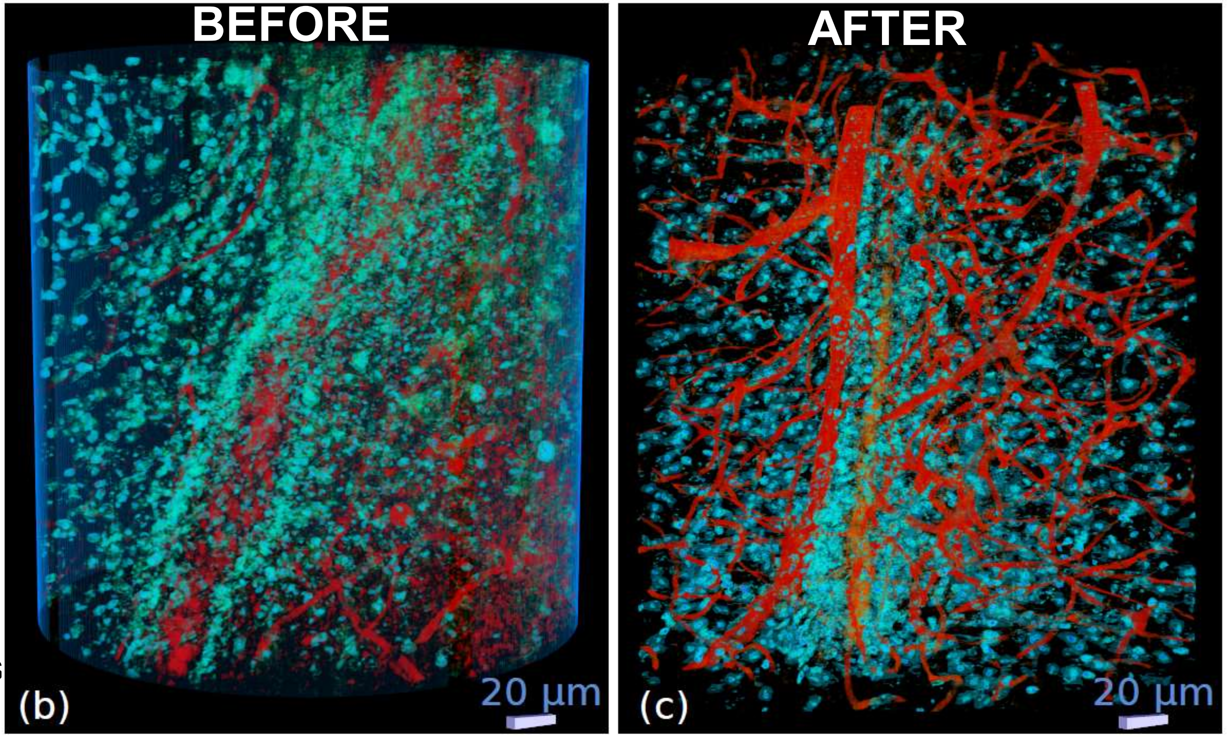

- Nanotomography of spinal cord in a Multiple Sclerosis mice model
- Regeneration of vascular network and motor neurons after treatment
- Sample size 2.5 x 5 mm, pixel size 130 nm, Epon embedded, Os stained for correlation with TEM

SAPIENZA UNIVERSITÀ DI ROMA

The European Synchrotron | ESRF

A. Cedola, A. Uccelli et al., Sci. Rep. 7: 5890 2017 | DOI:10.1038/s41598-017-06251-7

3D DISSECTION OF ALZHEIMER'S DISEASE PATHOLOGY

AMYLOID ANGIOPATHY AND MICROENVIROMENT

Micro – XPCT: WT | Micro – XPCT: APP/PS1

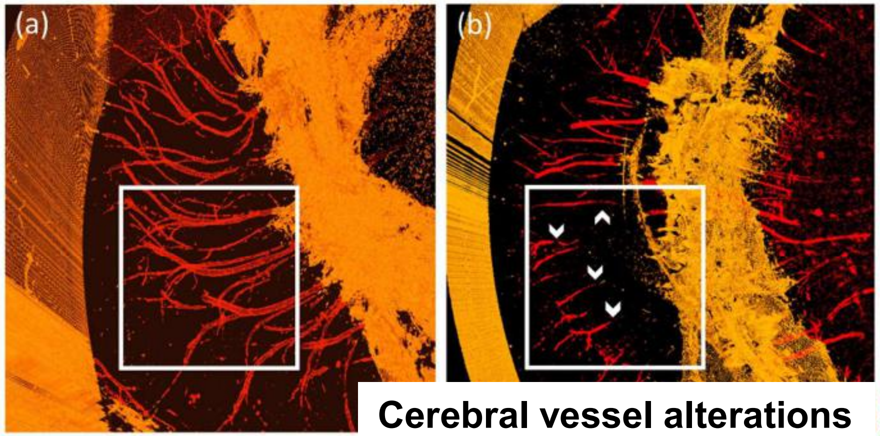

Cerebral vessel alterations

Nano – XPCT: APP/PS1

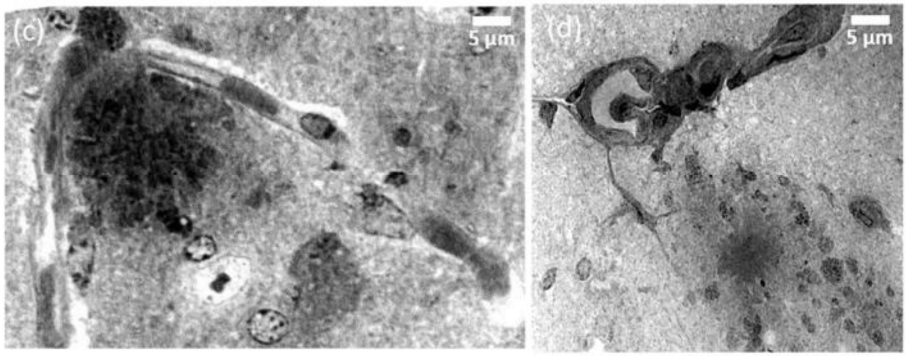

Nano – XPCT: APP/PS1

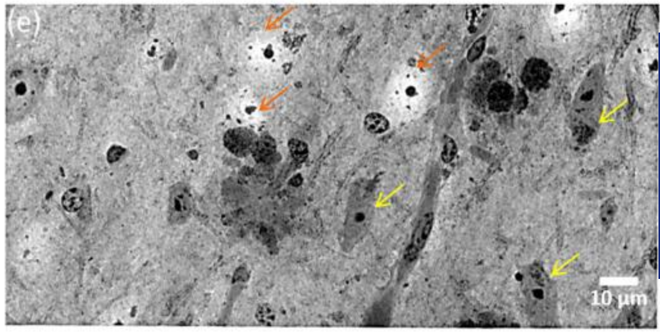

Healthy Neurons

Suffering Neurons

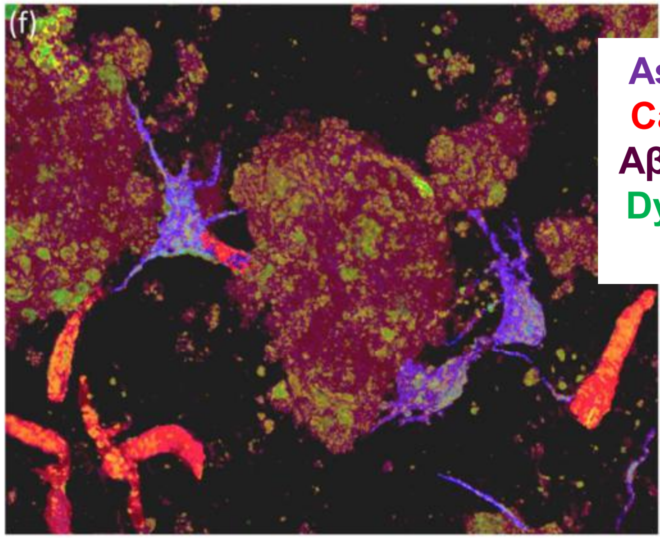

Astrocytes
Capillaries
Aβ plaques
Dystrophic neurites

AD mouse brain microenvironment

Future work:
evaluate the efficacy
of new therapeutic approaches

Phase Contrast Nano-tomography at ID16A
Micro-CT at Tomcat, SLS

L Massimi, A Cedola et al. *NeuroImage*, 184 (2018) 490

The European Synchrotron | ESRF

Cryo 3D Correlative Microscopy (first time)

ALBA MISTRAL

ESRF ID16A

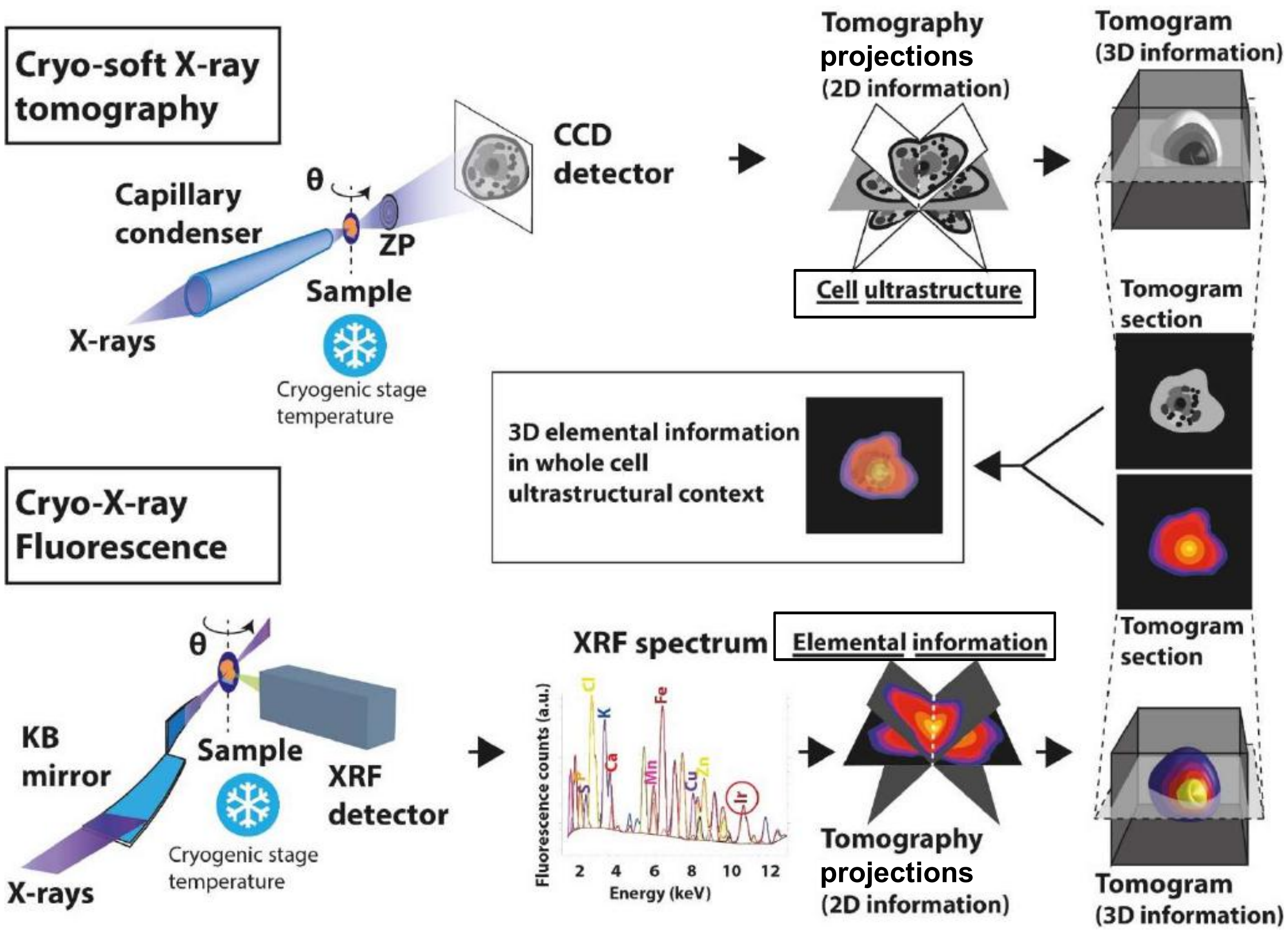

J Conesa, Y Yang, E Pereiro, A Pizarro et al., Angew. Chem., 59, 1270 (2020)

CNB imdea nanociencia ALBA The European Synchrotron ESRF

INTRACELLULAR LOCALIZATION OF POTENT ANTICANCER METALLODRUGS

Mitochondria (epifluo) Ir (XRF)

Ir (XRF) + Structure (SoftXT)

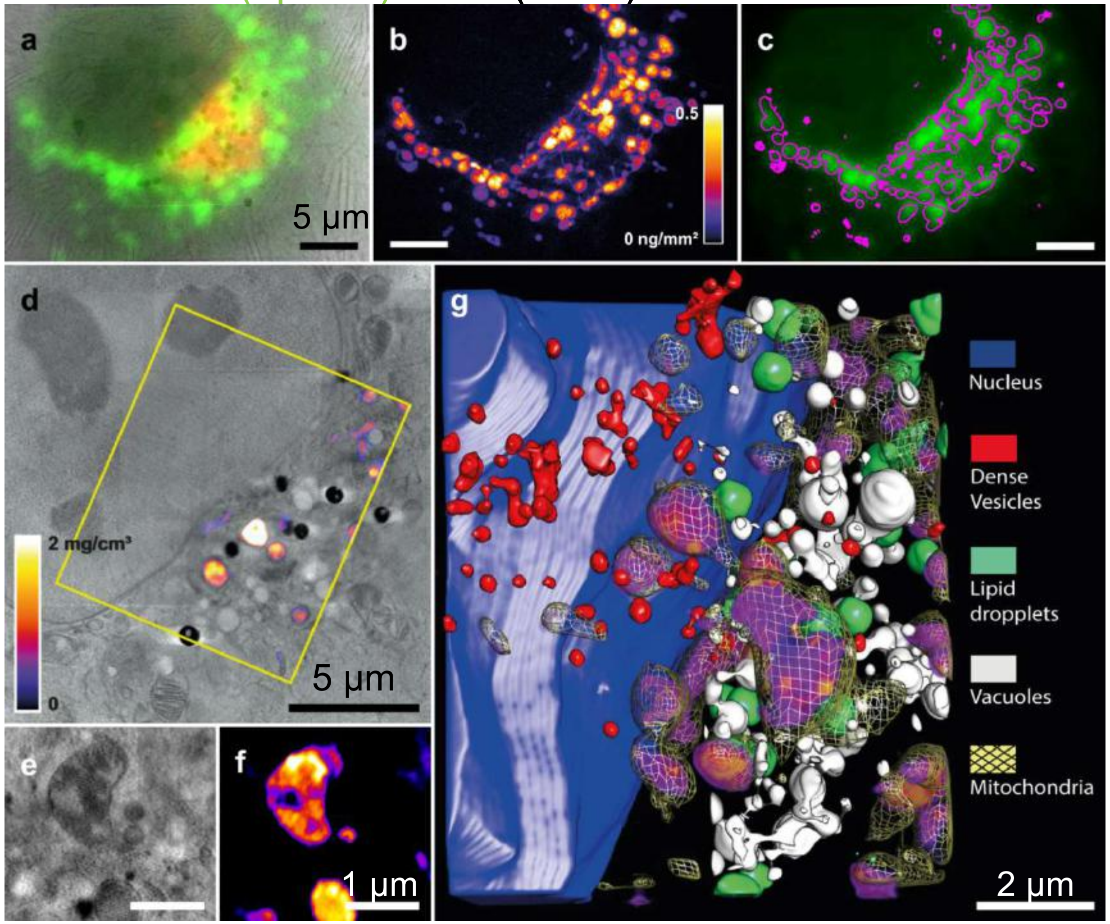

- Ir metallodrug is exclusively located in the *mitochondria*
- Triggers effects on cell death-related endogenous metals (Ca and K)

EBS outlook:

- *Time-dependent uptake* of drugs in the cellular environment (*pseudo 4D*)

J Conesa, Y Yang, E Pereiro, A Pizarro et al., Angew. Chem., 59, 1270 (2020)

Cryo 3D Correlative Microscopy

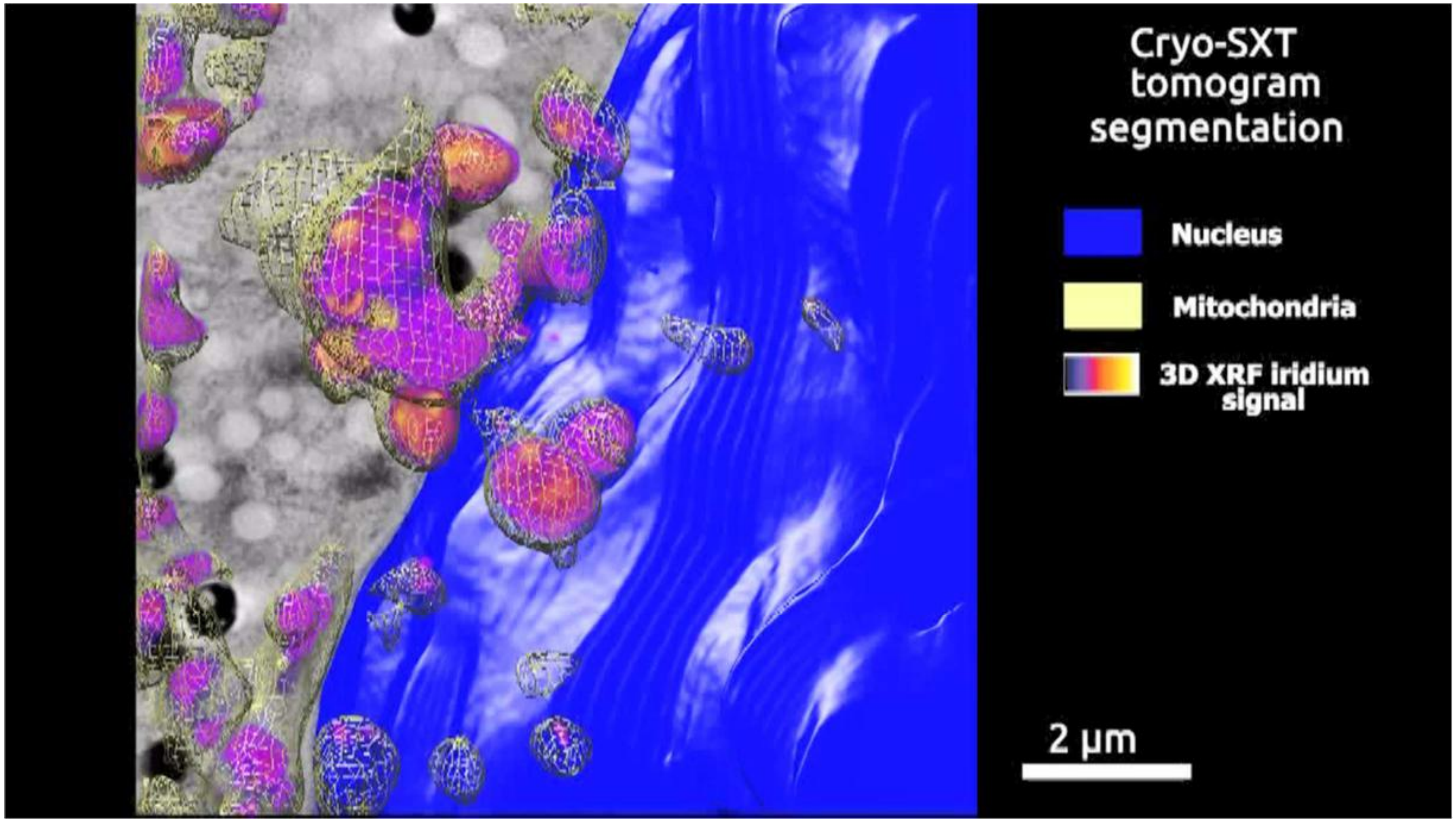

J Conesa, Y Yang, E Pereiro, A Pizarro et al., Angew. Chem., 59, 1270 (2020)

CNB imdea nanociencia ALBA The European Synchrotron ESRF

THE POWER OF PHASE CONTRAST ILLUSTRATED ON MOUSE CORTEX TISSUE

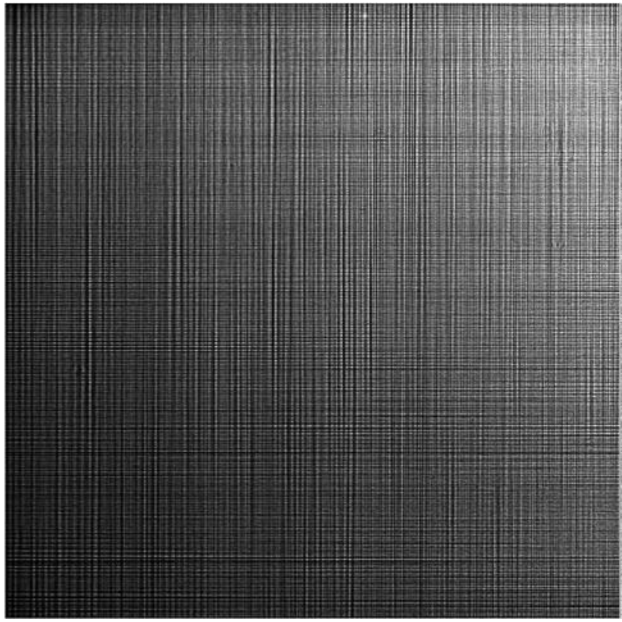

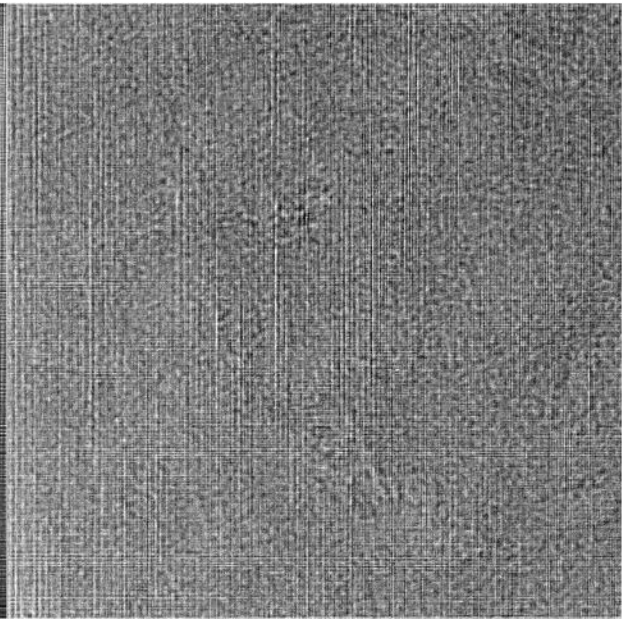

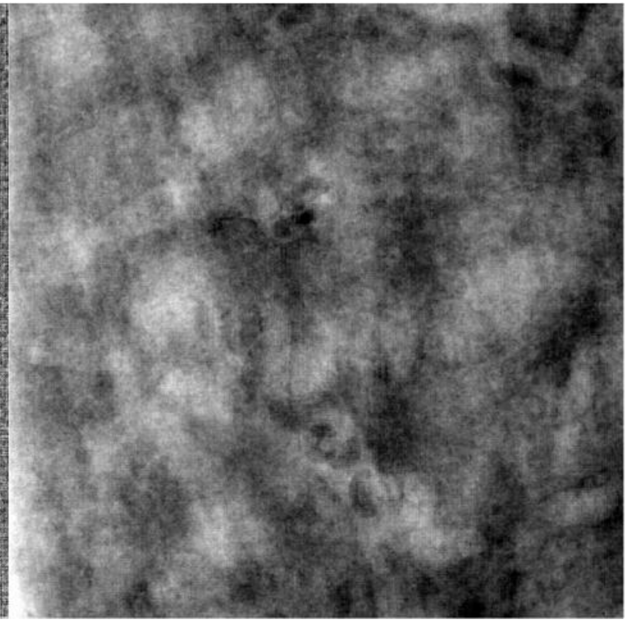

Raw data recorded by the detector → Empty beam corrected holograms → Phase maps

RESOLVING NEURAL NETWORKS (CONNECTOMICS)

Connectomics in mouse cortex – complementarity with FIB-SEM & TEM
Data collection ~4h

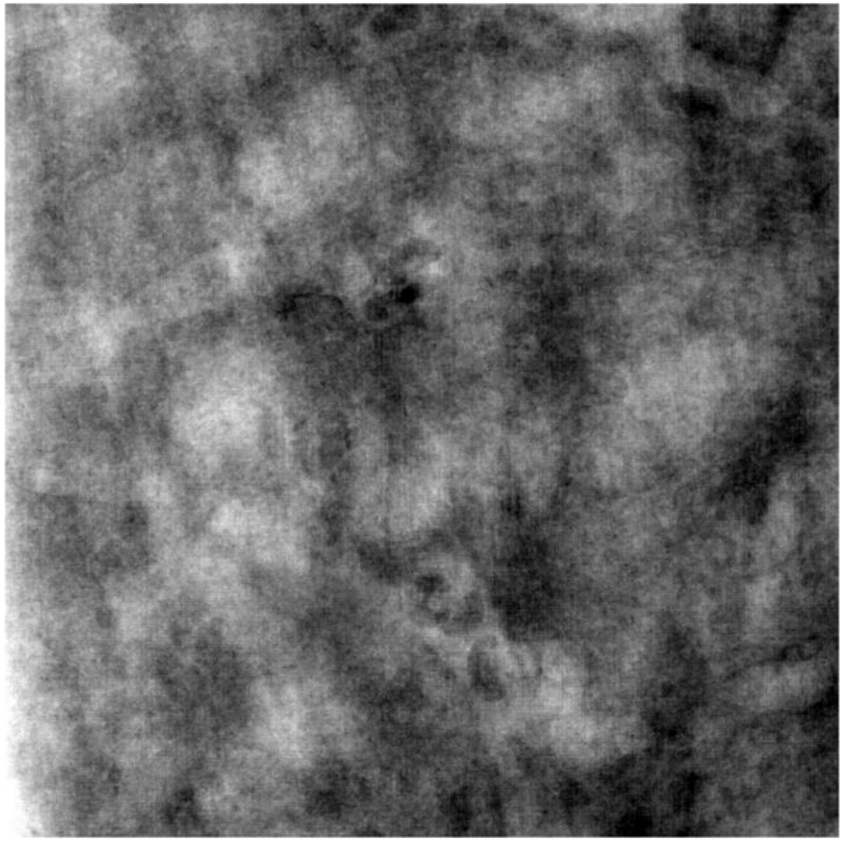

Phase maps

Tomographic reconstruction

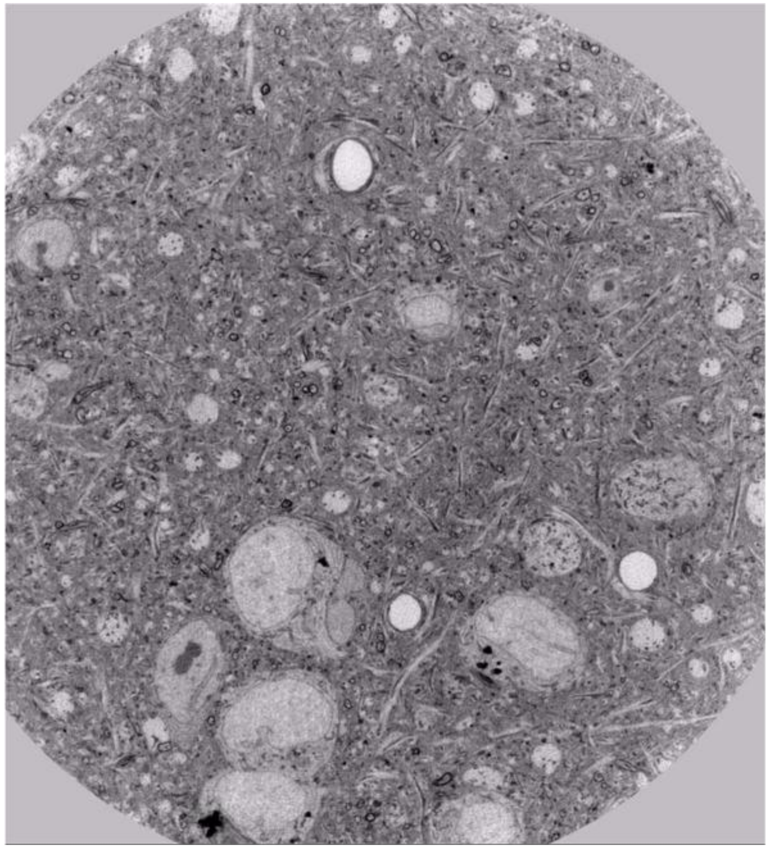

Pixel size 40 nm

Kuan, Maniates, Lee, Pacureanu* et al. Nat. Neuro. 2020*

HARVARD MEDICAL SCHOOL The European Synchrotron | ESRF

X-RAY HOLOTOMOGRAPHY ENABLES MULTISCALE IMAGING OF BRAIN VOLUMES WITH EM-LIKE QUALITY

Drosophila neuronal dendrites

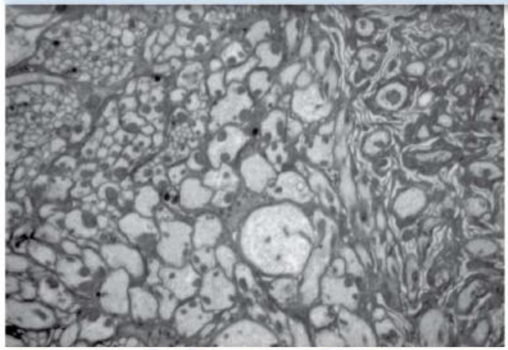

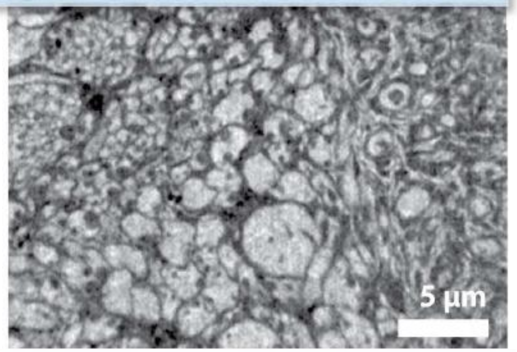

Transmission Electron Microscopy 12 nm pixels

X-ray holographic nano-tomography 50 nm pixels

Mouse cortex 30 nm voxel size

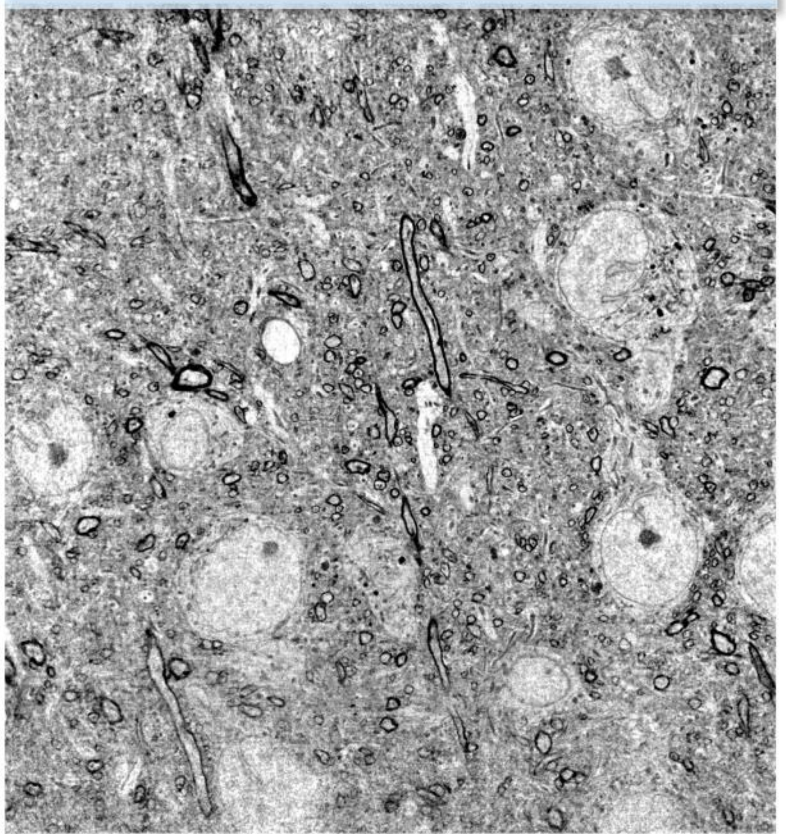

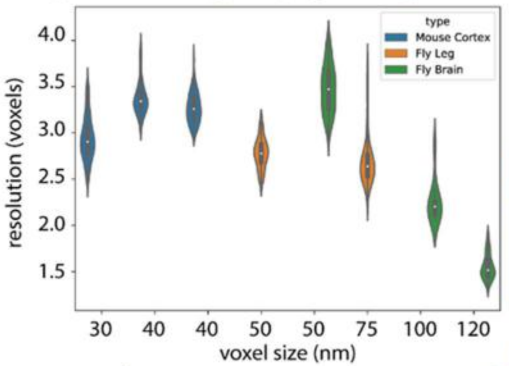

Thanks to EBS spatial resolution and throughput will be improved
➔ Synaptic resolution, large volumes, multiple samples

DENSE NEURONAL RECONSTRUCTION IN MILLIMETER SIZED SAMPLES

HOW NEURONS CONTROL AND COORDINATE WALKING

- *Drosophila* brain → first 3D image obtained with serial-section electron microscopy (Bock et al. *Cell* 2018). **Data collection took ~ 2 years.**
- X-ray holographic tomography → data collection for a brain takes **4 – 24 hours** *f*(voxel size).
- Legs are nearly impossible to section for EM → X-ray imaging was the only way to access the 3D information.

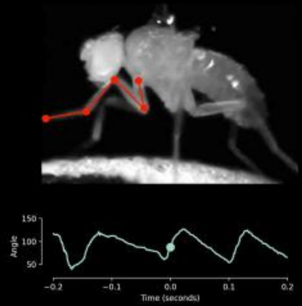

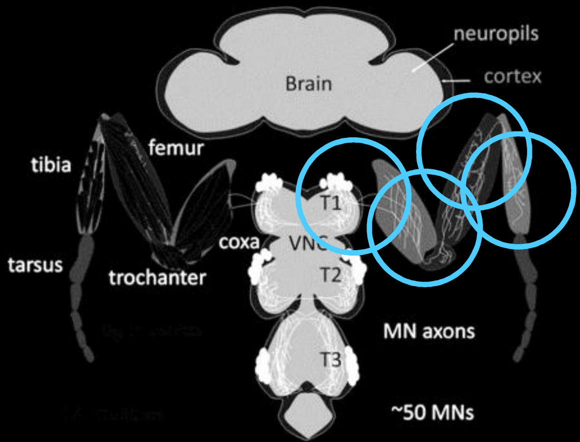

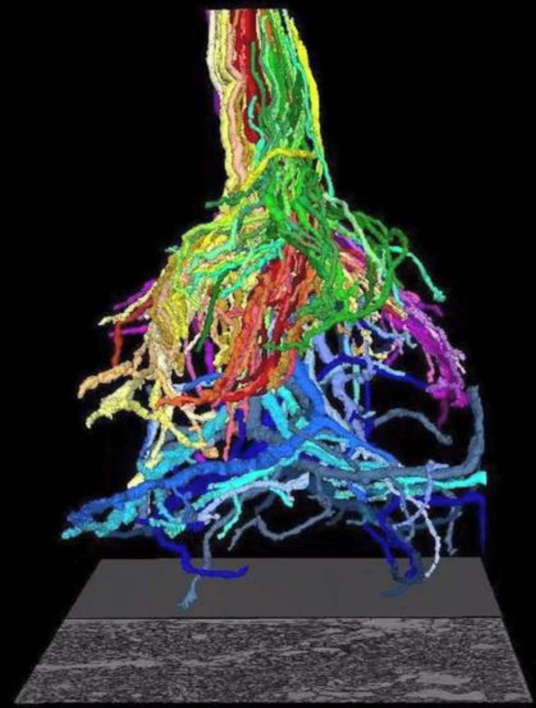

Automatic reconstruction of neurons connecting VNC (spinal cord) to muscles in the leg of *Drosophila*

Kuan, Maniates, Lee, Pacureanu* et al. Nat. Neuro. 2020*
See also: *Azevedo, Lee, Pacureanu, Tuthill et al., Nature 2024*

HARVARD MEDICAL SCHOOL
erc European Research Council 2020-2025
The European Synchrotron | ESRF

SELF-SUPERVISED DENOISING (ML)

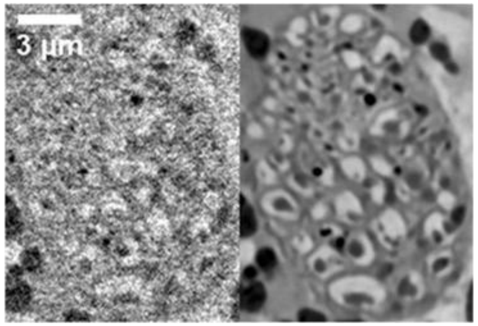

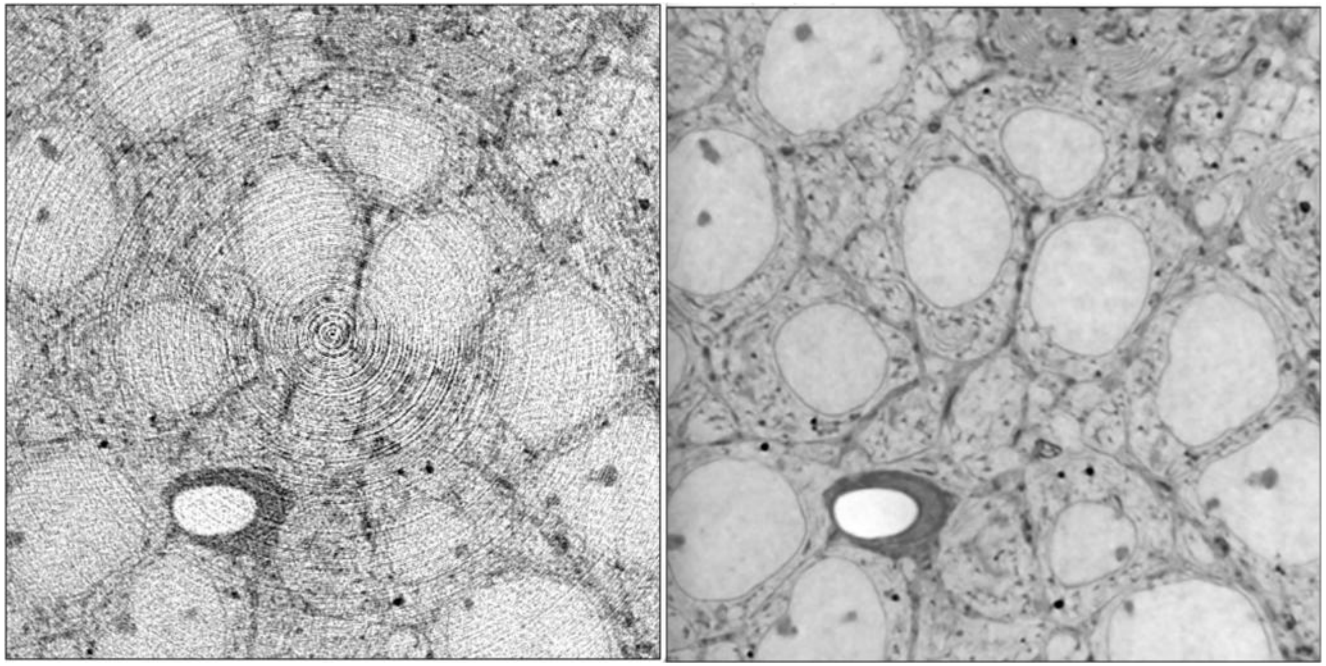

Alfred Laugros

QUANTIFICATION OF DEGRADATION IN LI-ION BATTERIES

Fracturing of secondary particles

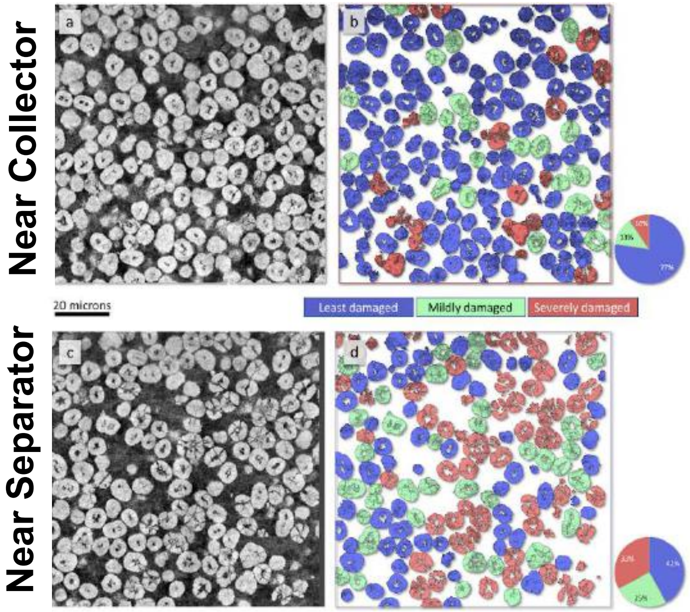

Li-NMC cathode

NMC-CBD detachment

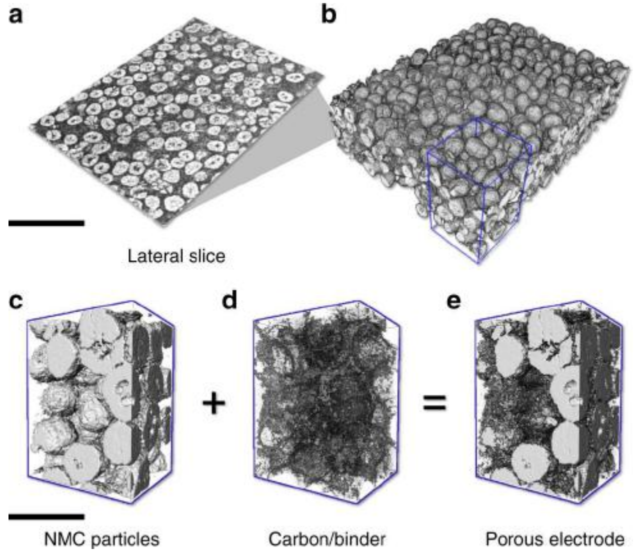

Electron Density vs State-Of-Charge

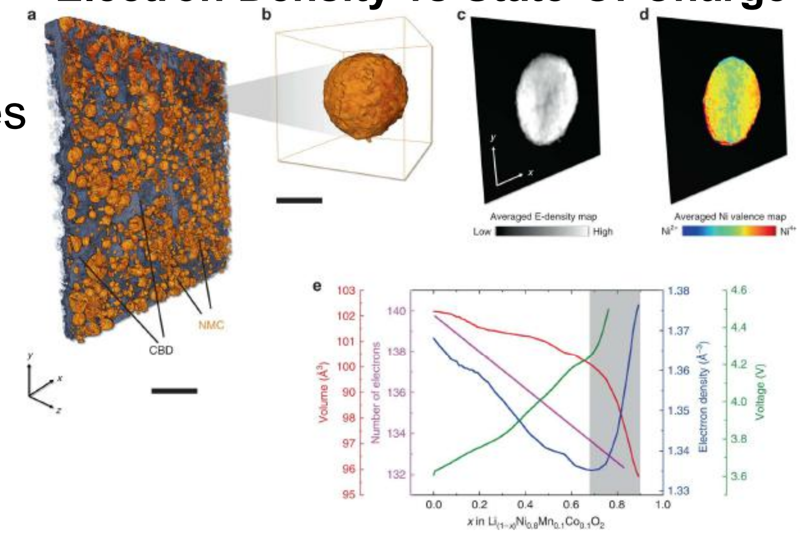

Heterogeneous fracturing of secondary particles in Ni-rich cathode materials

Quantification by Machine Learning of particle - carbon/binder detachment

Electron density as a proxy for the State-Of-Charge (SOC)

Yang, Liu et al. Adv. Energy Mater. 2019
Jiang, Liu et al. Nat. Commun. 2020

SLAC PURDUE UNIVERSITY VT VIRGINIA TECH | ESRF

Near-field ptychography with a structured illumination

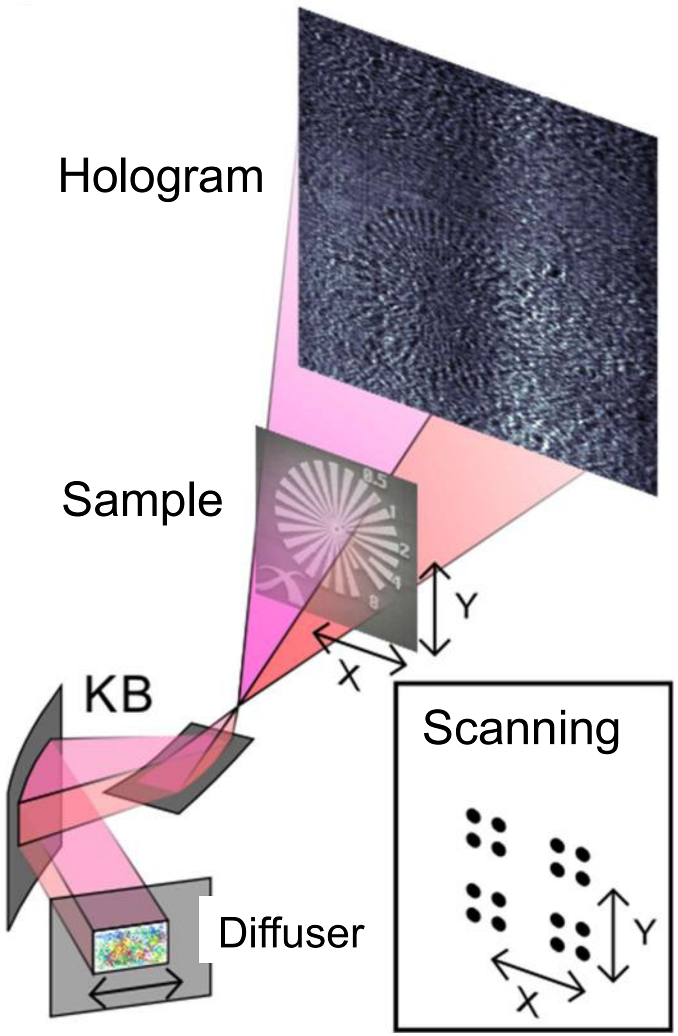

M. Stockmar, P. Cloetens, P. Thibault, Scientific Reports, 2013

A different flavor of transverse diversity

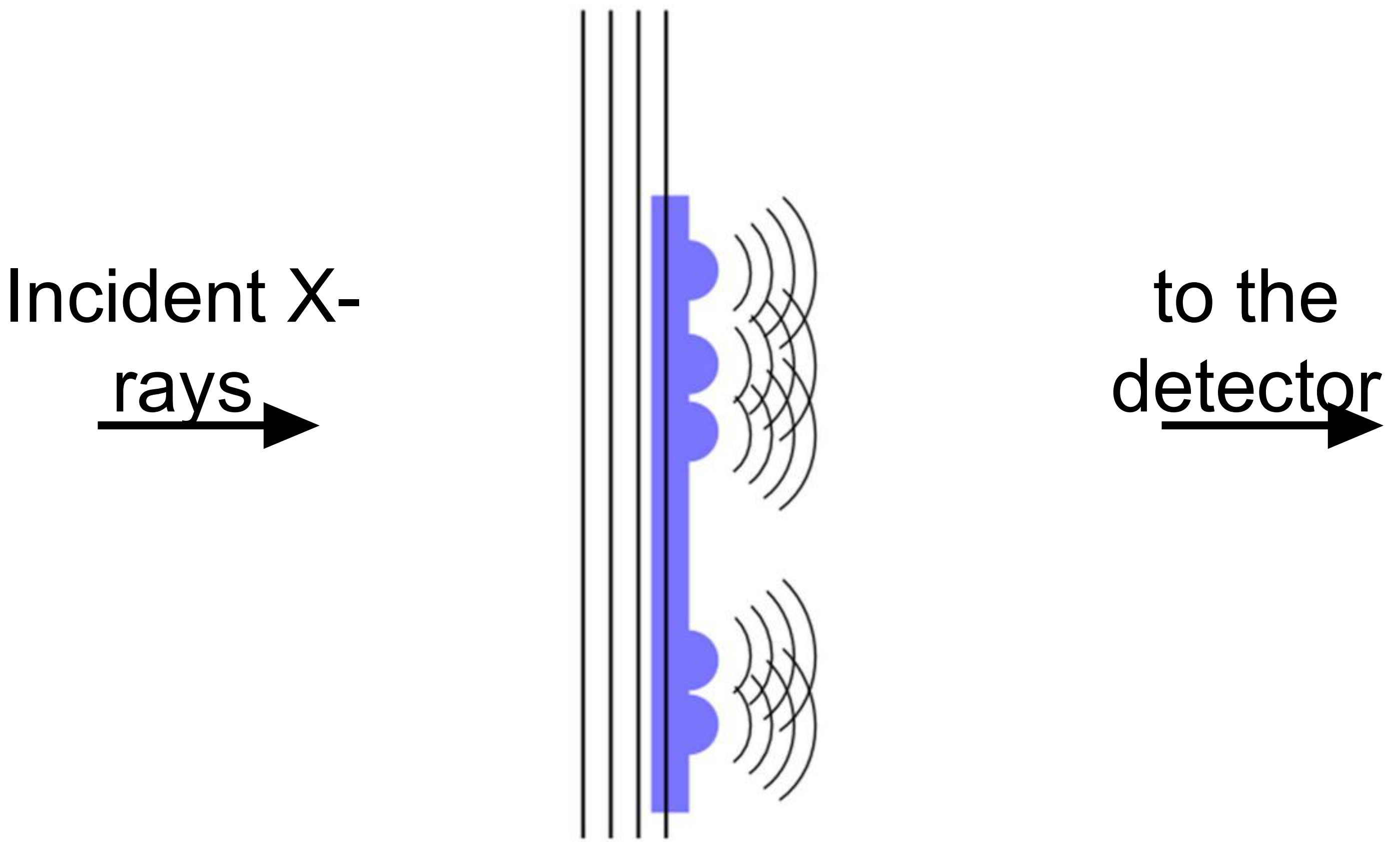

A different flavor of transverse diversity

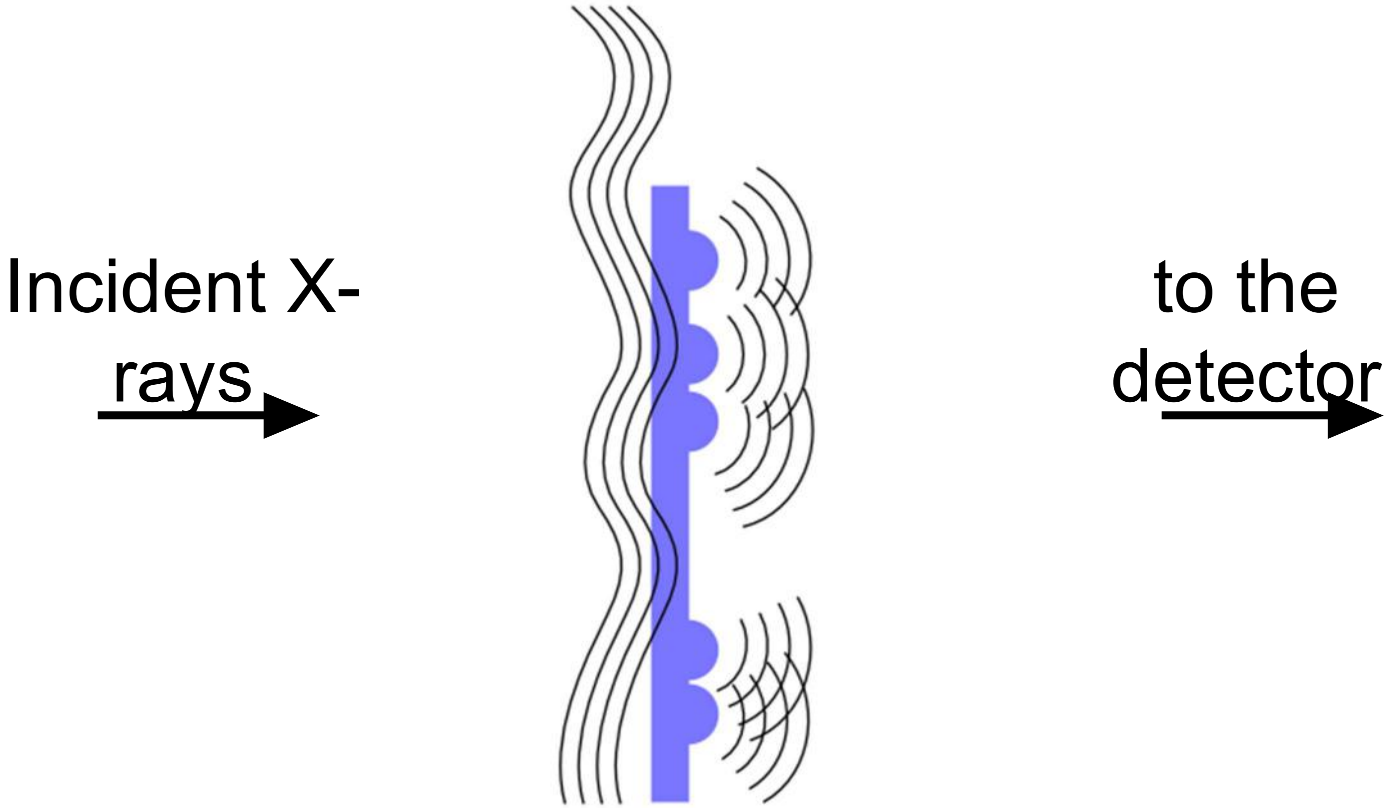

M. Stockmar *et al.*, Scientific Reports 3, 1927 (2013)

NEAR-FIELD PTYCHOGRAPHY

Object phase

Probe phase

Object amplitude

Probe amplitude

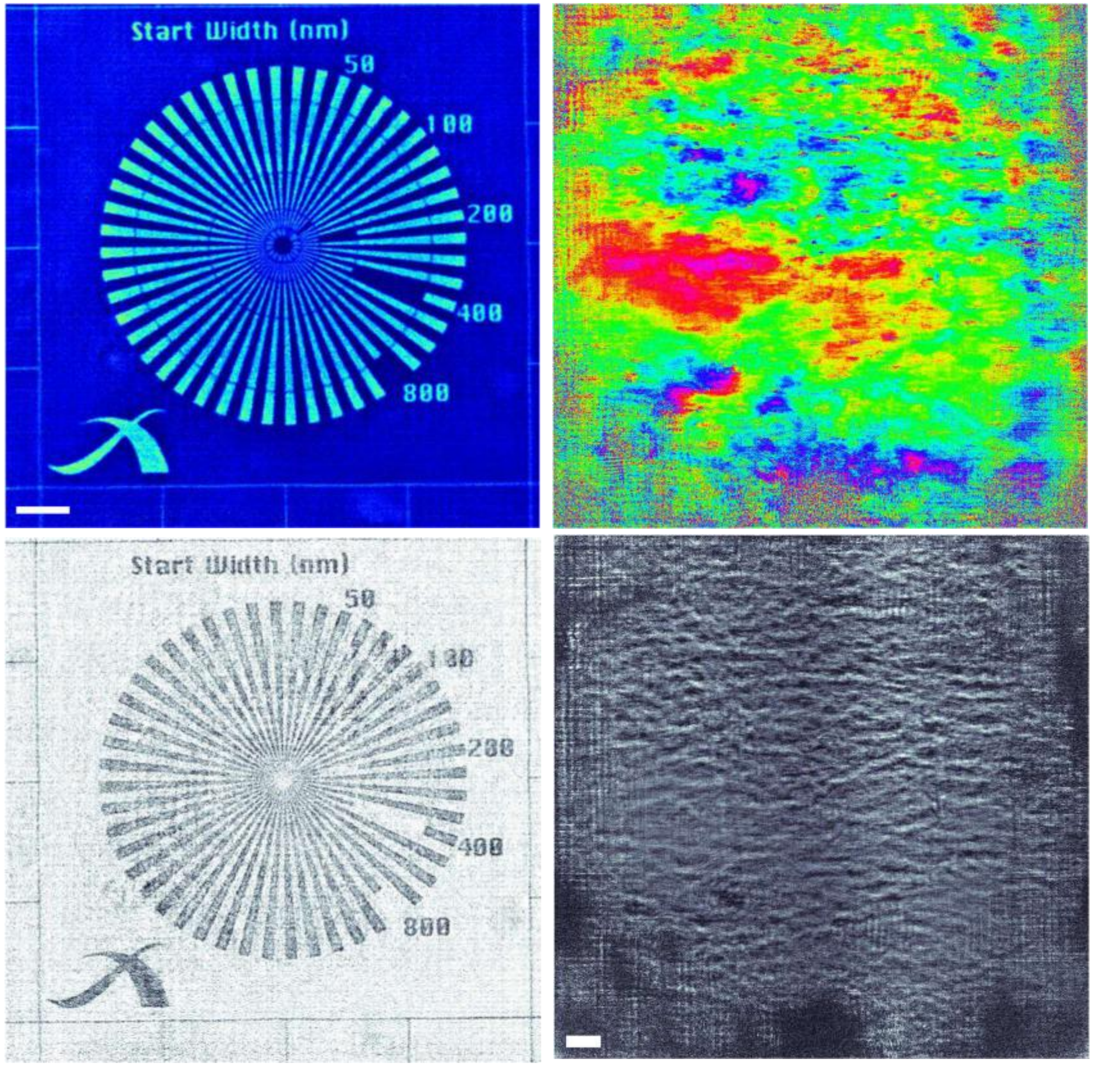

M. Stockmar *et al.*, Scientific Reports 3, 1927 (2013)

Successfully extended to (local) tomography!

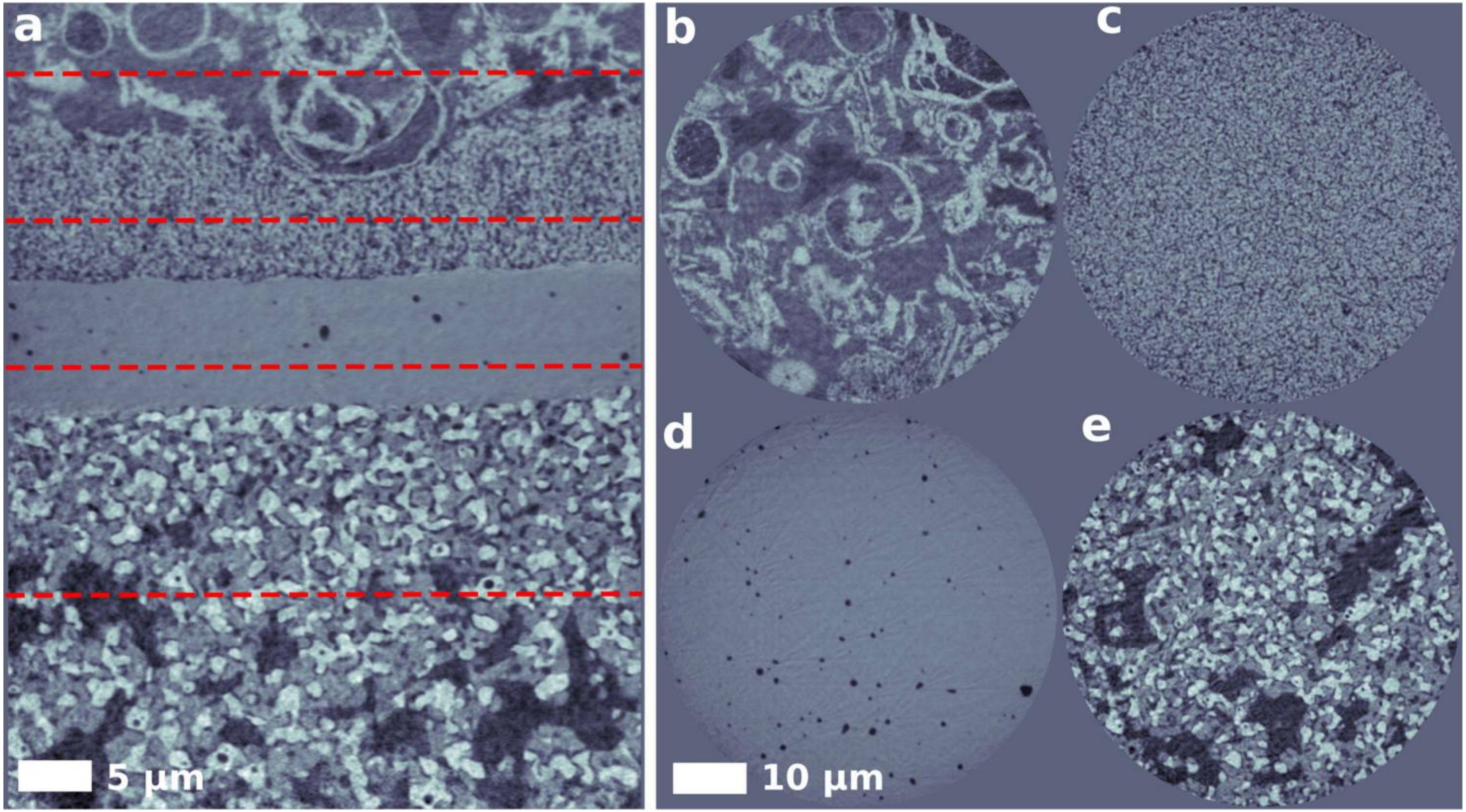

M. Stockmar, M. Hubert *et al.*, Opt. Express, 23, 12720 (2015)

EXPLORING THE RESOLUTION LIMITS ON PHOTONIC CRYSTALS

Single gyroid photonic crystals

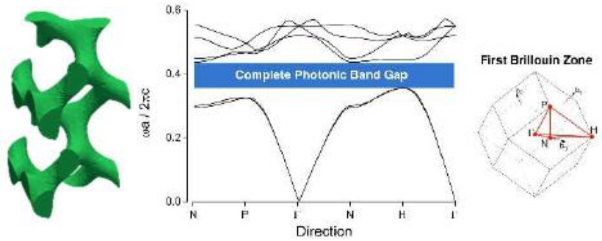

(left) *Eupholus schoenherri petiti.* Image by J. Rupérez. (right) *Callophrys rubi.* Image by A. Gor.

Visible light microscopy

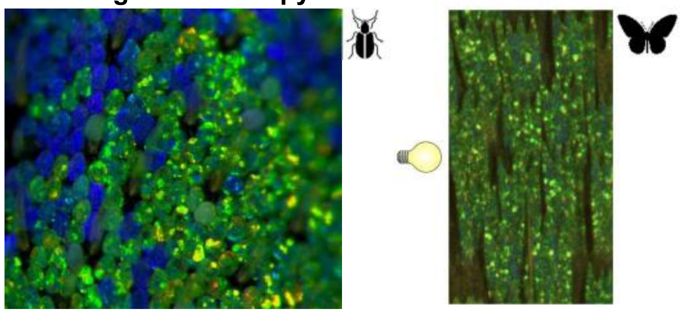

100 μm

100 μm

Near-field Ptychography: high-resolution 2D projections

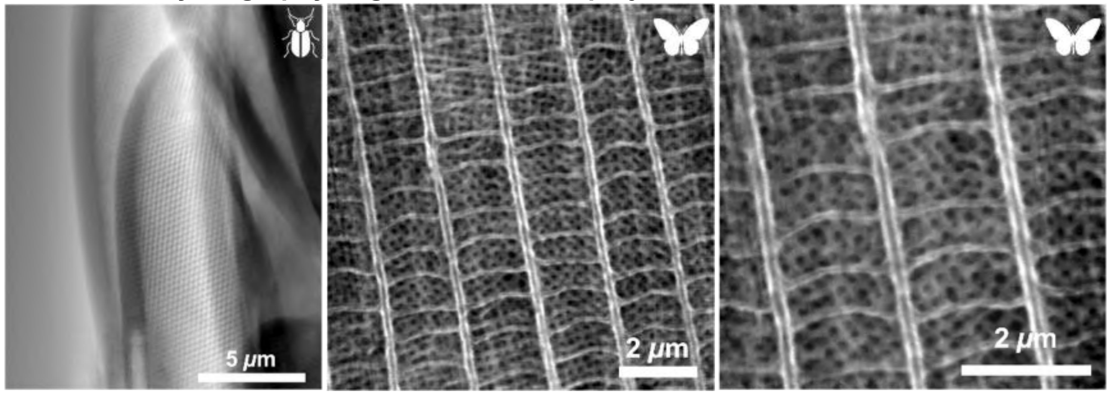

10 nm pixel size

5 nm pixel size

3 nm pixel size

HXCT: 50 nm pixel, overview scan

NF-PXCT: 10 nm pixel, high resolution scan

work in progress..

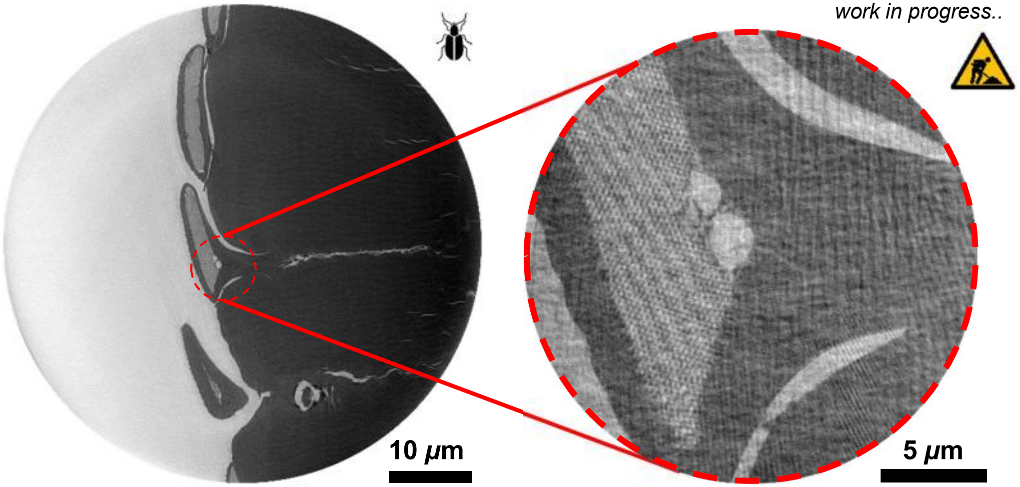

ESRF: THE EUROPEAN SYNCHROTRON

Main beamlines involved in X-ray Imaging

ID19, A. Rack
Abs./Phase Tomo
Ultra-fast

BM18
P. Tafforeau
Abs./Phase Tomo
Large FOV

ID17 Biomedical
Abs./Phase In-vivo

ID15A, M. Di Michiel
(Powder) Diffraction Tomo
Abs./Phase

ID13, M. Burghammer
SAXS Tomo

ID11, J. Wright, W. Ludwig
Diffraction Contrast Tomo
3DXRD

BM05, V. Honkimaki
Micro-tomography

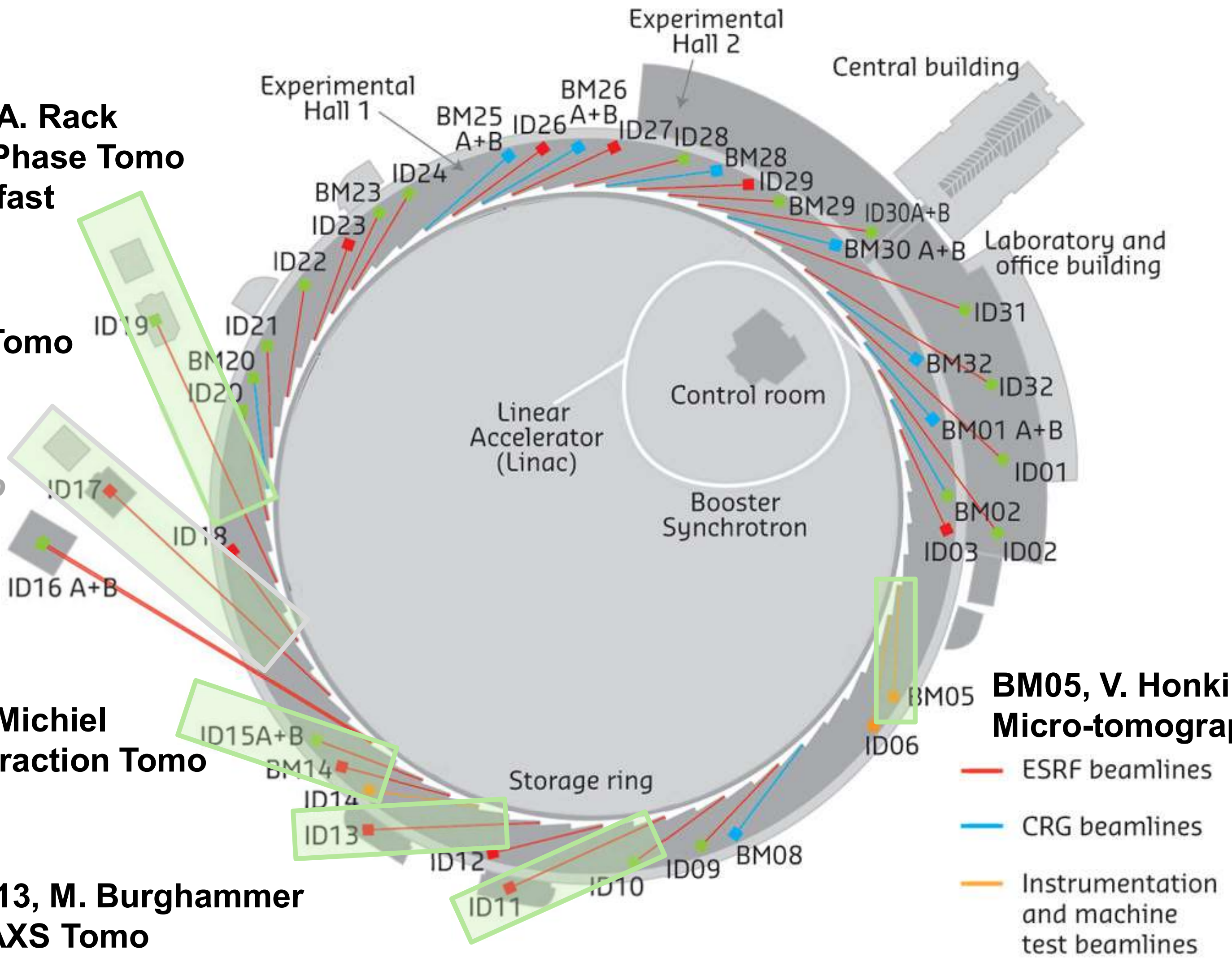

ESRF: THE EUROPEAN SYNCHROTRON

Main beamlines involved in X-ray Microscopy

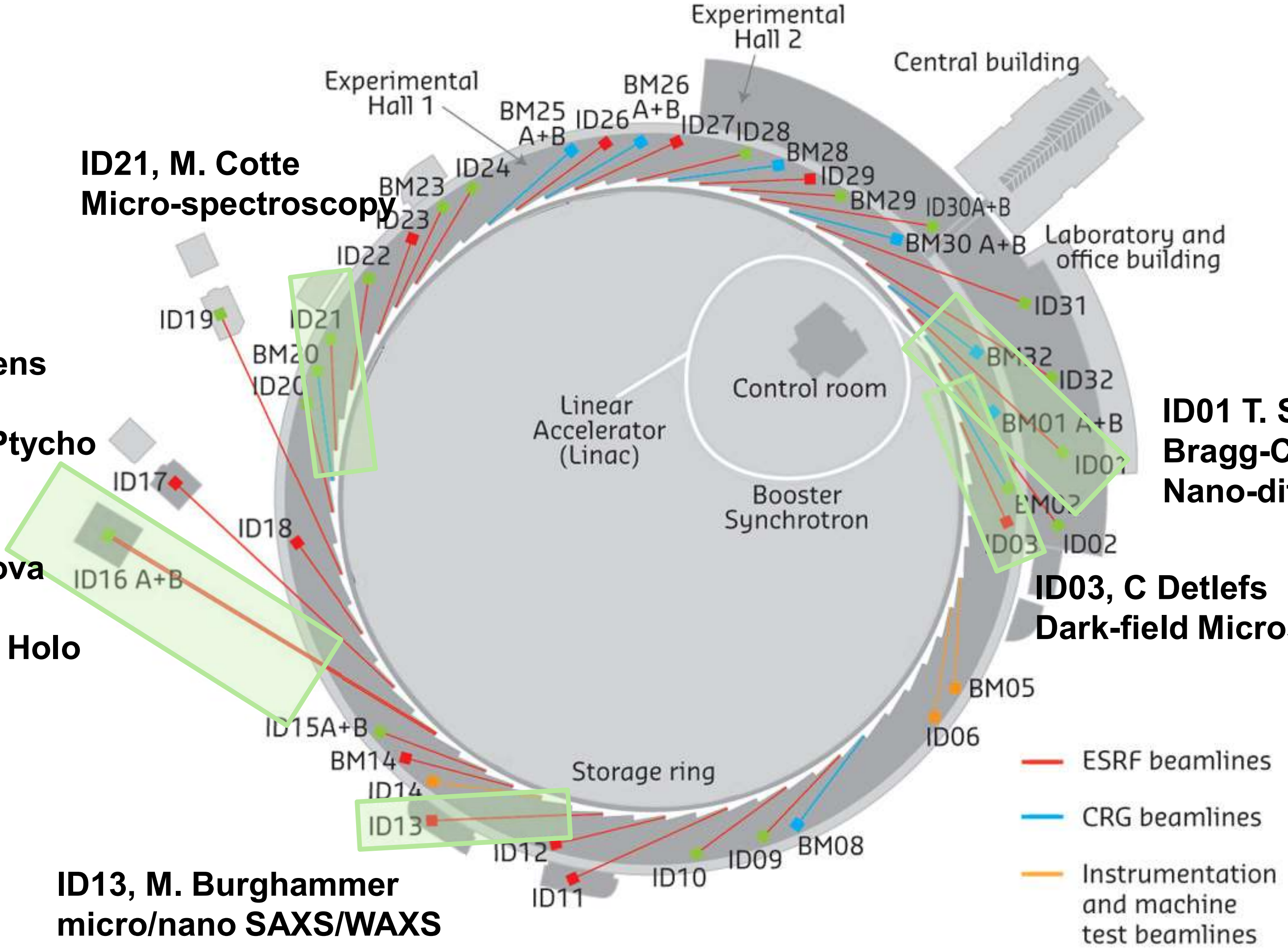

ID21, M. Cotte
Micro-spectroscopy

ID16A, P. Cloetens
Nano-Imaging
XRF, Holo, NF-Ptycho

ID16B, J. Villanova
Nano-Analysis
XRF, XRD, XAS, Holo

ID13, M. Burghammer
micro/nano SAXS/WAXS

ID01 T. Schulli
Bragg-CDI
Nano-diff

ID03, C Detlefs
Dark-field Microscopy


Thank you for your attention